Novel Polymerized Bentonites and Their Application as the Core of GCL Used in Aggressive Environment

September 2021

Graduate School of Science and Engineering
Saga University

NIE JIXIANG

Novel Polymerized Bentonites and Their Application as the Core of GCL Used in Aggressive Environment

A dissertation submitted in partial fulfillment of the requirement for the degree of Doctor of Philosophy in Geotechnical Engineering

By

NIE JIXIANG

Examination Committee:	Prof. Jinchun Chai (Supervisor) Prof. Yukihiro Ito Prof. Takenori Hino Dr. Takehito Negami
Nationality:	Chinese
Previous Degrees:	Bachelor of Engineering (Civil) Department of Civil Engineering and Architecture, Saga University, Japan Master of Engineering (Civil) Department of Civil Engineering and Architecture, Saga University, Japan
Scholarship Donor:	SIPOP (Strategic International Postgraduate Program), Saga University

Graduate School of Science and Engineering
Saga University, Japan
September 2021

ACKNOWLEDGEMENT

I would like to express my deepest gratitude to my supervisor Professor Jinchun Chai for during study. He gave me helps and suggestions for finding the topic and doing research. When I encounter difficulties in research, Professor Chai always gives me encouragement and useful suggestions to solve the problems, also taught me the methodology of analysis and scientific thinking. These suggestions are important to deal with the problems I will have in the future.

I am also very grateful to the examination committee members, Prof. Yukihiro Ito, Prof. Takenori Hino, Dr.Takehito Negami, who give valuable advices on the research work. I would like to thank Dr. Takehito Negami, who taught and supported me to do the SEM test in his busy time. I want to thank to the staff members of the Department of Civil Engineering and Architecture, Mr. Akinori Saito for his assistance on the experiment and other helps. I would like to acknowledge to the scholarship grant provided by SIPOP (Strategic International Postgraduate Program) for the opportunity and financial support of my study in Saga University.

I am grateful to my seniors, Dr. Rui Jia, Dr. Fang Xu, Dr. Yang Zhou, Dr. Yitian Lu, Dr. Hongtao Fu. I am also thanks to my colleagues, Mr. Junfeng Ni, Mr. Ziyang Gao, Mr. Rila Anda, Miss. Xiaoxiao Zhu, Mr. Ryoga Tanaka, Mr. Gehui Pang and my friend Mr. Weibin Li for kindly helping.

Finally, I express a lot of gratefulness to my family and relatives for all necessary helps.

ABSTRACT

To increase the swell potential and maintain lower permeability of bentonite in aggressive environments (high concentration cation solutions, very high or low pH solutions, etc.), novel polymerized bentonites (PBs) were produced, and their potential use as the core material of geosynthetic clay liner (GCL) to be used in the aggressive environments were evaluated.

(1) Polymerization method and suitable conditions. Novel PBs were produced using natural sodium bentonite (UB) and two monomers, acrylic acid (M_1) and acrylamide (M_2), using free radical polymerization method. The initiator (I) used was potassium persulfate, the deionized water (DI-W) as solvent. Using free swelling index (FSI) in 0.6 M NaCl solution as an index, the suitable polymerization conditions identified were: pH of 6, $I/(M_1 + M_2) = 0.5\%$, and $M_1/M_2 = 0.5$. Further, during the polymerization process, instead of using nitrogen gas to remove oxygen, a method of using vacuum pressure was established.

(2) Microstructures of novel PBs. Designating PB with polymer content of 10% as 0.1PB and so on, the results of X-ray diffraction (XRD) pattern shows that d-spacing of bentonite crystal of 0.1PB is the same as that of UB and the product was a microcomposite. For 0.2PB, its d-spacing was increased and the products was a nanocomposite. The SEM images of swelled PBs show large amount of polymer like net structures between bentonite particles. These polymers will have an important role for increasing the resistance of PBs to the aggressive cation solutions.

(3) Swelling and consolidation properties and permeabilities of the PBs. The properties of 0.1PB and 0.2PB were evaluated by a series of experiment test, i.e., FSI tests, swelling pressure tests, consolidation tests and permeability tests. The results from FSI tests and the swelling pressure tests show that the PBs have higher swelling

capacity than those of UB in DI-W and cation solutions (i.e., 0.6 M NaCl and 0.03-0.06 M $CaCl_2$). With 0.6 M NaCl solution, the FSI of 0.1PB is approximately 29 mL/2g. which exceed the requirement to be used as the core of GCLs (> 24 mL/2g). The mechanism that PBs had higher swelling capacity is that the novel PBs have two hydrophilic groups, -$CONH_2$ and -COONa. Due to both groups can be connected with exchangeable cations directly or indirectly by physical interaction, which contributes to reduce the amount of cations entering the diffuse double layers of bentonite particles. The results of the consolidation tests show that for all liquids tested, the compression indexes (C_c) of PBs are higher than that of UB. For a given void ratio, the order of permeability calculated from the consolidation test results is $k_{UB} > k_{0.1PB} > k_{0.2PB}$ (subscripts indicate the corresponding materials). For void ratios up to 5 for 0.1PB, the value of k is still smaller than 10^{-10} m/s in the 0.6 M NaCl and 0.03-0.06 M $CaCl_2$ solutions. The directly measured values of permeability from the flow rate test are comparable with that from the consolidation test results. Therefore, it is suggested that the novel PBs have potential to be used as a barrier material under high Na^+ concentration environments (e.g., sea water).

(4) Behavior GCLs with 0.1PB as core material (PB-GCLs). Leakage rate test results show that for the PB-GCL, with DI-W, a circular damage-hole up to 100 mm in diameter, and with 0.6 M NaCl solution, a damage-hole up to 15 mm in diameter were self-healed. In comparison, for UB-GCL in DI-W, a damage hole up to 60 mm in diameter and in 0.6 M NaCl solution up to 5 mm were self-healed. Therefore, PB-GCL had higher self-healing capacity. Further, the methods for predicting self-healing capacity of UB-GCL as well as PB-GCL with a circular damage-hole have been established. Good agreement between the measured and predicted self-healing ratios (healed area divided by the total damage area) was obtained. The prediction methods are useful for selecting a suitable GCL to be used under a given environment.

In summary, this research developed a new method for polymerizing bentonite and produced PBs which had higher swelling capacity and lower permeabilities with cation solutions. In addition, the leakage rate test results indicate that PB-GCLs (0.1PB) had very lower permeability and higher self-healing capacity. It is suggested that the novel PBs are potentially to be used as a barrier material under aggressive environments (e.g., seawater).

TABLE OF CONTENTS

LIST OF TABLES

LIST OF FIGURES

LIST OF NOTATIONS

CEC	Cation exchange capacity
C_c	Compressibility index
C_s	Swelling index
DI-W	Deionized water
DDL	Diffuse double layer
e	Void ratio
e_i	Initial void ratio
FSI	Free swelling index
GCL	Geosynthetic clay liner
G	Specific gravity
I	Initiator
k	Permeability
LOI	Loss on ignition
LVDT	Linear variable differential transducer
M_1	Acrylic acid
M_2	Acrylamide
PB	Polymerized bentonite
0.1PB	PB with a polymer to bentonite ratio of 0.1 and using two monomers
0.2PB	PB with a polymer to bentonite ratio of 0.2 and using two monomers
0.4PB	PB with a polymer to bentonite ratio of 0.4 and using two monomers
0.1PB-AA	PB with a polymer to bentonite ratio of 0.1 and using acrylic acid

	as monomer
0.4PB-AA	PB with a polymer to bentonite ratio of 0.4 and using acrylic acid as monomer
0.1PB-AM	PB with a polymer to bentonite ratio of 0.1 and using acrylamide as monomer
0.4PB-AM	PB with a polymer to bentonite ratio of 0.4 and using acrylamide as monomer
UB	Natural sodium bentonite
w_i	Initial water content
w_l	Liquid limit
w_p	Plastic limit
XRD	X-ray diffraction
ψ_{hole}	Permittivity of the damage holes
Q_{intact}	The steady flow rate of the intact sample
Q_{damage}	The steady flow rate of the damaged sample
A_{damage}	The damage area
A_{total}	The total cross-sectional area of the specimen
Δh	The water head difference
α	Self-healing ratio
m_b	The amount (mass) of bentonite
D	The diameter of a damage-hole
D_0	A constant (= 50 mm)
m_0	A constant (= 3 g for natural bentonite)
w_l	The liquid limit of bentonite with the liquid tested
w_{l0}	The liquid limit of bentonite using DI-W

p_a	Atmospheric pressure
p'	The overburden pressure on the GCL
t_b	The initial thickness of bentonite layer in the GCL
t_{b0}	A reference thickness
λ	Corresponds to the length of the X-ray radiation
n	Any positive integer
d	The space between layers in the clay lattice
θ	Measured diffraction angle.
T	Thickness of the PB entered the holes
σ_v'	Effective vertical stress

CHAPTER ONE
INTRODUCTION

1.1 Background

The majority municipal solid waste (MSW) from urban areas is landfilled in many countries, in design landfills, how economically and efficiently to protect ground environment from hazardous materials in the landfill is an essential issue. Over the past three decades, as shown in Fig. 1.1 (Kong et al. 2017), engineers and environmental agencies have increasingly adopted in the use of geosynthetic clay liners (GCLs) as a liner of waste containment facilities (e.g., landfills). This is because GCLs often have a very low permeability to water (typically $\leq 5\times10^{-11}$ m/s when permeated by deionized (DI) water at 35 kPa as per ASTM D5887) and ease of installation in the field (Koerner et al. 2012; Sari and Chai 2013) as shown in Fig. 1.2. They have also been adopted in applications such as secondary liners for underground storage tanks at fuel stations for groundwater protection, and as single liners for canals, ponds or surface impoundments (Bouazza 2002).

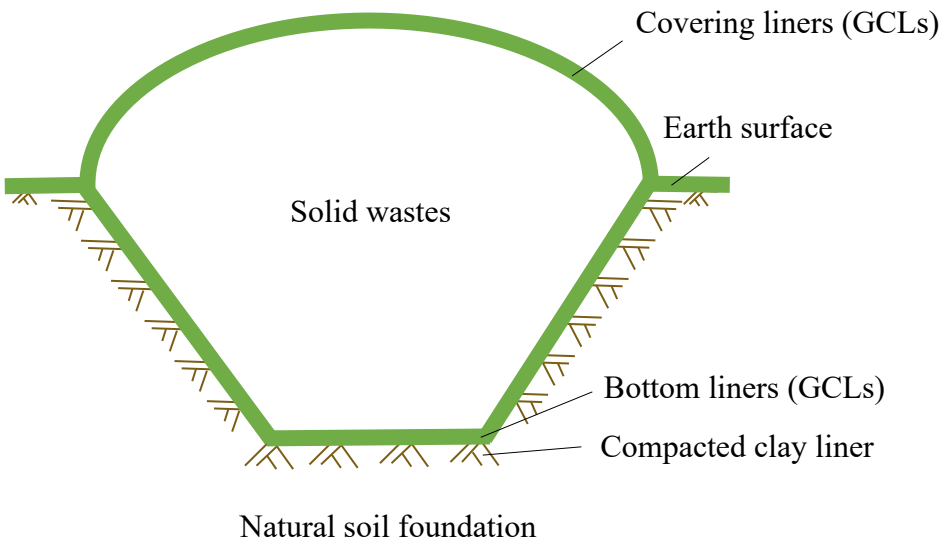

Fig. 1.1 Structure of a typical landfill

(a) (b)

Fig. 1.2 Installation of GCL in the field (from terrafixgeo.com)

The GCLs are factory-manufactured hydraulic barriers consisting of a thin layer of bentonite (3-5.0 kg/m^2) sandwiched between two geotextiles or bonded to a geomembrane, therefore, the properties of the GCLs are controlled by the properties of the encased bentonite. The lower permeability of the bentonite is attributed to the higher swelling capacity of bentonite in water (Chai and Shen 2018). However, in the field, The GCLs are easily to contact with cation solutions (e.g., seawater, leachates from landfill). With cation solutions, the swelling capacity of the sodium bentonite will be reduced and permeability increased (Petrov and Rowe 1997, Shackelford et al. 2000, Guyonnet et al. 2009, Sari and Chai 2013, Chai et al. 2016, Tian et al. 2016a, Chai and Shen 2018, Rowe et al. 2019). This is because the cation solutions can reduce the repulsive force between bentonite particles (Mitchell and Soga 2005, Chai and Shen 2018). To use GCLs as a barrier under an environment with cation leakage, it is required a core material of GCL to have higher swelling capacity and lower permeability under those conditions. For example, the Geosynthetic Research Institute standard GRI-GCL3 (GI 2016) requires a minimum free swelling index (FSI) of 24 mL/2g in DI water for bentonite to be used in GCLs, and in chemical containment applications, it is required that the permeability of

GCL is less than 5×10^{-11} m/s.

To increase swelling capacity of bentonite with cation solutions, one of the techniques is to polymerize bentonite (PB) (Bohnhoff and Shackelford 2013; De Camillis et al. 2016; Chai and Prongmanee 2020; Chen et al. 2019; Christian et al. 2020; Di Emidio et al. 2015; Ozhan 2018; Prongmanee et al. 2018; Scalia et al. 2011; Tian et al. 2019). Generally, there are two methods for preparing the PB. One is by mixing granular sodium bentonite with polymer (Di Emidio et al. 2015, Tian et al. 2019, Christian et al. 2020), and other is to mix the monomer with bentonite first, and then polymerize it (Scalia et al. 2014, Prongmanee et al. 2018, Nie et al. 2020). Although the latter one is a little bit complicated, it can produce more uniform PB and high quality PB. Previous researchers have reported that the mechanisms for lower permeability of PBs are increasing swelling capacity, preventing cation exchange, and pore-clogging by polymers. It is verified that PBs can keep lower permeability and higher swelling capacity in cation solutions (Chen et al. 2019; Prongmanee et al. 2018; Tian et al. 2019).

In Japan, some landfills are built in shallow sea areas, such as Tokyo bay landfill sites, and there are possibilities the liner system will be contacted with seawater. In addition, some municipal solid wastes have higher concentrations of Na^+, Ca^{2+}, etc. While for higher concentration cationic solutions, such as 0.6 M NaCl solutions (like seawater), the literature reported PBs (10% polymer) still cannot meet the requirement for use as a core material of GCLs (Prongmanee et al. 2018), i.e., the free swelling index (FSI) is less than 24 mL/2g (Guyonnet et al. 2009, GI 2016).

Further, the free radical polymerization method generally includes several steps, such as mixing monomer and initiator with bentonite; removing oxygen using nitrogen gas; polymerization; washing the product to remove impure materials; drying and crushing it into powder. It is desirable to simplify the procedure without lose the quality

of PBs produced (Ahmed 2015).

1.2 Structure of geosynthetics clay liners (GCLs)

Geosynthetic clay liners (GCLs) consist of bentonite and geosynthetics. The geosynthetics are either geotextiles or geomembranes. For geotextile-encased GCL (GT-GCL), the bentonite is contained by geotextiles on both sides. The geotextiles are bonded with an adhesive, needle- punching, or stitch-bonding as shown in Figs.1.3 (a) to (c) (EPA 2017) . The needle punching process causes some fibers from the top geotextile to extend through the bentonite to bottom geotextile, bonding the entire structure together. The fibers are potentially creating a stronger bond between the two geotextiles. Alternatively, the reinforcement can be carried out by sewing the entire geotextiles-bentonite composite together with parallel rows of stitch-bonded yarns.

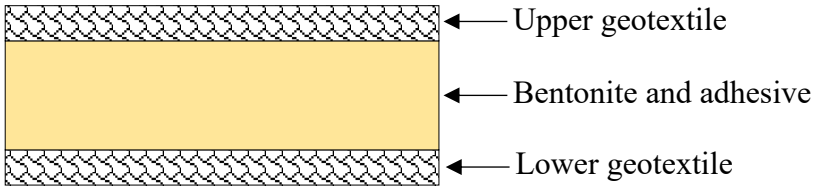

(a) Bentonite bound with adhesive to upper and lower geotextile

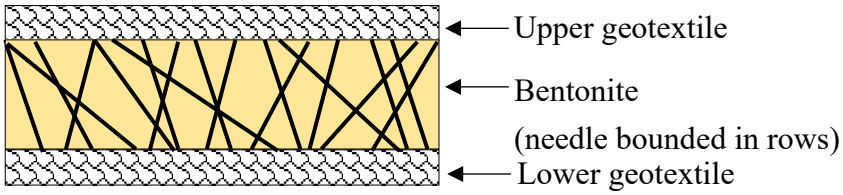

(b) Bentonite needle- punching through upper and lower geotextile

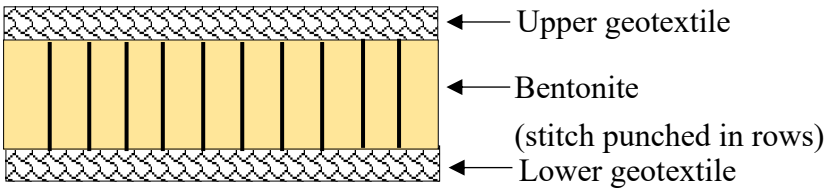

(c) Bentonite stitch-bonding between upper and lower geotextile

Fig. 1.3 (a) to (c) Cross section of GT-GCLs (modified from (EPA 2017))

.

Fig. 1.4 Cross section of GM-GCLs (modified from (EPA 2017))

For the geomembrane-supported GCL (GM-GCL) as shown in Fig.1.4, the bentonite is bonded to the geomembrane using a nonpolluting adhesive and a thin open weave spun-bound geotextile is adhered to the bentonite for protection purposes during installation. The primary differences between GCLs are the type and form of bentonite (e.g., powder versus granular, sodium versus calcium, etc.) used in the GCL, the type of geotextile (e.g., woven versus nonwoven geotextiles) and or the type of geomembranes, as well as the bonding methods.

1.3 Objectives

The objectives of this study are (1) developing a novel PB (polymer content 10%) to meet the FSI value more than 24 mL/2g in aggressive cation solution (0.6 M NaCl); (2) Investigating the physical properties, hydraulic properties, and self-healing capacity of GCLs with the PB as core material.

The objectives have been achieved by the following steps:

(1) developing a novel PB

Basic idea is to use free radical polymerization method to produce PB under the monomer to bentonite ratio of 0.1, Variables to be considered are: single monomer or due monomers; amount of the initiator, pH values, polymerization temperature, etc. Adopted conditions will be evaluated by free swelling index of the PBs produced.

(2) Properties of the PB.

Properties of the PB will be evaluated by microstructure analyses, the microstructure

(X-ray diffraction (XRD) and scanning Electron Microscopy (SEM) test), and hydraulic properties (the swelling pressures and permeability). Solution will be used are deionized water, 0.6 M NaCl and 0.03-0.06 M $CaCl_2$.

(3) Behavior of the GCL using PB as a core material

The hydraulic properties of geotextile encased GCL using PB as a core will investigated by permeability test, and self-healing capacity test using deionized water and 0.6 M NaCl solution.

1.4 Organization of the dissertation

The dissertation contains six chapters. The introductory Chapter 1 describes the background and objectives of the study. Chapter 2 reviews the literatures about bentonite, the polymerized bentonite (PB), the property of the PB, and the performance of the GCL with PB. Chapter 3 presents the method for producing new PB, the adopted polymerization condition as well as the microstructure of the PB. Chapter 4 presents the property of the novel PB by swelling capacity (e.g., FSI test, and swelling pressure test) and hydraulic properties in aggressive solution. Chapter 5 presents the behavior of GCLs using PB as the core by permeability test and self-healing capacity test. Finally, the conclusions drawn from this study and recommendations for future works are given in Chapter 6. The flowchart and contents of this dissertation is given in Fig. 1.4.

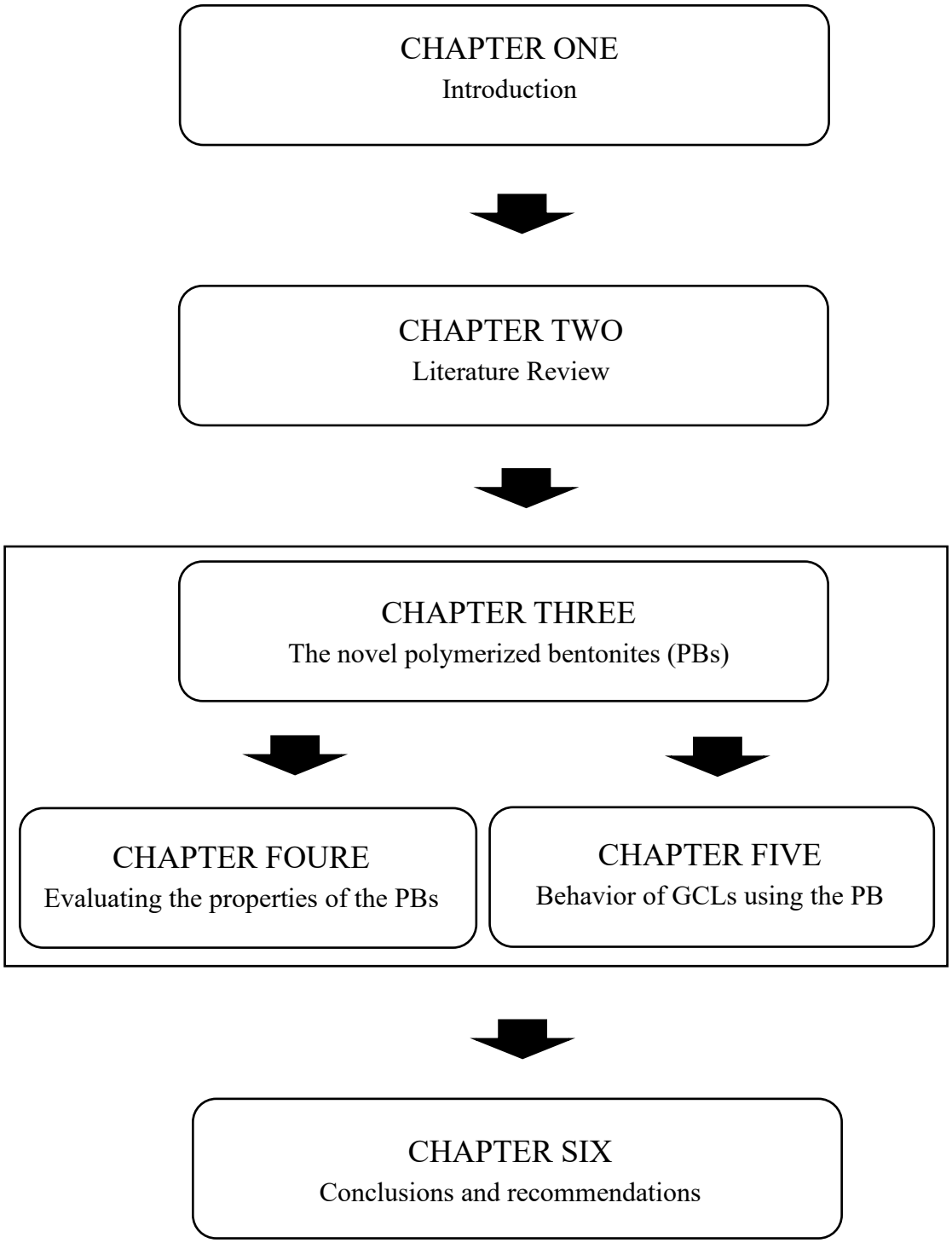

Fig. 1.5 Flowchart of the study

CHAPTER TWO
LITERATURE REVIEW

2.1 Introduction

Geosynthetic clay liners (GCLs) are increasingly being used in landfill liner system because of their ease of installation and low permeability. It is well known that the hydraulic performance of the GCLs highly depends on the properties of its core material, bentonite. Bentonite has low permeability (k) and high swelling capacity in water (Benson and Meer 2009; Chai and Prongmanee 2020; Sari and Chai 2013; Shackelford et al. 2000). However, for high concentration cation solutions, their swelling capacity will decrease and k will increase. To improve the hydraulic performance of bentonite in cation solutions, one of the methods is to mix bentonite and polymers, or polymerize bentonite, i.e., polymerized bentonite (PB).

In this chapter, firstly, the structure and swelling mechanism of bentonite will be reviewed, then the polymerization method and clay-polymer composite structure are discussed. Subsequently, the reported results about the properties of the PBs and the performance of GCLs use UB and PBs are reviewed.

2.2 Bentonite (UB)

The property of GCLs is controlled primarily by its core, bentonite. Bentonite is a highly expansive clay, consists mainly of montmorillonite mineral (approximately 65 to 90% of montmorillonite) (Shackelford et al. 2000). For engineering purpose, it is mostly used for lining material (i.e., GCLs), drilling mud and absorbent due to its highly colloidal behavior and expansion capacity. The types of bentonites are classified by the majority cations carried by the bentonite particles. For civil and environmental engineering, there are two common bentonites, which is widely used i.e., sodium (Na^{+}) and calcium (Ca^{2+}) bentonites.

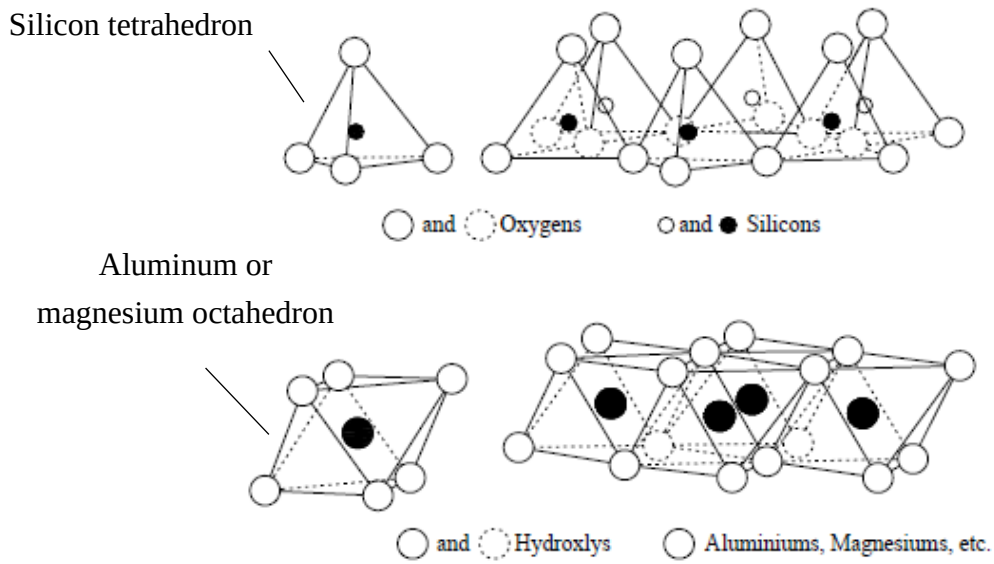

(a) Unit and sheet structure

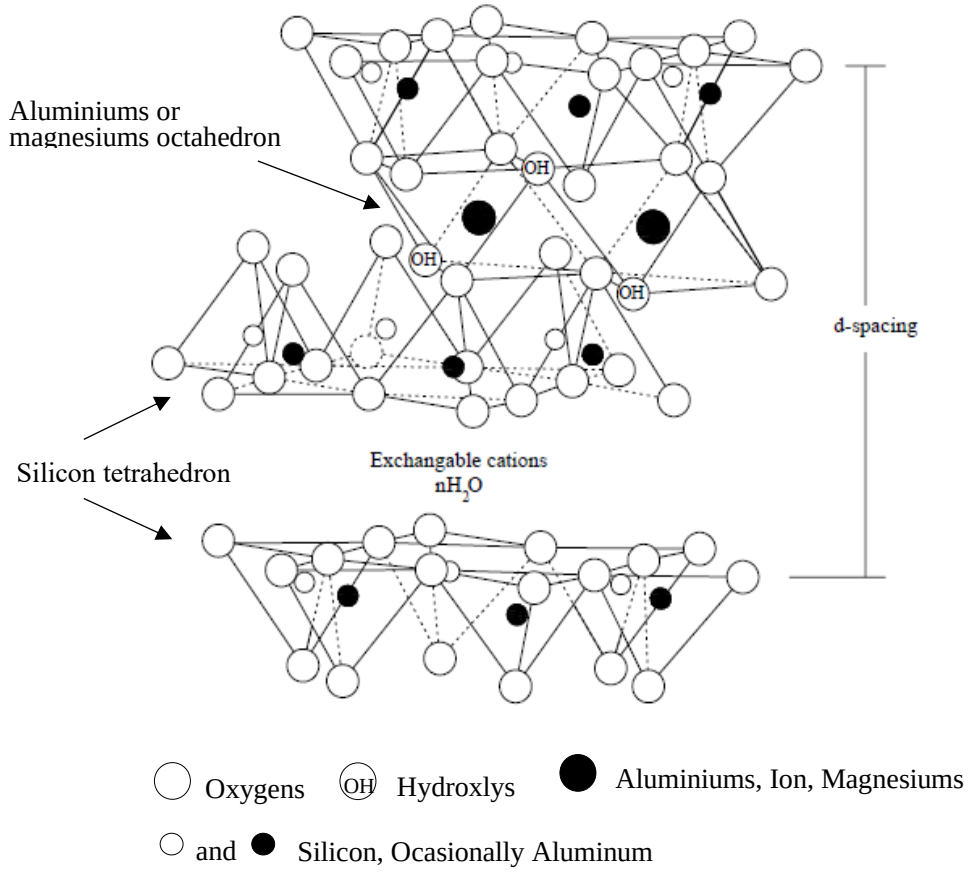

(b) Montmorillonite structure

Fig. 2.1 Unit and sheet structure and montmorillonite structure (modified from Mitchell and Soga, 2005)

The Na^+-bentonite has high swelling ability in water, while calcium bentonite is generally used as an adsorbent of ions in chemical solution due to its high cation exchange capacity. Na^+-bentonite has excellent barrier properties (e.g., swelling, permeability (k), self-healing) (Chai and Shen 2018, Nie et al. 2020).

2.2.1 Bentonite structure

In general, clay minerals have very small particle with net-negatively charge on their surface, which is balanced by the adsorption of cations. The basic unit of clay mineral are the silicon tetrahedron and the aluminum or magnesium octahedron as shown in Fig. 2.1 (a).

The Montmorillonite structure is shown in Fig. 2.1(b). It is well known that clay minerals have negative charge on their surface, which is balanced by the adsorption of cations. The basic unit of clay mineral are the silicon tetrahedron and the aluminum or magnesium octahedron (Mitchell and Soga 2005). Montmorillonite knows as 2:1 clay structure, which is an octahedral sheet sandwiched by two layers of silicon tetrahedron sheets as shown diagrammatically in three dimensions in Fig. 2.1. The bonding between the particles is van der Waals forces. These bonds are weak and can be easily separated by adsorption of water molecules. Moreover, the spacing between adjacent sheets, d-spacing, is created by balancing between the attractive (van der Waals) and the electrical repulsive force when it absorbs water molecules, and the d-spacing is varying on the degree of saturation. The d-spacing of the montmorillonite structure can be from approximately of 9.6 Å to complete separation (after Mitchell and Soga, 2005).

2.2.2 Cation exchange capacity (CEC)

The montmorillonite content in bentonite also is reflected indirectly by the cation exchange capacity (CEC) of the bentonite. The CEC is a measure of the total adsorption

capacity of a soil for cations, which increases with greater surface charge deficiency and greater specific surface of the clay mineral portion of the soil. In addition, the CEC of bentonites typically is lower than the CEC of pure montmorillonite, the latter typically ranging from 80 to 150 meq/100g (Shackelford et al. 2000). The difference between the CEC of bentonite and pure montmorillonite can be attributed to other non-adsorbing minerals in the bentonite, such as quartz. Thus, as the montmorillonite content of bentonite increases, the CEC of the bentonite should approach the CEC of pure montmorillonite (Shackelford et al. 2000).

2.2.3 Diffuse double layer (DDL)

The diffuse double layer (DDL) theory is often referred to as the Gouy-Chapman theory, and it can reasonably describe only for smectite (montmorillonite) particles suspended in monovalent electrolyte solution at very low concentration (< 0.001 M) (Sposito 2008) as well as predicting the swelling pressure of bentonites (Chai et al. 2016).

The idealizing assumptions of the DDL theory are: firstly, there are no interactions between the ions, and they are considered as point charges; secondly, the charge on the particle surface is considered to have a uniform distribution; and thirdly, the permittivity of the medium adjacent to the particle surface does not depend on their location; and lastly, the DDL theory is determined in the one-dimensional condition only and the particle surface must be considered as a plate.

For dry clay particles, some adsorbed cations are tightly adsorbed on surfaces of negative charged clay particles. When the clay absorbs water molecules from a solution, the concentration of cations will be higher near the surface of the particles, and it try to diffuse away for equalizing concentrations throughout the pore fluid. The escaping tendency due to diffusion and the opposing electrostatic attraction leads to ion distributions adjacent to a single clay particle in suspension as shown in Fig. 2.2.

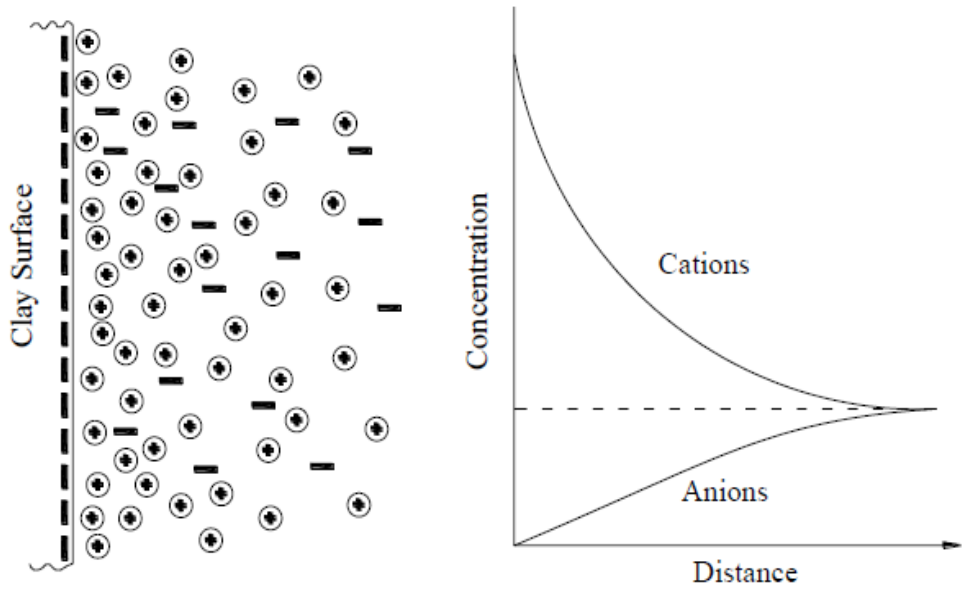

Fig. 2.2 Montmorillonite structure (after Mitchell and Soga, 2005)

2.2.4 Osmotic swelling

For the procedure of bentonite swelling, there are two distinct phases to be considered: the crystalline phase and the osmotic phase (Norrish and Quirk 1954). Crystalline swelling occurs first as water molecules move into the interlayer space hydrating the mineral surface and associated cations. Crystalline swelling causes the interlayer to separate by a distance corresponding to several water molecules (McBride 1994). Completion of crystalline swelling corresponds to a gravimetric water content in bentonite of approximately 35% (Guyonnet et al. 2005). Osmotic swelling follows crystalline swelling as water molecules flow into the interlayer region in response to the concentration gradient between the interlayer region and the free pore water. Osmotic swelling can produce far greater swell than crystalline swelling alone and is responsible for the high swelling capacity and low permeability of sodium bentonite in deionized water. The magnitude of osmotic swell is a function of the ionic strength of the pore water, with greater swell occurring when the pore water is more dilute (Kolstad et al.

2004). Osmotic swelling only occurs, however, when cations occupying the interlayer space during hydration are predominantly monovalent. When divalent cations are predominant, osmotic swelling capacity will be reduced significantly during hydration (Norrish and Quirk 1954; McBride 1994; Guyonnet et al. 2005).

The Na^+-bentonite used in GCLs has Na^+ as the predominant interlayer cation. When hydrated with water or dilute leachate, Na^+-bentonite undergoes osmotic swelling due to "chemico-osmosis," i.e., the flow of water molecule from lower ion concentration outside the interlayer region of the montmorillonite particles to higher ion concentration inside the interlayer region of the montmorillonite particles, which results in the formation of a thick layer of ions and water molecules (so-called "diffuse double layer") around the montmorillonite particles (McBride, 1994). This thick diffuse double layer causes separation of the naturally aggregated montmorillonite particles which reduces the intergranular pore spaces in the bentonite fabric resulting in low permeability ($<1.0 \times 10^{-10}$ m/s) (Chen et al. 2018; Kolstad et al. 2004; Shackelford et al. 2000). Furthermore, the ability of Na^+-bentonite to swell enables small defects like punctures that may occur during installation of GCLs to self-heal (Rowe 2020; Sari and Chai 2013).

However, aggressive leachates such as those that predominantly have high ionic strength (e.g., >300 mM), polyvalent cations, and/or extreme pH ($2 > pH > 12$) can inhibit osmotic swelling of Na^+-bentonite due to the low concentration gradient between the permeant solution and the interlayer region of the montmorillonite particles, resulting in a thin diffuse double layer, large intergranular pore spaces, and consequently high permeability of Na^+ - bentonite GCL ($<1.0 \times 10^{-10}$ m/s) (Chen et al. 2018; Christian et al. 2020; Kolstad et al. 2004; Petrov and Rowe 1997; Shackelford et al. 2000; Tian et al. 2019).

The influence of valence has been shown to be evident in free swelling index tests conducted by Shackelford et al. (2000). The bentonite was hydrated with deionized water and three different 0.025 M chloride solutions (i.e., LiCl, $MgCl_2$, and $AlCl_3$). Results in Fig. 2.3 show the swell volume of each solution. The highest valence cation, Al^{3+}, has the largest effect on the swelling capacity of the clay. The swell volume in deionized water is only slightly larger than in the LiCl, due to the monovalent of the cation.

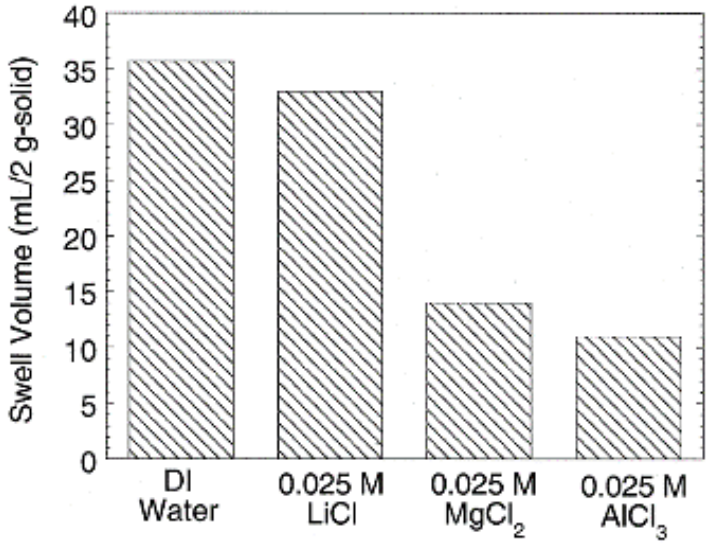

Fig. 2.3 Effect of cation valence on FSI (after Shackelford et al., 2000)

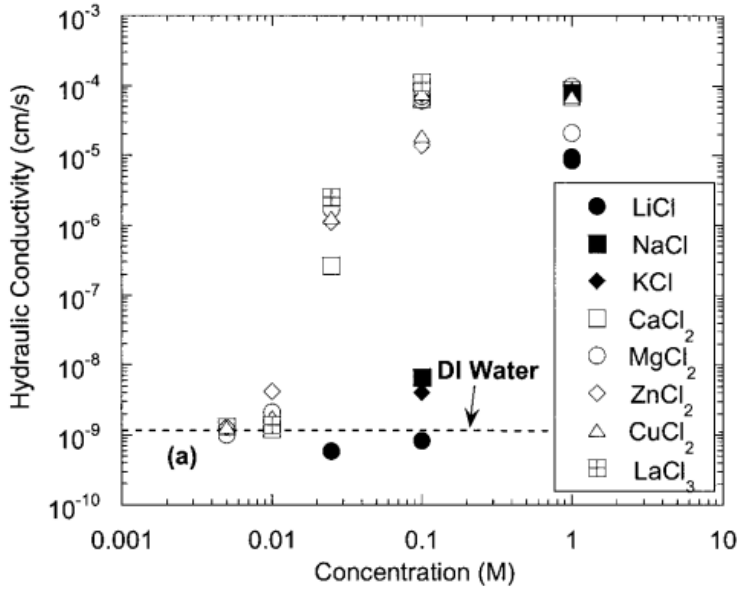

Fig. 2.4 Hydraulic conductivity as function of concentration (after Jo et al., 2001)

Jo et al. (2001) investigated the influence of salt solutions with various concentration, cation valence on hydraulic conductivity (k) of GCLs. They reported that the k-value of the GCL increase with increasing in concentration of solutions. Moreover, they also found that monovalent cations reduce the value of k to different degrees depending on the hydrated radius of the cation (Fig. 2.4).

2.3 Polymerized bentonite (PB)

2.3.1 Polymer

Polymers are widely used in modern society human daily life. For example, they have been used as a water barrier and sealing material, due to their advantages of high and fast water absorption rate, strong water retention capacity, safety and non-toxicity (Alexandre and Dubois 2000). Polymers are long-chain molecules composed of unit cells (monomers) linked in either straight or branched chains to form macromolecules (Painter and Coleman 1998). A single macromolecule may contain thousands of monomers. When dissolved in water, some polymers form a hydrogel like a web of polymer strands and associated water molecules with a gelatinous structure. The polymers used in bentonite-polymer composite generally form hydrogels when hydrated (Tian et al. 2016b, 2019).

Absorbent polymers have a very high swelling capacity. Christian et al. (2020) reported that polymers generally can be classified into two main categories, depending on the basic structure of the polymer: water-soluble linear polymers and superabsorbent crosslinked polymers. Water-soluble linear polymers can disperse and swell in water to form a viscous polymer gel (Williams 2007). Superabsorbent crosslinked polymers are networks of linear polymer chains bonded together either chemically or physically and not soluble in water, which can absorb a large amount of water (Behera and Mahanwar 2020). Crosslinked polymers are not soluble in water due to presence of the crosslinkers, but are capable of imbibing large amounts of water when hydrated to form discrete

polymer hydrogels. So, they are commonly referred to as superabsorbent polymers (SAP) (Behera and Mahanwar, 2020).

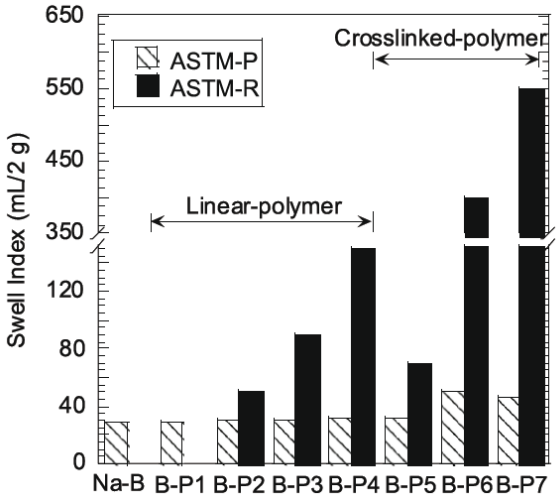

Fig. 2.5 Comparison of swell indices of sodium bentonite (Na-B) and bentonite - polymer (B–P) specimens prepared following ASTM standard method (after Christian et al. 2020)

Christian et al. (2020) uses seven types of bentonite-polymer composites from same manufacturer, among them, four types belong to linear polymer and others belong to crosslinked polymer. The result of free swelling index (FSI) demonstrate that crosslinked polymer has better swelling ability than that of the linear polymer as shown in Fig. 2.5.

Polymers are commercially manufactured in four main physical forms: powders, emulsions, beads, and liquid solutions (Billmeyer 1984). Powdered polymers are typically manufactured through bulk polymerization of monomers into dried gels, then milled and screened into powder (Billmeyer 1984; Williams 2007).

The conformation of polymers in solution is sensitive to environmental conditions such as pH, ionic strength, temperature, electrical potential, and photo-irradiation (Kim and Palomino 2011). Low pH or high ionic strength generally results in a coiled polymer

conformation, whereas high pH or low ionic strength generally results in an extended polymer conformation. Chemical environments leading to a coiled conformation have a destabilizing effect on polymers in solution, resulting in so-called salting out (precipitation), whereas conditions leading to extended polymer conformation have a so-called salting-in (solubilization) effect (Swann et al. 2010). Differences in polymer conformation affect the macroscopic properties of a polymer hydrogel (Kim and Palomino 2011). Although the bentonite and polymer are completely different stuff, it is noticed that they almost have a same tendency regarding to limit swelling and extend, when contact the low pH or high ionic strength.

2.3.2 Polymerization method

(1) Free-radical polymerization

Free-radical polymerization process is based on a repetitive reaction in which a monomer is converted into a polymer segment. Organic radicals play an important role in polymer syntheses. Free radical polymerization is very important in the field of industrial polymer synthesis and is the preferred route to commercial polymers. Industrially, more than 50% of all plastics produced in the world are synthesized through radical polymerization processes because this method has a number of merits for vinyl polymer syntheses. Indeed, free radical polymerization is very easy to perform and is adaptable to many types of monomers under mild conditions using convenient equipment, and often shows substantial reproducibility. In most cases, monomer purification is not required to a high extent and initiator residues need not be removed from the polymer because they have little or no effect on polymer properties. Moreover, free radical polymerization processes can be readily and economically performed in the bulk and in suspension which is a distinct advantage from industrial point of view. Free radical polymerization is probably the most important commercial process leading to

high molar mass polymers. This is due to the large variety of monomers which can be polymerized and copolymerized radically and to the relatively simple experimental conditions which require the absence of oxygen but which can be carried out in the presence of water, e.g., as in suspension or emulsion polymerizations, and within a convenient temperature range, typically 0- 100°C.

The free radical copolymerization proceeds via initiation, propagation, and various types of chain-stopping reactions (such as chain transfer to various types of substrate and radical–radical termination via combination or disproportionation) (Matyjaszewski and Davis 2002; Mishra and Yagci 2016). Figs. 2.6 (a) to (d) show the reaction scheme of free-radical polymerization.

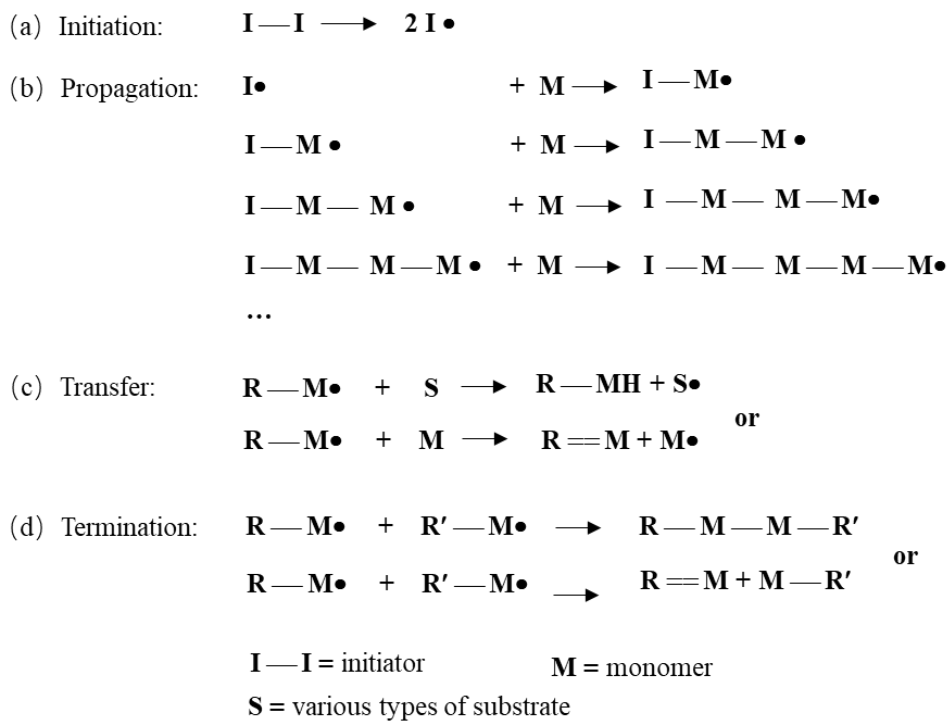

Fig. 2.6 General reaction scheme for free-radical polymerization, (a) initiation, (b) propagation, (c) transfer and (d) termination (after Matyjaszewski and Davis 2002)

(a) initiation, the creation of the radical from nonradical species;

(b) propagation, the successive additions of monomer to the radical;

(c) transfer, the termination of a polymer chain and the subsequent initiation of a new polymer chain;

(d) termination, the mutual reaction of two radicals to produce inactive polymer.

(2) Polymerization processes

The commercial polymerization processes included of emulsion polymerization, solution polymerization, suspension polymerization, and precipitation polymerization are widely used.

(a) Emulsion polymerization

Emulsion polymerization is usually starting with an emulsion incorporating water, monomer, and surfactant. The most common type of emulsion polymerization is an oil-in-water emulsion, in which droplets of monomer (the oil) are emulsified (with surfactants) in a continuous phase of water.

(b) Solution polymerization

The compositions of the solution polymerization include of monomer, initiator and solvent. In this method, the choosing polymer should be soluble in the chosen solvent. For the advantages of this method, heat released by the reaction is absorbed by the solvent, and so the reaction rate is reduced. The viscosity of the reaction mixture is also reduced, which is not allowing auto acceleration at high monomer concentrations. This process is easy and commonly used in the production of sodium polyacrylate, a superabsorbent polymer used in disposable diapers (Zohuriaan-Mehr and Kabiri, 2008).

(c) Suspension polymerization

Suspension polymerization is a heterogeneous radical polymerization process that uses mechanical agitation to mix a monomer in a liquid phase, while the monomers polymerize, forming spheres of polymer. This process is used in the production of commercial resins,

including polyvinyl chloride (PVC), a widely used plastic, styrene resins including polystyrene, expanded polystyrene, and high-impact polystyrene.

(d) Precipitation polymerization

This polymerization method is a heterogeneous polymerization process that begins initially as a homogeneous system in the continuous phase, where the monomer and initiator are completely soluble, but upon initiation the formed polymer is insoluble and thus precipitates.

2.3.3 Clay-polymer composite structure

Various parameters including clay structure, polymer type and preparation method influence the properties and structure of the composite. Generally, according to the state of the long chains of the polymers insertion into the silicate layer of sodium bentonite, clay-polymer composite structure can be classified into three types, which include one microcomposite (phase separated) structure and two nanocomposite (intercalated and exfoliated) structures (Alexandre and Dubois 2000).

(a) Phase-separated structure is a structure that the polymer cannot be embedded between the silicate sheets of bentonite, and a phase separation is to obtain composite materials which are coated by the polymer (Fig. 2.7a). The performance of the material remains the same as the traditional material of microcomposites. The phase separated clay-polymer composites is in the group of micro composites.

(b) Intercalated structure is structure that one or more chains of polymers are inserted into the interlayer of clay, and a certain extent d-spacing of the lamellar silicate sheet of clay, but the lamellar of clay still retains a certain layered ordered structure, which may be used as anisotropic functional materials, such as barrier materials. The intercalated bentonite/polymer composite is classified as nanocomposite (Fig. 2.7b).

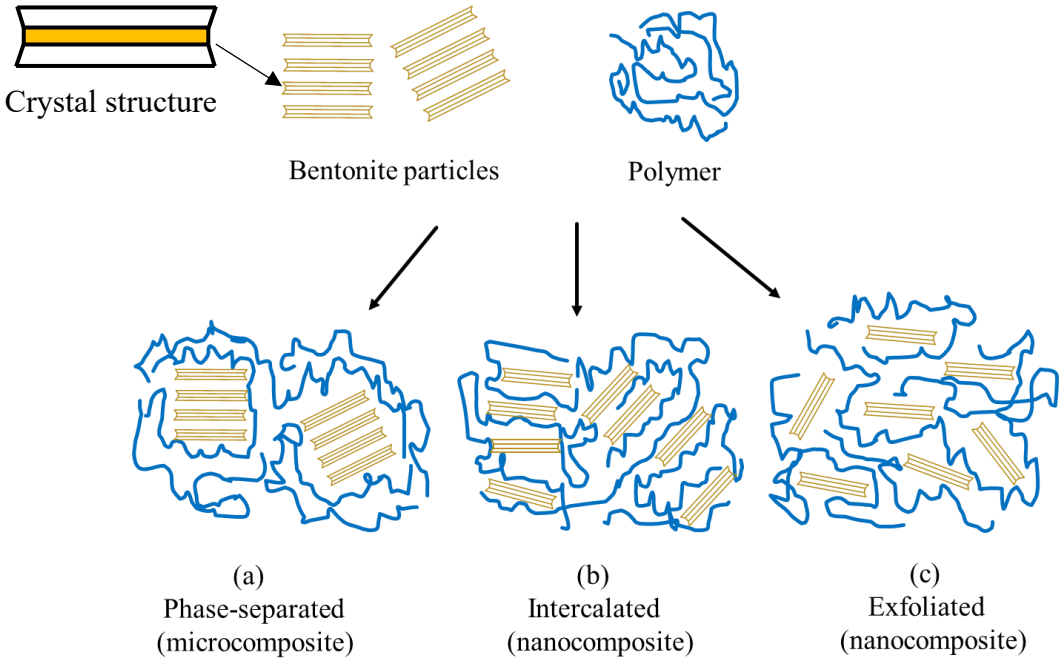

Fig. 2.7 Scheme of different types of composites arising from the interaction of layered silicates and polymers (modified Alexandre and Dubois 2000)

(c) Exfoliated structure is demonstrated that the ordered structure of exfoliated layered silicate is completely destroyed, and the lamellar layer is completely exfoliated, and is randomly dispersed in the polymer matrix. The montmorillonite lamellar layer and the polymer achieve uniform mixing. Due to the large specific surface area of the dispersed phase, it is closely bound to the matrix, and theoretically it has better physical and mechanical properties than conventional composite materials. The exfoliated bentonite/polymer composite is also classified as nanocomposite (Fig. 2.7c). (Alexandre and Dubois, 2000).

2.4 Properties of PBs

The low permeability of bentonites is primarily due to adsorbed immobile water molecules and hydrated ions in the interlayer region of bentonite clays that restrict the

pore space available for the flow and cause tortuous flow pathways (Di Emidio et al. 2011; Prongmanee et al. 2018; Tian et al. 2019). In solutions with high ion concentration and valence cause the thickness of the diffuse double layer to collapse and the osmotic swelling to decrease (Guyonnet et al. 2005; Scalia et al. 2018), therefore, the permeability was increased when in contact with aggressive cation solutions. To improve the chemical compatibility of bentonite to aggressive permeants, several types of PBs have been developed in the past decade (Di Emidio et al. 2011, 2015, Scalia et al. 2011, Bohnhoff and Shackelford 2013b, Scalia et al. 2014, Tian et al. 2016a, 2019, Kong et al. 2017, Prongmanee et al. 2018, Chen et al. 2019, Chai and Prongmanee 2020, Christian et al. 2020).

2.4.1 Structural characterization of bentonite-polymer composites

To understand the mechanism of a polymer treated bentonite, microstructure analysis is widely used, such as the X-ray diffraction (XRD) analysis and scanning electron microscope (SEM) image.

(1) X-ray diffraction (XRD) analysis

X-ray diffraction (XRD) is a technique for identifying type of minerals in a substance and basal-spacing (d-spacing) of crystal structure (Abhilash et al. 2016; Guyonnet et al. 2005). If the polymer entered the intercalated crystal structures of bentonite particles, its basal spacing will be changed and XRD was used to identify whether this kind change was occurred (Kim and Palomino 2011). It is well known that bentonite show a characteristic peak in the X-ray diffraction (XRD) pattern due to their regular layered structures. interlayer spacing of montmorillonite is an important parameter to investigate the effect of organic montmorillonite treatment and the type of nanocomposites. Intercalation of polymer molecules into the clay particle increases the interlayer spacing, resulting in a shift of the diffraction peak towards lower diffraction angle. Any change

in the inter-layer of a clay lattice by polymer causes the change in the position, broadness and intensity of the characteristic peak in the XRD pattern. Fig. 2.8 is a schematic diagram of the measurement of the layer spacing by X-ray diffraction (XRD).

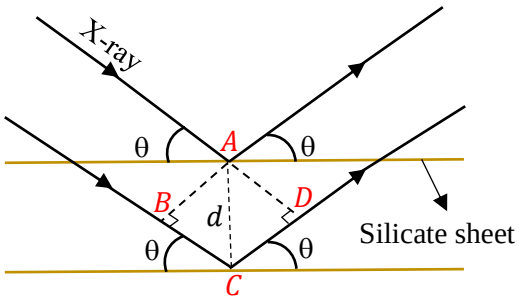

Fig. 2.8 A schematic diagram of the measurement of the layer spacing by XRD

X-rays with a wavelength of λ are incident on the surface of the montmorillonite layer at an incident angle θ, two sets of diffracted waves are formed on each surface of montmorillonite layers in the adjacent, and d is the distance between adjacent montmorillonite layers. If the two sets of X-rays appear as shown in the Fig. 2.8, and the diffraction peak appears on the X-ray diffraction results, then according to the principle of X-ray diffraction, the wavelength difference between the two sets of X-rays must be an integral multiple of the wavelength. Using the peak width at half maximum height and peak position (2θ) in the XRD pattern, the d-spacing can be calculated utilizing Bragg's law (Eq. 2.1).

$$2dSin\theta = n\,\lambda \tag{2.1}$$

Where λ corresponds to the length of the X-ray radiation, and n is any positive integer, also known as the diffraction order, d is the space between layers in the clay lattice and θ is measured diffraction angle.

Gao and Heimann (1993) reported the result of XRD using the monomer

acrylamide (AM) polymerized with Na-montmorillonite (PAM- montmorillonite) with AM to bentonite

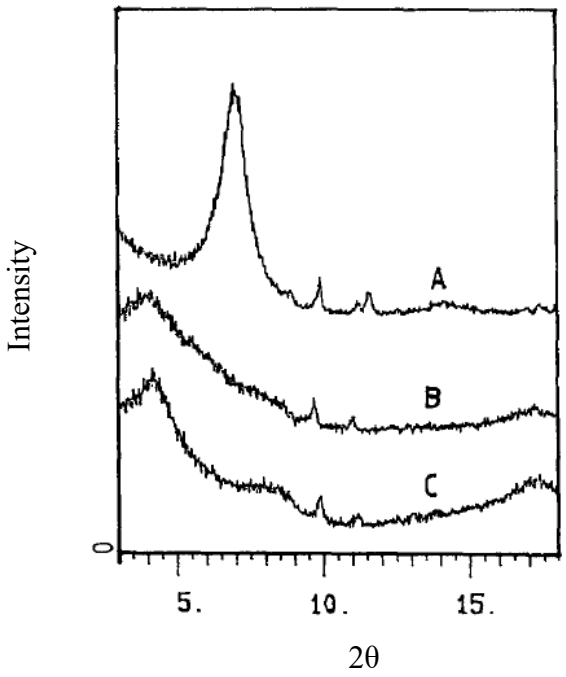

Fig. 2.9 XRD interplanar spacings (CuKα) of (A) Na-montmorillonite, (B) PAM-montmorillonite (1:4) composite, and (C) PAM-montmorillonite (1:1) composite (after Gao and Heimann, 1993)

ratio of 1:4 and 1:1. It is clearly that a peak of the PAM-montmorillonite composite both (B) and (C) is lower than that of the Na-montmorillonite (A) as shown in Fig. 2.9. Both samples (B) and (C) the value of the interplanar spacing changed from 1.27 nm (hydrated complex with Na^+ as exchangeable interlayer cation) (A) to 2.12 nm which indicates that the polymer was intercalated into the clay. The expansion of the interlayer region was thus 0.85 nm (Gao and Heimann 1993).

(2) Scanning electron microscope (SEM) image

In Fig. 2.10 shows the extensive three-dimensional network of polymer hydrogel

between bentonite clusters when the bentonite polymer composite (BPC) GCL was hydrated with deionized water. Tian et al. (2016a) attributed the low permeability of the BPC GCLs to polymer hydrogel blocking flow paths between bentonite granules. Scanning electron micrographs (SEMs) confirmed that hydrogel filled the voids between the bentonite granules, which could block permeable flow paths and lower the permeability. They concluded that maintaining low permeability requires retention of hydrogel in the pore space under a hydraulic gradient.

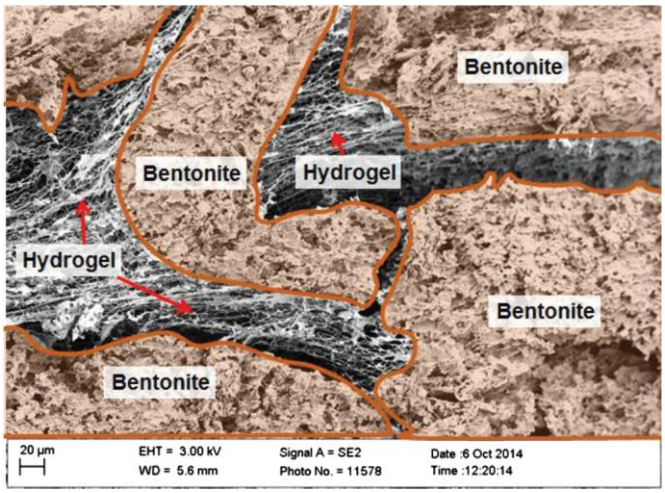

Fig. 2.10 (Color) SEM image of bentonite–polymer from CPH GCL in DI water after freeze-drying; brown color represents bentonite clusters (after Tian et al. 2016)

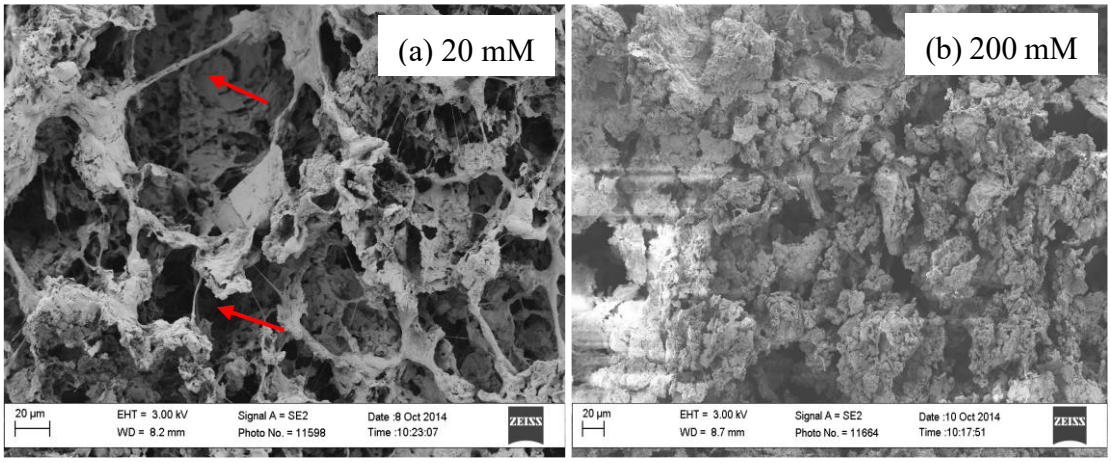

Fig. 2.11 SEM images of freeze-dried Bentonite-polymer mixtures initially hydrated in

(a) 20 and (b) 200 mM $CaCl_2$. The redarrows in (a) point to the polymer chains (after Tian et al. 2016b)

In terms of cation solutions, SEM images reported by (Tian et al. 2016b) illustrate how the chemistry of the permeant liquid affects conformation of the polymer and retention of the hydrogel in the pore space. In Fig 2.11, SEM images on the bentonite polymer composite GCL permeated with 20 mM $CaCl_2$ solution and 500 mM $CaCl_2$ solution showed the $CaCl_2$ concentration increased, the polymer hydrogel was composed of fewer and larger polymer strands that were less effective in bridging between bentonite clusters and blocking flow paths.

2.4.2 Various types of polymer combined with bentonite

According to Theng (1979), clay-polymer interactions can be classified according to the polymer's surface charge; nonionic polymers are electrically neutral whereas anionic and cationic polymers carry net negative and positive surface charges, respectively.

Nonionic polymer is possibly adsorbed to surfaces of the sodium bentonite by H-bounding (Deng et al. 2006; Theng 1979), Few publications used a nonionic polymer treated bentonite.

Cationic polymers are able to protect the clay from cation exchange because a cationic polymer chain contains thousands of cations that would need to be exchanged simultaneously (Ashmawy et al. 2002). Due to the cationic polymer tends to aggregate clay particles, with a consequent compression of the diffuse double-layer thickness, which is not beneficial for the hydraulic performance of the clayey barrier (Di Emidio et al. 2015). Ashmawy et al. (2002) reported that the clays treated with cationic polymers showed higher or similar permeability compared with that of untreated clays. For instance, the permeability to water of this type of treated clays is between 3.0×10^{-9} and

1.0×10^{-7} m/s compared with that of untreated clays ranging between 3.0×10^{-9} and 1.0×10^{-8} m/s (Ashmawy et al. 2002).

Anionic polymers onto clay surface is promoted by the presence of polyvalent cations which act as bridges between the anionic groups on the polymer and the negatively charged sites on the clay (Stutzmann and Siffert 1977; Theng 1982). Stutzmann and Siffert (1977) stated that the adsorption of anionic polymers onto clays occurs through ionic exchange. Di Emidio et al. (2011) developed a chemical-resistant clay (HYPER clay), a bentonite treated with the anionic polymer sodium carboxymethyl cellulose (Na-CMC), with deionized water, seawater, and a 5 mM $CaCl_2$ solution. Permeability of the HYPER clay was one order of magnitude lower than the permeability of an untreated sodium bentonite (NaB) when permeated with sea water, and 2.6 times lower than NaB when permeated with 5 mM $CaCl_2$. Prongmanee et al. (2018) reported using synthesis of sodium acrylate and sodium bentonite to produce the anionic polymerized bentonite (PB), The PB has higher swelling capacity and lower permeability than those of untreated bentonite in 0.6 M NaCl.

As shown above, the anionic polymers were effectively to improve the hydraulic performance of bentonite in aggressive solutions.

2.4.3 Swelling capacity and permeability

Scalia et al (2011) and Scalia et al. (2014) developed a bentonite polymer nanocomposite (BPN) (polymer content 12.7%) by polymerizing an organic monomer (acrylic acid) in a bentonite slurry using the free radical polymerization method. They reported that in deionized (DI) water, BPN exhibited more than twice the swell capacity compared to that of Na-bentonite (i.e., 73.0 vs. 30.5 mL/2g). The results showed that swell indexes (Fig. 2.12) of the BPC were higher than those of the untreated bentonite (Na-B) in different concentration of $CaCl_2$ solutions.

In DI water and 5, 50, and 500 mM $CaCl_2$ solutions, the flow test of the GCLs use BPN show the permeability k is less than 3×10^{-10} cm/s for all solutions tested. In contrast, the k of specimens prepared with natural sodium bentonite was more than 4 orders of magnitude higher (> 2×10^{-5} m/s) when permeated with 50 and 500 mM $CaCl_2$. The hydraulic conductivities of GCLs from Na-bentonite or BPN are compared in Fig. 2.13.

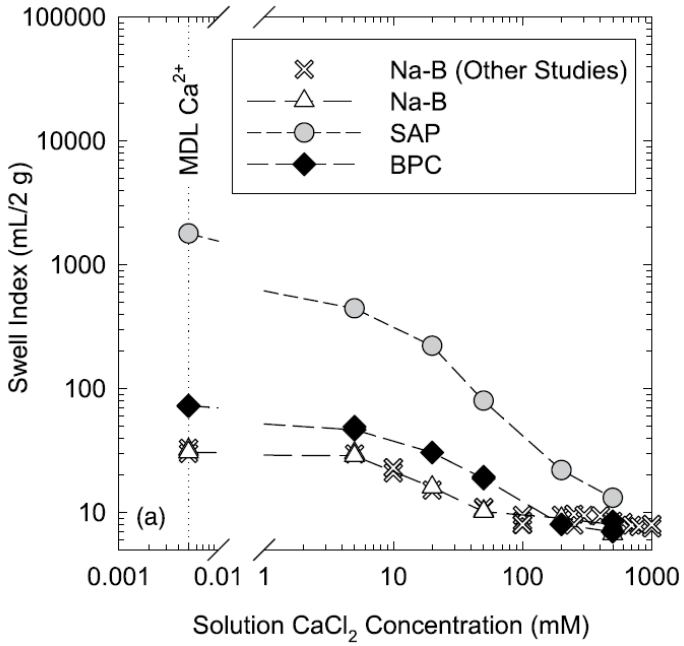

Fig. 2.12 Swelling index versus solution $CaCl_2$ concentration (after Scalia et al., 2014)

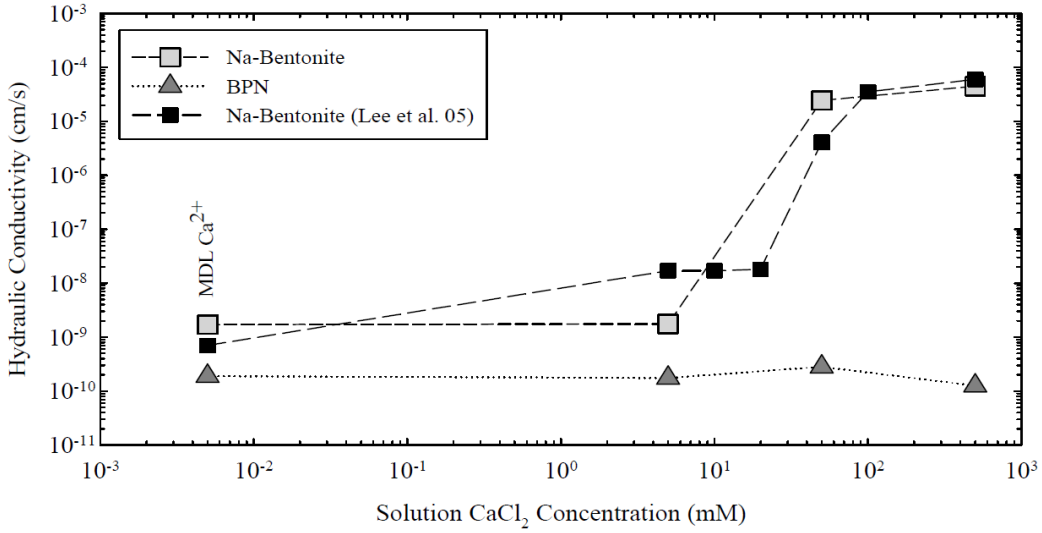

Fig. 2.13 Permeability of Na-bentonite, BPN, and Na-bentonite GCLs tested by Lee et al. 2005 (after Scalia et al. 2011)

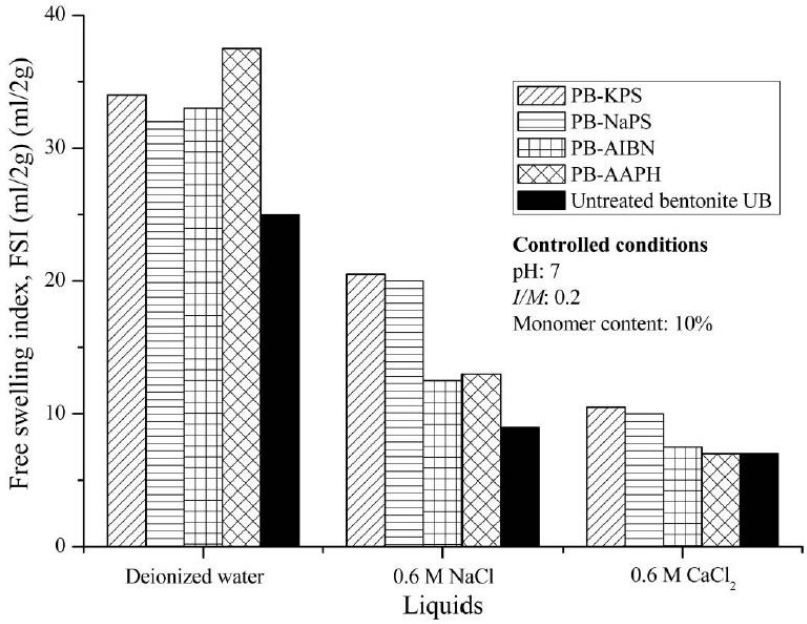

Fig. 2.14 Effect of liquids on FSI with various initiators (after Prongmanee et al. 2018)

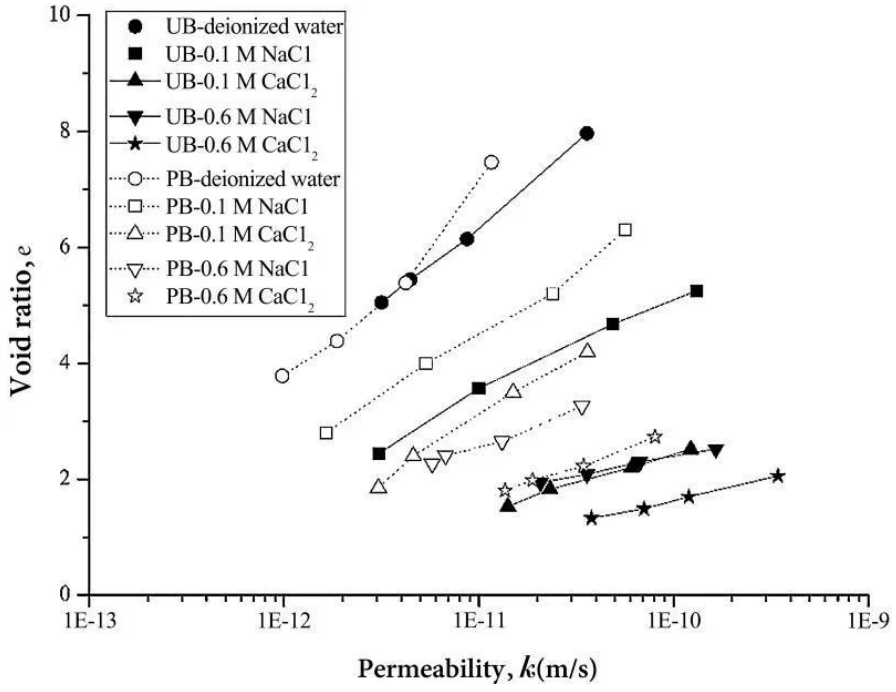

Fig. 2.15 The relationship between the void ratio and permeability (after Chai and Prongmanee 2020)

Prongmanee et al. (2018) and chai and Prongmanee. (2020) produced polymerized

bentonite (PB) (polymer content 10%), which is using the monomer acrylic acid to sodium bentonite ratio of 0.1. The results of FSI demonstrated that PBs producing with various initiators have larger value of FSI than that of UB in aggressive cation solutions as shown in Fig. 2.14. The values of *k* of the PBs were lower compared with that of the corresponding sodium bentonite in various cation solutions as shown in Fig. 2.15.

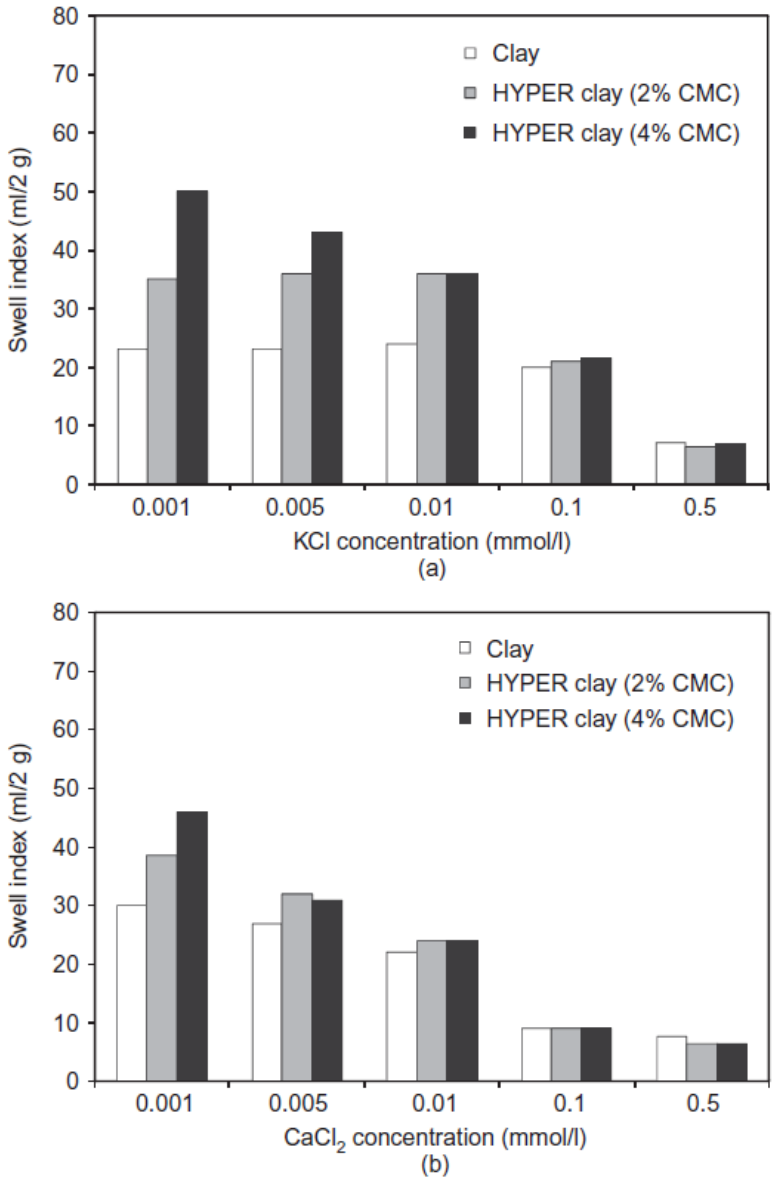

Fig. 2.16 The addition of CMC to the clay improved its swelling ability in: (a) KCl solutions and (b) $CaCl_2$ solutions (after Di Emidio et al. 2015)

Di Edimio et al. (2015) mixed a sodium bentonite and an anionic sodium

carboxymethyl cellulose (CMC) with commercial name as HYPER clay. They investigated both swelling and permeability (*k*). The test results show that the HYPER clay had higher swelling capacity (Fig. 2.16) and a lower permeability (Figs. 2.17 (a) and (b)) compared with that of the untreated bentonite.

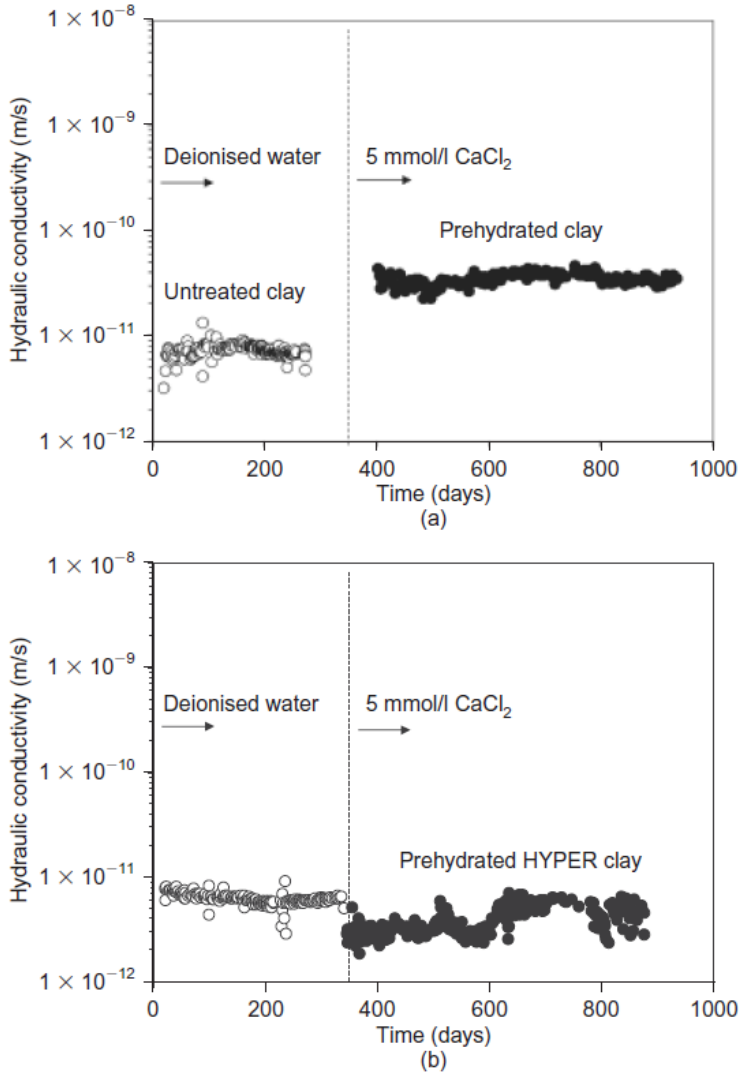

Fig. 2.17 Permeability to 5 m mol/l $CaCl_2$ solution of: (a) untreated clay and (b) the HYPER clay after prehydration with water (after Di Emidio et al. 2015)

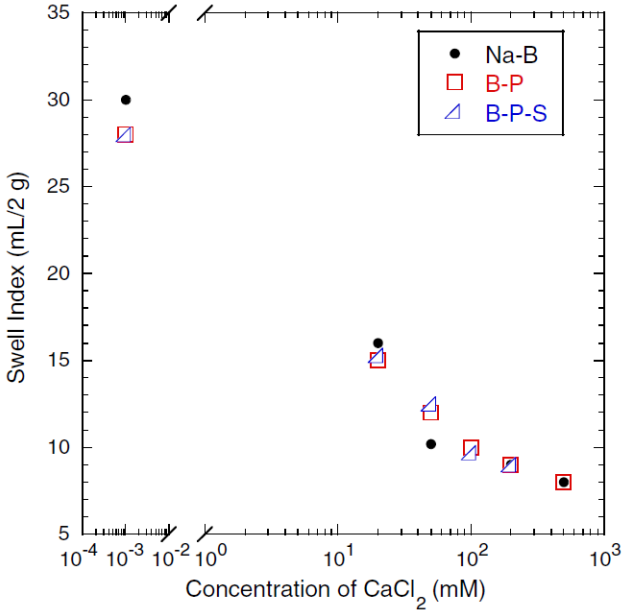

Fig. 2.18 Swell index for BP and NaB in DI water and $CaCl_2$ solutions with concentrations ranging from 5 to 500 mM. DI water shown at 0.001 mM (after Tian et al. 2019)

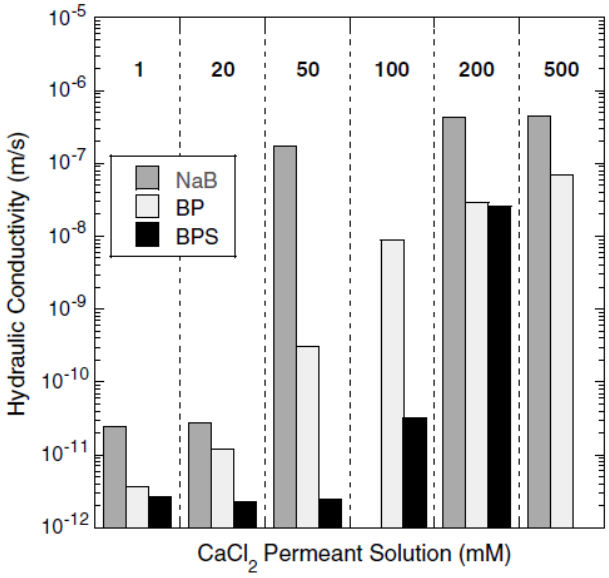

Fig. 2.19 Permeability of BP and BPS GCLs to DI water and $CaCl_2$ solutions (after Tian et al. 2019)

Tian et al. 2019 used two commercially available GCLs containing the same dry-blended bentonite-polymer mixture including 5.1% polymer content: a bentonite polymer GCL (BP GCL) and bentonite-polymer GCL with silt film (BPS GCL). The FSI results was reported that the swell index for the BPCs and the conventional NaB decreases with increasing $CaCl_2$ concentration as shown in Fig. 2.18. The BP and BPS GCLs are approximately one to four orders of magnitude less permeable than the NaB GCL over the entire range of $CaCl_2$ solutions as shown in Fig. 2.19.

Chen et al. (2019) used commercial GCL that contained a mixture of proprietary polymer blended with granular sodium bentonite (NaB), and the other GCL used was created using a slurry polymerization process prepared with NaB and 12.7% polymer (iBPC) as described in Scalia et al. (2014). The polymer composites have lower permeability in coal combustion product (CCP) leachates than that of the untreated bentonite as shown in Fig. 2.20. Others are bentonite-polymer composite GCLs with numerical suffix equal to polymer loading in percentage by dry mass. Enclosed zone

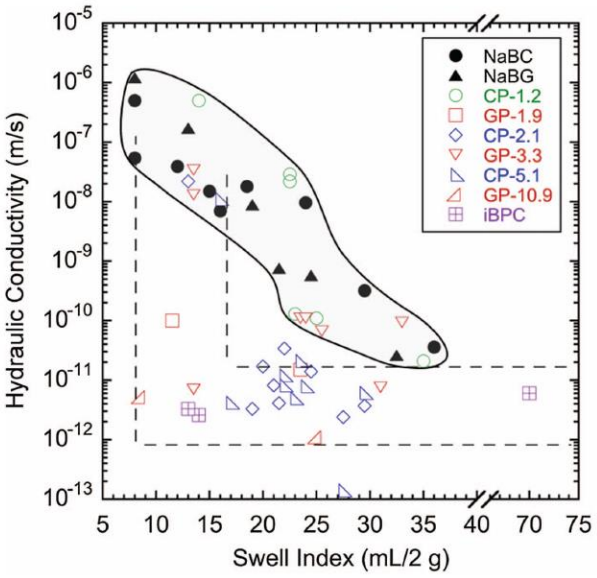

Fig. 2.20 (Color) Permeability versus swell index for different CCP leachates and GCLs. Solid symbols are conventional GCLs with Na bentonite (data from Chen et al. 2018) (after Chen et al. 2019)

covers conventional NaB GCLs and BPC GCLs with low polymer loading (<1.9%). In terms of lower permeability, they reported that relatively immobile water molecules bound to the polymer in the hydrogel and to the bentonite surface via osmotic swelling likely contributed to small and tortuous pore spaces for flow.

2.5 Self-healing performances of the GCL with UB and PB

In the field, it is difficult to avoid the damage such as punctures and/or tears of GCLs (Sari and Chai 2013; Sawada et al. 2019). Fig. 2.21 is a photograph showing the self-healed result of a GCL pierced by a bolt (Koerner 1990). Mazzieri and Pasqualini (1997) reported that puncturing by plant roots might induce negative impact on the permeability (k) of adhesive bonded GCLs (Fig. 2.22). Rowe et al. (2017) reported roots that had penetrated through the cover geotextile and bentonite then run along the lower bentonite carrier geotextile interface (desiccation is due to oven drying) as shown in Fig. 2.23. Additionally, after installation and before waste coverage, due to day-night temperature variations, water vapor-drop cycles are generated on the GCL, which can cause down-slope erosion of the bentonite resulting in areas without bentonite as shown in Fig. 2.24.

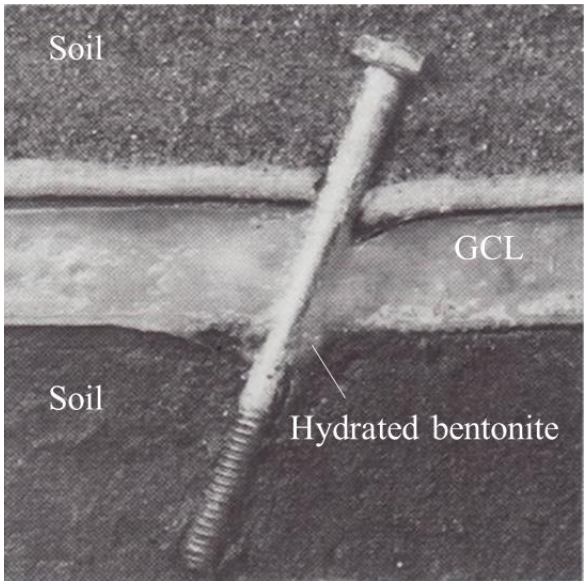

Fig. 2.21 Self-healing of GCL pierced by a bolt (modified from Koerner, 1990)

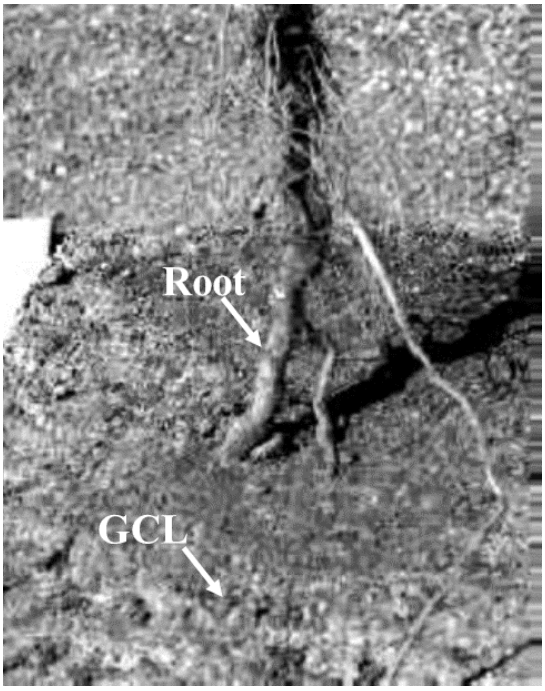

Fig. 2.22 GCL damaged caused by roots (after Mazzieri and Pasqualini, 1997)

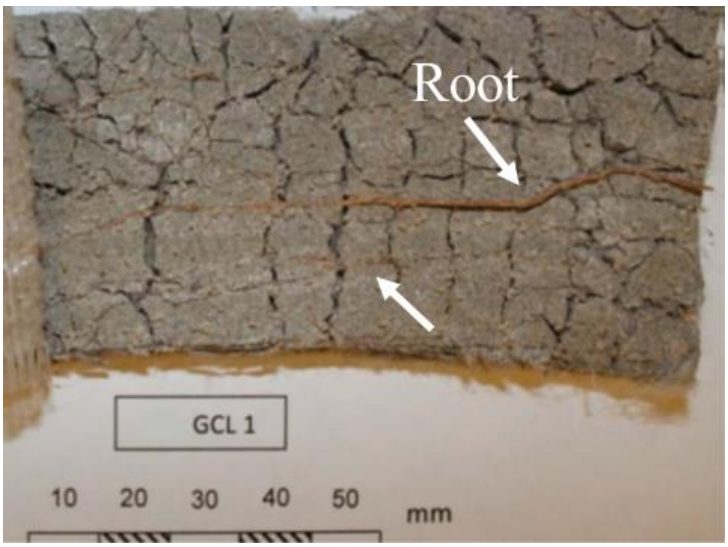

Fig. 2.23 Roots running in the GCL (after from Rowe et al., 2017)

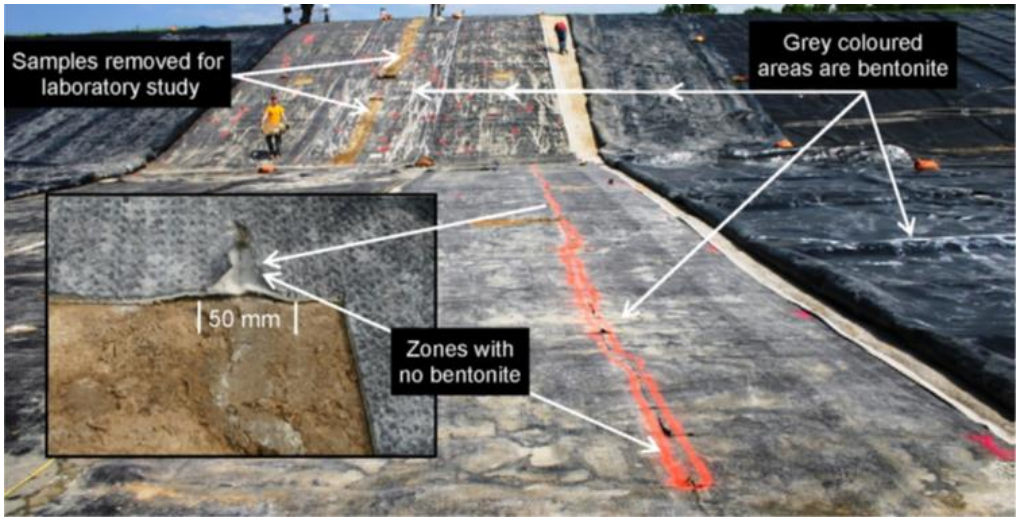

Fig. 2.24 Down slope erosion of GCL (from Rowe et al. 2016a)

Due to the expansion of hydrated bentonite, part of or the entire damage hole can be healed, and this mechanism is called the "self-healing capacity" (Babu et al. 2001; Chai et al. 2016; Chai and Prongmanee 2020).

Sari and Chai (2013) examined self-healing of holes ranging from 5 to 50 mm diameter (in a 150 mm-diameter specimen) hydrated with tap water, a 10 g/L NaCl solution, and a 100 ml/L ethanol/water solution under a range of overburden stress up to 200 kPa. GCLs with holes ≤ 30 mm-diameter self-healed when hydrated with tap water or the ethanol-tap water solution, but not the 10 g/L NaCl.

Chai et al. (2016) investigated the self-healing ratio (healed area/total area of a hole) of GCLs with a fully penetrating hole by laboratory leakage rate test and an explicit empirical equation was proposed for predicting the self-healing ratio, which uses basic physical properties of a GCL, the liquid limit and swelling index of the bentonite in the GCL with the corresponding liquid. Generally, a good agreement was found between the laboratory measured self-healing ratio and the predicated using this empirical method.

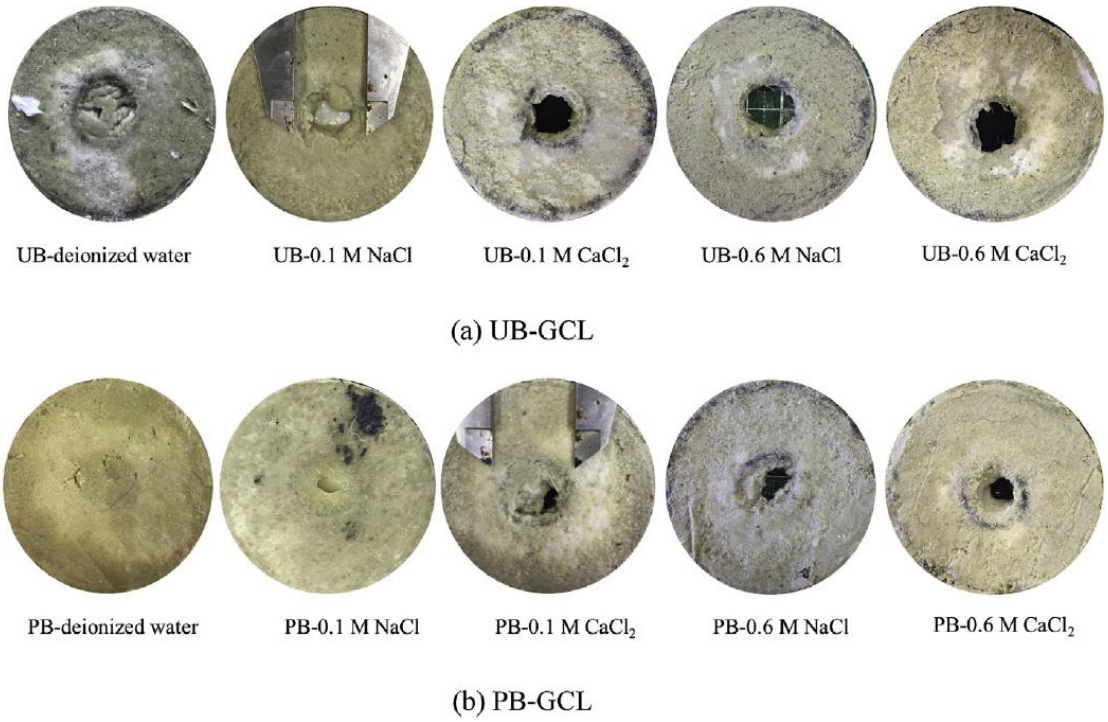

Fig. 2.25 The healing samples of GCL after the leakage rate test for UB and PB (specimen diameter: 60 mm, damage hole diameter: 20 mm) (after Chai and Prongmanee 2020)

However, the amount of bentonite expansion can be significantly reduced with an increase in the cation concentration in the liquid (Rowe et al. 2019; Sari and Chai 2013), Chai and Prongmanee (2020) reported that the self-healing capacity of a GCL using the PB were investigated in five differenet test liquids included of deizonized water, NaCl solutions (0.1 M and 0.6 M) and $CaCl_2$ solutions (0.1 M and 0.6 M). As shown in Fig. 2.25, with deionized water and a damage hole of 20-mm-diameter, the damage hole was fully self-healed for both the UB-GCL and PB-GCL specimens. However, with increasing cation concentrations and valence of the cations in the liquids, the self-healing capacity of both the UB-GCL and PB-GCL specimens decreased. While the PB-GCL specimen had a higher self-healing capacity compared with that of the UB-GCL

specimen for all the cationic solutions used.

2.6 Summary

As shown above, polymerized bentonites (PB) and bentonite blended with dry polymer have been used in barrier applications to improve their chemical resistance to aggressive permeants. In particular, the treated bentonite with anionic polymers showed higher swelling capacity and lower permeability compared to untreated bentonite (UB). In cation solutions, PBs have higher values of FSI than those of UBs, however, In 0.6 M NaCl solution, FSI of PB is still do not meet the requirement for use as the core material of GCLs (Prongmanee et al. 2018), i.e., the free swelling index (FSI) is less than 24 mL/2g (Guyonnet et al. 2009, GI, 2016). GCLs with PB had higher self-healing capacity than that using natural bentonite.

In summary, there are two main issues need to be investigated, i.e. (1) develop a novel PB of higher swelling capacity in aggressive cation solution and simplify the process of polymerization for large-scale producing; (2) the self-healing capacity of the novel PB in aggressive cation solution (e.g., 0.6 M NaCl).

CHAPTER THREE
The NOVEL POLYMERIZED BENTONITES (PBs)

3.1 Introduction

One of the techniques used to increase the swelling capacity of bentonite is polymerization of bentonite (Bohnhoff and Shackelford 2013; De Camillis et al. 2016; Chen et al. 2019; Christian et al. 2020; Di Emidio et al. 2015; Nie et al. 2020; Nie and Chai 2021; Ozhan 2018; Prongmanee et al. 2018; Scalia et al. 2011; Tian et al. 2019). They have been verified that PBs can maintain low permeability and high swelling capacity in solutions of cations (Chen et al. 2019; Christian et al. 2020; Tian et al. 2019; Ozhan 2018; Prongmanee *et al*. 2018).

Generally, there are two methods for preparing polymer bentonite composites. One involves mixing granular sodium bentonite and the particles of premade polymer (Di Emidio *et al*. 2015; Tian *et al*. 2019; Christian *et al*. 2020), and the other is to mix the monomer with bentonite first, and then polymerize it (Scalia *et al*. 2014; Prongmanee *et al*. 2018; Nie *et al*. 2020). Although the latter method is slightly complicated, it can produce more uniform polymerized bentonite (PB) (Gao and Heimann. 1993). The traditional free radical polymerization method involves several steps, i.e. mixing monomer and initiator with bentonite; removing oxygen using nitrogen gas; polymerization; washing the product to remove impure materials; and drying and crushing it into powder (Ahmed 2015; Prongmanee et al. 2018). It is desirable to simplify it without loose the quality of the products.

For higher concentrations of cation solutions, such as 0.6 M NaCl solutions (as found in seawater), there are literature reports that 10% polymer PBs still do not meet the requirement for use as the core material of GCLs to be used in such an environment (Prongmanee et al. 2018), i.e., the free swelling index (FSI) is less than 24 mL/2g

(Guyonnet *et al.*, 2009; GI 2016).

This chapter presents the method for producing novel polymerized bentonites (PBs) that, will have a free swelling index (FSI) value more than 24 mL/2g when immersed in aggressive cation solutions (such as sea water). The method and the conditions adopted for the polymerization are described first. Then the microstructure analysis of the various PBs, based on X-ray diffraction (XRD), Scanning electron microscopy (SEM) were reported.

3.2 Materials and polymerization method

3.2.1 Materials

(1) Bentonite

Natural sodium bentonite (UB) from Wyoming (USA) was used. Chemical properties of the bentonite are listed in Table 3.1. The pH value was measured with a solid/liquid ratio of 1/10. The value of cation exchange capacity (CEC) was measured using the semi-micro Schollenberger method and was 77 meq/100g. The bentonite mainly consisted of dioctahedral smectite and its content accounted for approximately 85% of the total weight (Chai and Shen 2018).

To remove the impurities from the bentonite, the natural bentonite was stirred uniformly in deionized water with a solid/liquid ratio of 1/25 for more than 30 minutes, and then the mixture was left for 48 hours to allow impurities to precipitate. After that, the upper slurry without impure material was poured out of the container, and the impure material was left at the bottom. The upper slurry of bentonite was oven dried at 105°C and then crushed and sieved using sieve No. 200 (smaller than 0.075 mm) (UB). The CEC of pure UB was 92 meq/100g.

(2) Chemicals

The chemicals used were liquid acrylic acid ($C_3H_4O_2$, 98% purity), acrylamide

(C_3H_5NO, 99% purity), potassium persulfate ($K_2S_2O_8$, 95% purity), sodium hydroxide (NaOH, 97% purity), sodium chloride (NaCl, 99.5% purity), and calcium chloride ($CaCl_2$, 95% purity). Acrylamide is a harmful chemical, while polyacrylamide is safe. Therefore, it should be careful when handling acrylamide, and full polymerization should be ensured (Gao and Heimann. 1993).

Table 3.1 Chemical properties of the sodium bentonite

Property	Unit	Value
Chemical composition		
SiO_2	%	73.8
Al_2O_3	%	13.8
Fe_2O_3	%	4.3
MgO	%	1.6
CaO	%	1.5
Na_2O	%	1.7
K_2O	%	0.5
LOI	%	1.6
Total		98.8
Cation exchange capacity, *CEC*	meq/100g	77.0
pH (ASTM 4972)	-	9.3

Table 3.2 Properties of the deionized water and cationic liquids

Liquids	Concentration		pH	*EC*
	(mol)	(mg/L)		(mS/cm)
Deionized water	0	0	6.33	0.002
0.6 M NaCl	0.60	35.06	5.88	34.91
0.03 M $CaCl_2$	0.03	3.33	5.61	5.65
0.06 M $CaCl_2$	0.06	6.66	5.41	11.06

The solutions tested were deionized water (DI-W), the cation solutions with 0.6 M NaCl, and 0.03-0.06 M $CaCl_2$. The 0.6 M NaCl solution simulates the conditions of seawater and the aggressive cation solution. These $CaCl_2$ solutions were chosen to

evaluate the performance of the PB against di-valence cation solutions. Table 3.2 reports the results of concentration, pH and electro-conductivity (EC) of the liquids tested.

（3）Structure of monomer and polymer

The molecule structure of monomers acrylic acid and acrylamide were shown in Fig. 3.1 (a) and (b), respectively. Sodium acrylamide was produced by neutralization with sodium hydroxide (NaOH) solution and the molecule structure was shown in Fig. 3.1 (c) (Barvenik 1994).

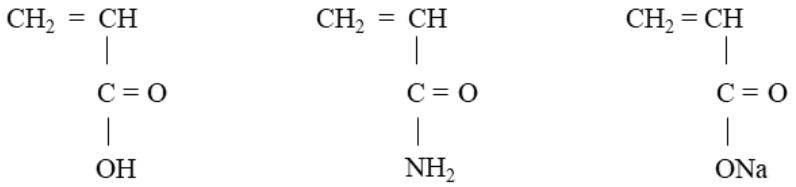

(a) (b) (c)

Fig. 3.1 Molecule structure of monomers (a) acrylic acid; (b) acrylamide; (c) sodium acrylate.

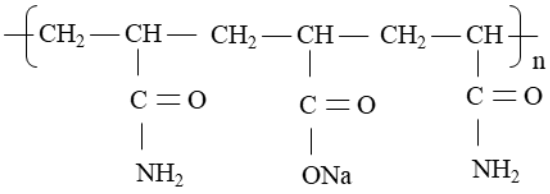

(a) Anionic polyacrylamide

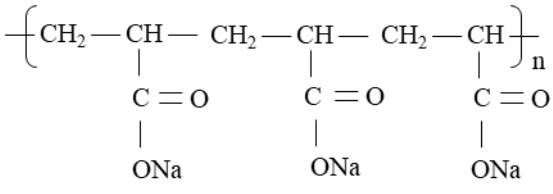

(b) Anionic sodium polyacrylate

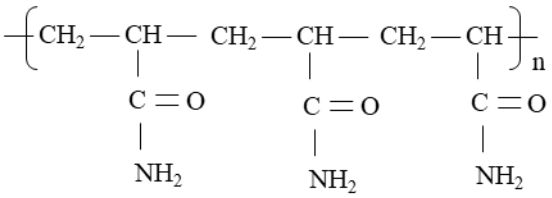

(c) Nonionic polyacrylamide

Fig. 3.2 Molecule structure of polymers (a) anionic polyacrylamide; (b) sodium polyacrylate; (c) nonionic polyacrylamide

Three molecule structures of polymers were shown in Fig. 3.2. The anionic acrylamide was obtained by copolymerization with due monomer acrylic acid and acrylamide (Barvenik 1994) as shown in Fig. 3.2 (a) . The anionic sodium polyacrylate was produced by polymerization with sodium acrylate (Barvenik 1994) (Fig. 3.2 (b)), and the nonionic polyacrylamide was produced by polymerization with acrylamide (Fig. 3.2 (c)).

3.2.2 Polymerization method

Acrylic acid (M_1) and acrylamide (M_2) as monomers, potassium persulfate as initiator (I), and deionized water as solvent were used in the polymerization process. Firstly, a monomer to bentonite (($M_1 + M_2$)/UB) ratio of 0.1 was fixed, and then M_1 / M_2 ratios ranging from 0.2 ~ 2, I/($M_1 + M_2$) ratios ranging from 0.1% ~ 10%, and pH ranging from 4 ~ 10 were used. The procedures for polymerization were as follows:

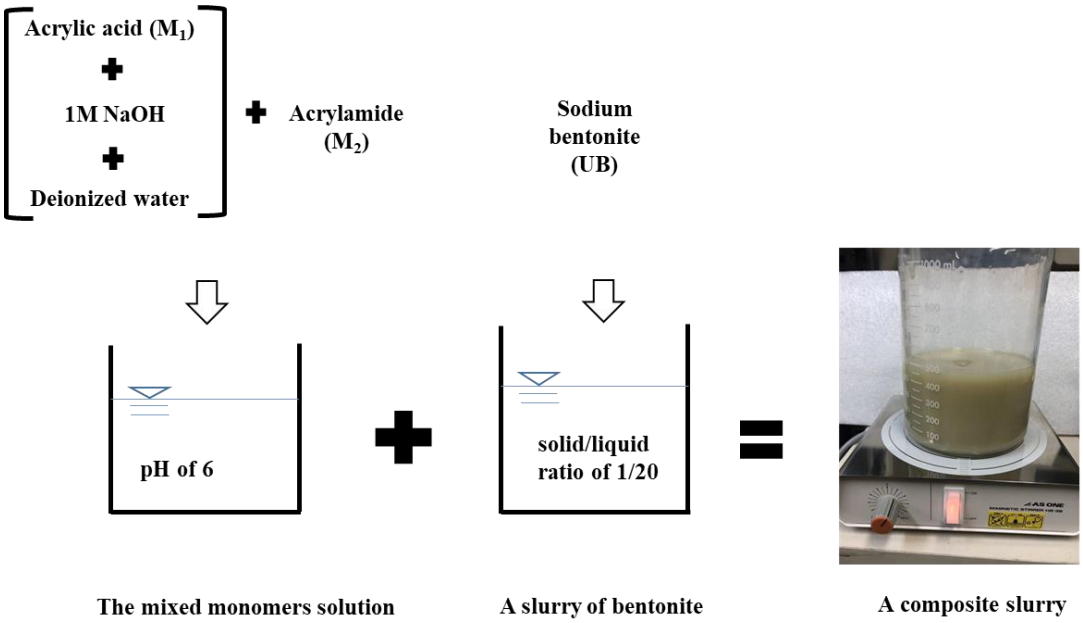

Fig. 3.3 Prepared composite slurry by mixture monomer and bentonite

(1) The sodium bentonite slurry was prepared by weighing. Mixing 20 g dried UB

into 400 ml deionized water at a ratio of 1/20 and stirring for 1 hour and allowing it to stand for more than 12 hours to form a homogeneous sodium bentonite slurry as shown in Fig. 3.3.

(2) Then, for $(M_1 + M_2)/UB = 0.1$, and M_1/M_2 ratio of 0.2 ~ 2, the amount of acrylic acid (M_1) was calculated to be 0.333 g and 1.335 g. A predetermined amount of M_1 was dissolved into 60 ml of deionized water, which was neutralized with 1 M NaOH solution to achieve the desired pH value. Then, the amount of M_2 with the desired ratio of M_1/M_2 (varied from 0.2 to 2) was added to the neutralized solution and stirred evenly for 1 minute to form a mixed monomer solution as shown in Fig. 3.3.

Fig. 3.4 The process of producing PB

(3) Prepare composite slurry. The mixed monomer solution was added into the bentonite slurry and stirred for 20 minutes to form a homogeneous slurry. Then, potassium persulfate with the desired ratio $I/(M_1+M_2)$ was dissolved in 40 ml deionized water, which was added to the mixture slurry and stirred for 10 minutes to form a composite slurry as shown in Fig. 3.3.

(4) Polymerization. The composite slurry was placed under vacuum in an airtight container using 100 kPa vacuum pressure for 2 hours to remove O_2 (Fig. 3.4(a)). After that, the whole composite slurry was put into an aluminum container (Fig. 3.4(b)), and polymerized in an oven at 100°C. Then kept it in the oven and dried for up to 24 hours (Fig. 3.4(c)). Finally, PB was crashed and sieved using 0.075 mm sieve and oven dried at 100°C before use (Fig. 3.4 (e) and (f)).

When use one monomer (either M_1 or M_2) to produce the PB, only the method for step No. (2) is different. The monomer M_1 is acid and need to adjust the pH of 6, whereas the monomer M_2 is neutral and not need to adjust the pH.

3.3 Conditions adopted for polymerization using two monomers

3.3.1 Test conditions and used liquid

The polymerization method used was free radical polymerization. The pH value, the ratio of acrylic acid to acrylamide (M_1/M_2), and the amount of initiator ($I/(M_1+M_2)$) used during the polymerization process were determined using FSI values of the product PBs with 10% polymer ($((M_1 + M_2)/UB) = 0.1$) in 0.6 M NaCl solution. FSI tests were performed following ASTM procedure D5890 (ASTM2006). 2 g dried PB was slowly and evenly dropped into the desired solution of 100 ml at a rate of 0.1 g per 10 min. The final volume of the swelled sample was measured after 24 h. Each case was repeated three times to check the repeatability of the tests, and the adopted values of FSI are mean

values.

3.3.2 Effect of ratio of acrylic acid to acrylamide

With $(M_1+M_2)/UB = 0.1$, $I/(M_1+M_2) = 0.5\%$, and pH = 6, the results of FSI for PBs with different M_1/M_2 ratios are plotted in Fig. 3.5. The M_1/M_2 ratio of 0.5 resulted in the highest FSI. Therefore, $M_1/M_2 = 0.5$ was adopted.

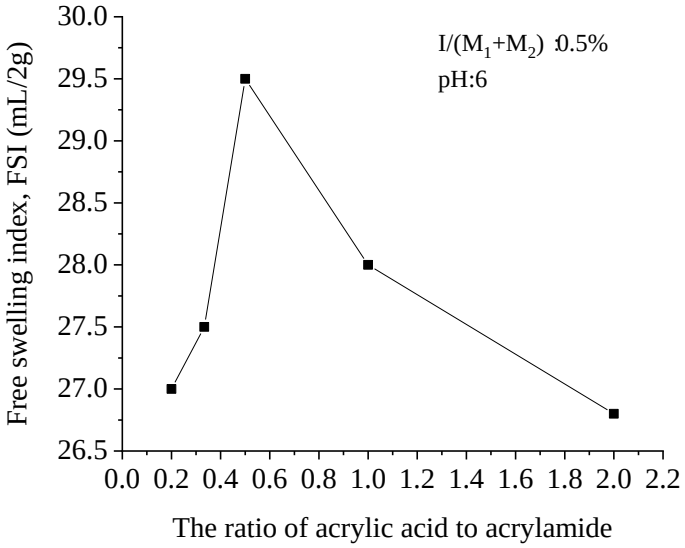

Fig. 3.5 Effect of M_1/M_2 ratio on FSI value of PB

3.3.3 Effect of amount of initiator

With $(M_1+M_2)/UB = 0.1$, $M_1/M_2 = 0.5$, and pH = 6, the FSI values of PBs with different amounts of initiator were determined and are shown in Fig. 3.6. The ratios $I/(M_1+M_2)$ tested ranged from 0.1% to 10%. When the ratio $I/(M_1+M_2)$ was within the range 0.5% to 2%, the variation in the FSI was very small, and we chose 0.5%.

3.3.4 Effect of pH values

Fig. 3.7 shows the FSI value of PB produced with various pH values for the monomer

mixture. When the pH was less than 6, the FSI value of PB increased with increasing pH. The FSI value was almost the same when the pH value was greater than 6. The pH value of 6 for the monomer mixture was used in this study.

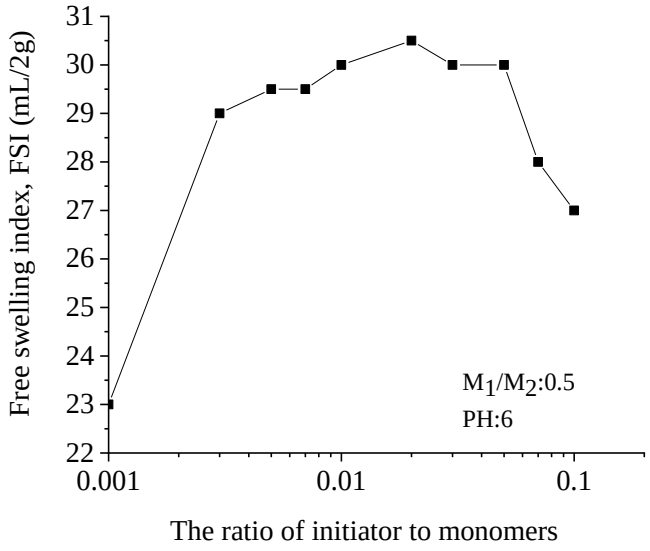

Fig. 3.6 Effect of I/ (M_1 + M_2) ratio on FSI value of PB

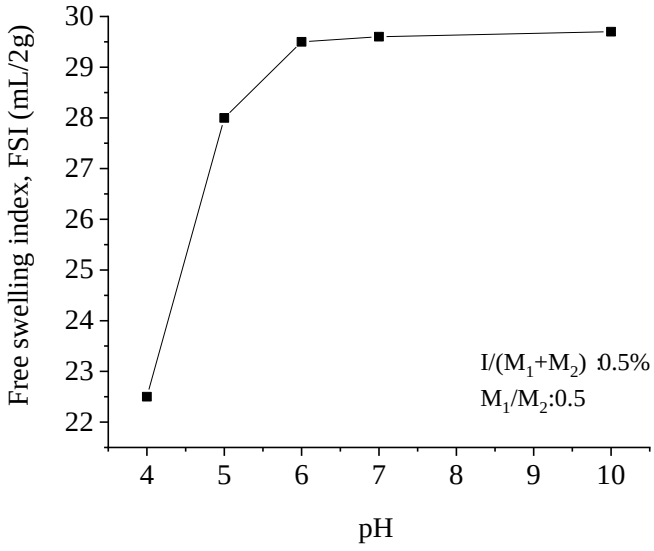

Fig. 3.7 Effect of pH on FSI value of PB

3.3.5 Summary of the conditions adopted

PBs were produced with monomer-to-bentonite ratios ((M_1+M_2)/UB) of 0.1. The conditions adopted for polymerization using two monomers were M_1/M_2 = 0.5, I/(M_1 +

M_2) = 0.5%, and pH = 6. Various PBs with different polymerization conditions were designated in Table 3.3. In the table, 0.2PB means polymer/bentonite ratio of 0.2 and using two monomers; 0.1PB-AA means polymer/bentonite ratio of 0.1 and using acrylic acid as monomer; and 0.1PB-AM means polymer/bentonite ratio of 0.1 and using acrylamide as monomer. The CEC of 0.1PB was 120 meq/100g, which was larger than that of UB. This show that the 0.1PB have higher cation exchange capacity than that of UB.

Table 3.3 Various PBs with different polymerization conditions

No.	Polymerization conditions	Initiator (I)	pH	Denoted name
1	$(M_1+M_2)/UB = 0.1$, $M_1/M_2 = 0.5$	0.5%	6	0.1PB
2	$(M_1+M_2)/UB = 0.2$, $M_1/M_2 = 0.5$	0.5%	6	0.2PB
3	$(M_1+M_2)/UB = 0.4$, $M_1/M_2 = 0.5$	0.5%	6	0.4PB
4	$M_1/UB = 0.1$	0.5%	6	0.1PB-AA
5	$M_1/UB = 0.4$	0.5%	6	0.4PB-AA
6	$M_2/UB = 0.1$	0.5%	-	0.1PB-AM
7	$M_2/UB = 0.4$	0.5%	-	0.4PB-AM

3.4 Microstructure analysis

3.4.1 X-ray diffraction (XRD) analysis

(1) Test methods

XRD studies were conducted using a SHIMADZU XRD -6000 diffractometer. Before the tests, the PBs or UB were heated for 4 hours in an oven at 105°C, and then the sample was put into a specimen container 20 mm in diameter and 1.25 mm in height at room temperature. The voltage and current of the X-ray tubes adopted were 40 kV and 30 mA, respectively. For nanocomposites, generally low angel XRD is used to

compare the positions of the diffraction peaks (Abhilash et al. 2016; Guyonnet et al. 2005). The scanned range was from 2.5° to 15° and a scanning rate of 0.02°/s was used in this study.

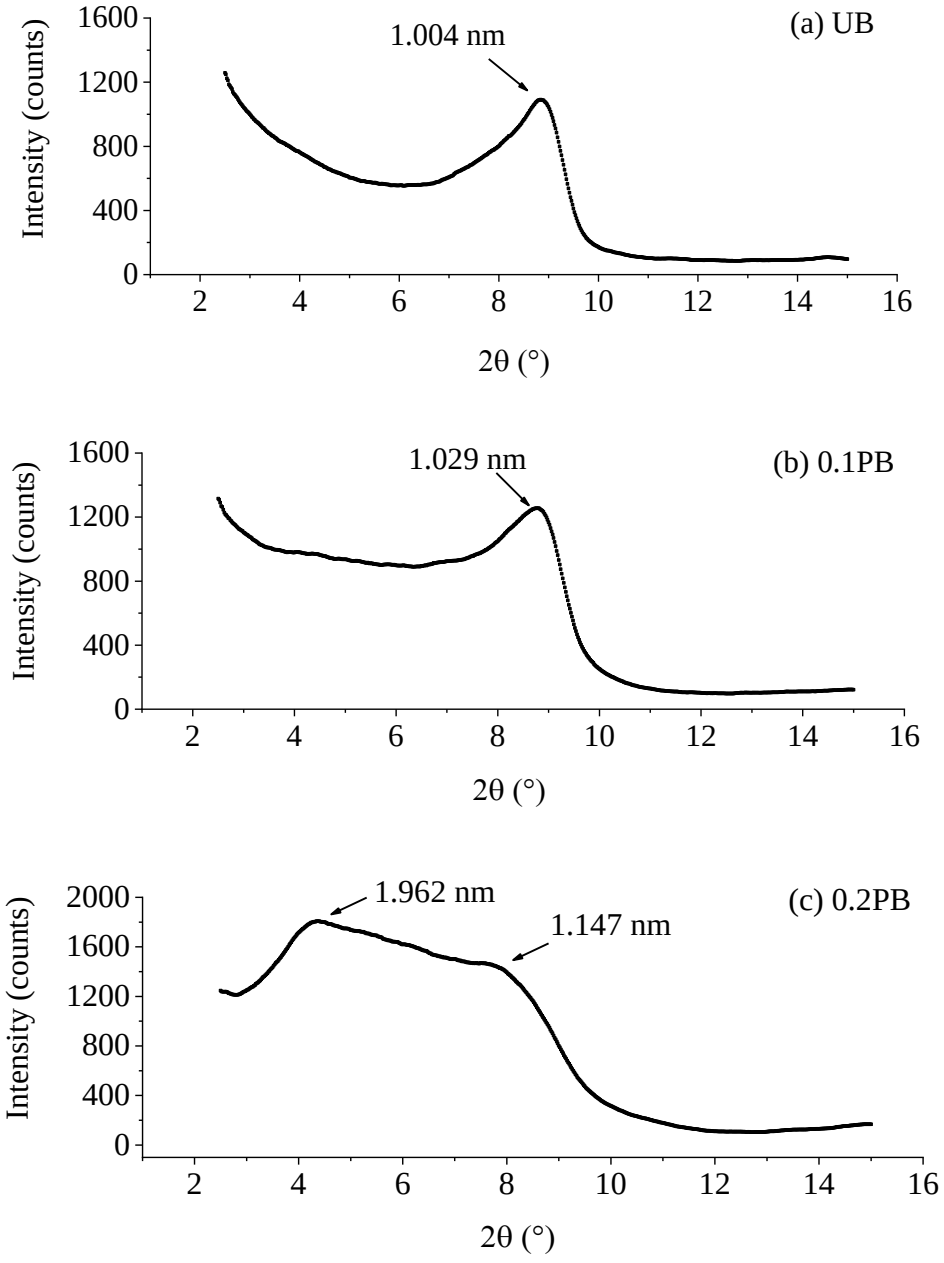

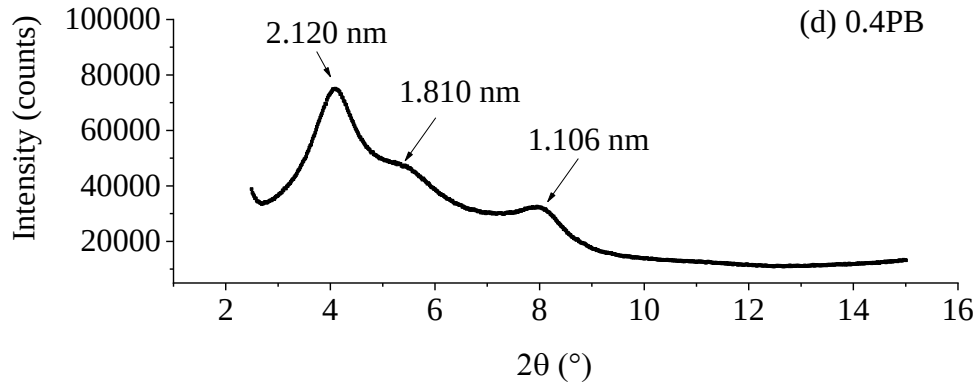

Fig. 3.8 X-ray diffraction (XRD) patterns of (a) UB, (b) 0.1PB, (c) 0.2PB, and (d) 0.4PB

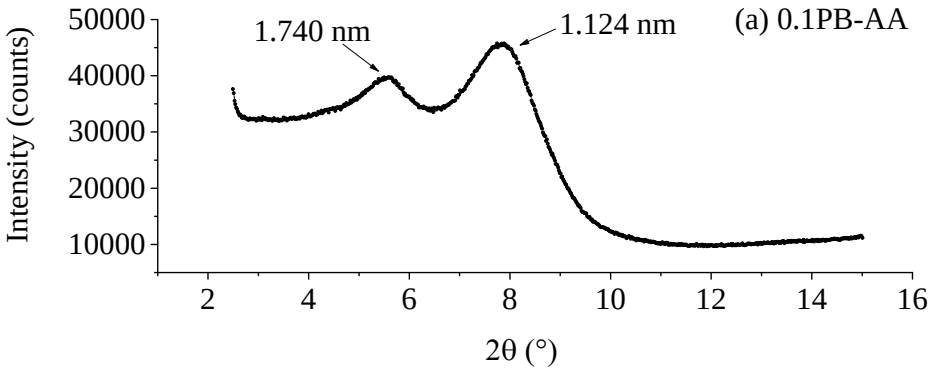

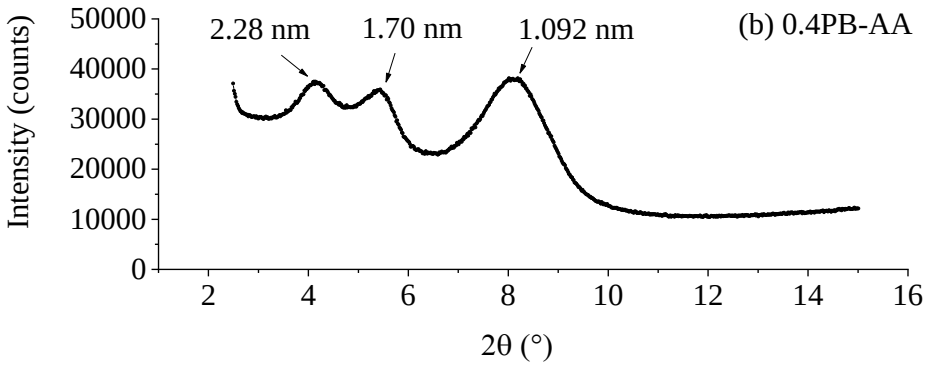

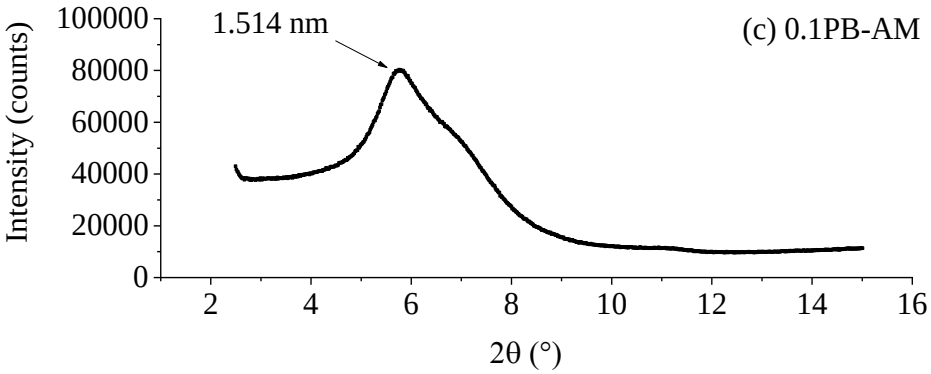

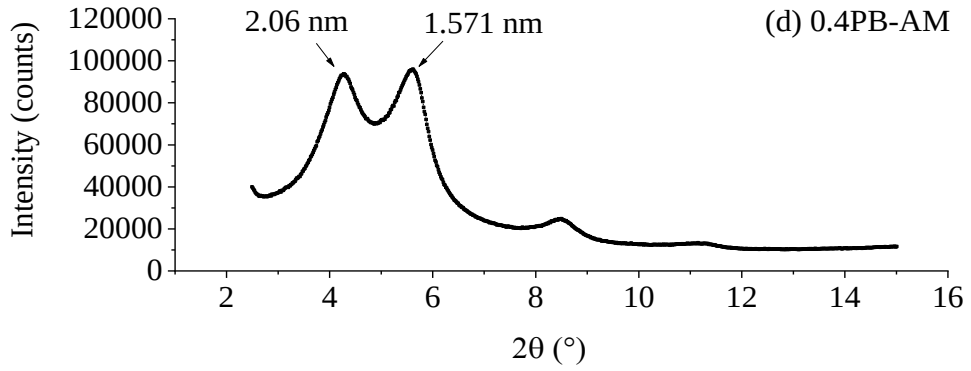

Fig. 3.9 X-ray diffraction (XRD) patterns of (a) 0.1PB-AA, (b) 0.4PB-AA, (c) 0.1PB-AM, and (d) 0.4PB-AM

(2) Results of UB and PBs

Fig. 3.8 shows the XRD results obtained for (a) UB, (b) 0.1PB, (c) 0.2PB, and (d) 0.4PB. The position of the diffraction peak of 0.1PB was almost the same as that of UB, and the interlayer basal spacings (d-spacing) for UB and 0.1PB were 1.004 nm and 1.029 nm, respectively, which indicates that the interlayer basal spacing of sodium bentonite was almost not modified by polymerization. As for the value of basal spacing of bentonite, Gao and Heimann (1993) reported values from 1.02 to 1.27 nm, which were comparable with the values we measured. However, the angle of the diffraction peak for 0.2PB and 0.4PB as shown in Fig. 3.8 (c) and (d) were smaller than that of UB, and the basal spacing of 0.2PB was 1.962 nm and 2.12 nm for 0.4PB. As shown in Fig. 3.8, for 0.1PB, the d-spacing of the bentonite particles was not changed (approximately equal to that of UB), and as shown in Fig. 2.5 it is postulated that the structure is of the phase-separated type and that the product is a microcomposite. For 0.2PB and 0.4PB, the d-spacing of the bentonite particles was increased, and it is postulated that the structure is intercalated and that the product is a nanocomposite.

Fig. 3.9 shows XRD patterns of (a) 0.1PB-AA, (b) 0.4PB-AA, (c) 0.1PB-AM, and (d) 0.4PB-AM. The position of the diffraction peak of the four types PBs were lower

than that of UB. These show that the interlayer d-spacings of four types PBs were larger than that of the UB and some polymers had been intercalated between bentonite particles. It is postulated that the structure of four types of PBs were nanocomposite. The patterns of 0.1PB-AA and 0.1PB-AM are different from that of 0.1PB, i.e. larger d-spacing. Although the exact reason is not clear yet, the samples tested may not absolutely uniform, and if we look at different place, we may get different result.

In addition, From Fig. 3.8 and Fig. 3.9 we know that the d-spacing of PBs increased with increasing polymer content (e.g., 0.4PB > 0.2PB > 0.1PB; 0.4PB-AA > 0.1PB-AA; 0.4PB-AM > 0.1PB-AM).

3.4.2 Scanning electron microscopy (SEM)

Due to the various monomers polymerized with bentonite have a different microstructure, which will be influenced the swelling capacity PBs. Seven types PBs (as shown in section 3.3 with Table 3.3) were analyzed using SEM.

(1) Test methods

Scaning Electron Microscopy (SEM) image was used to observe the morphology of the UB and the PB particles. The SEM used a JEOL JSM-7900F type of Japan and the voltage was 5 kV. The SEM specimens of UB was prepared by using the slurry of UB, which was oven dried to make block, and then swelled in DI-W for 48 hours as shown in Fig. 3.10 (a) and (b). The specimen of PBs were prepared by using a sheet of dry PBs as shown in Fig. 3.12, then, put into deionized water to swell for 48 hours.

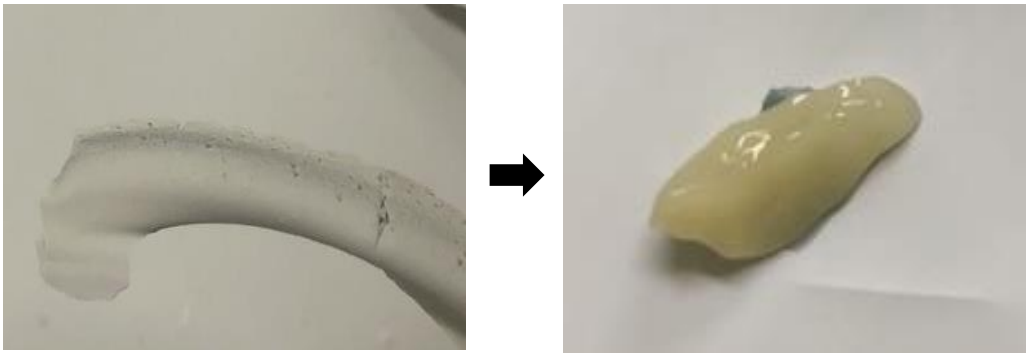

(a) Dry UB (b) Swelling imagine of UB

Fig. 3.10 The dried UB and swelled UB in DI-W

The swelled UB and PBs were frozen dried to make SEM specimens. The SEM specimens were frozen by immersing them in liquid nitrogen for 5 minutes and evacuated at a pressure of 0.5 Pa at - 49°C for 5 days before taking the SEM images. The SEM images all observed from the vertical planes perpendicular to surface of a sheet swelled specimen as shown in Fig. 3.11.

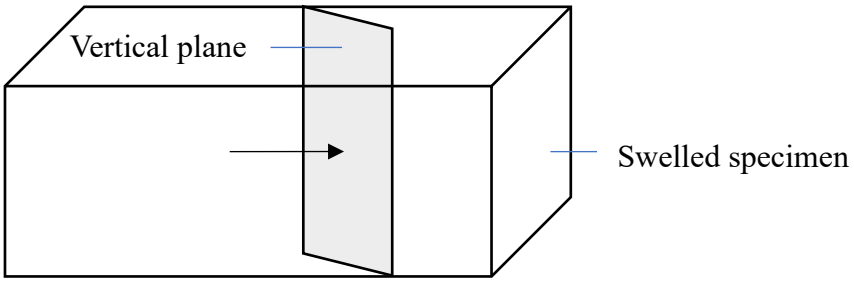

Fig. 3.11 Vertical plane of swelled specimen

Fig. 3.12 shows the various sheets of dry PBs. Under the monomer to bentonite ratio of 0.2 and 0.4, 0.2PB, 0.4PB and 0.4PB-AA were observed that they have a clearly transparency. This shows that using high polymer content can produce more uniform PB than using low polymer content. However, 0.4PB-AM have a little difference with 0.1PB-AM for transparency. Fig. 3.13 shows the imagines of various swelled PBs in DI-

W from a square dry PBs piece of 10 mm side. We find that the swelled PBs from Fig. 3.13 (a)-(d) which polymerized with two monomers (M_1 and M_2) or only one monomer (M_1) are like gel and transparency. The swelled PBs of Fig. 3.13 (e) and (f) which used M_2 are not transparency.

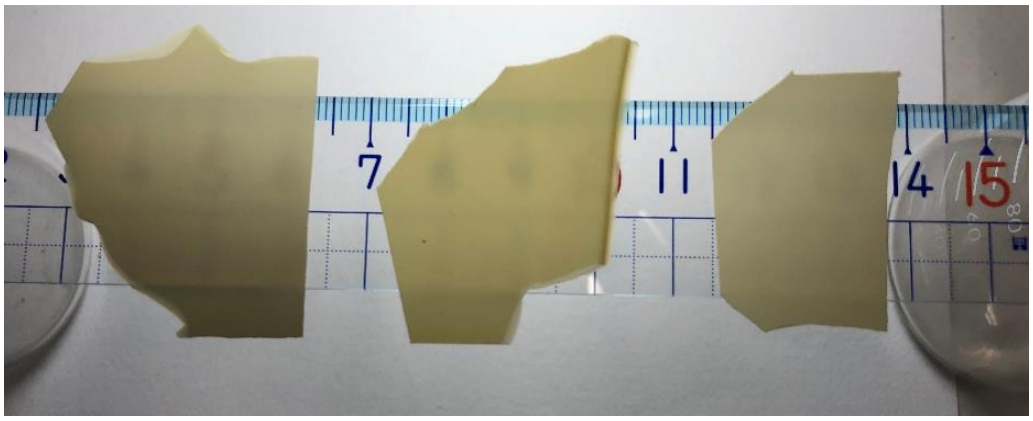

(a) 0.1PB; (b) 0.1PB-AA; (c) 0.1PB-AM

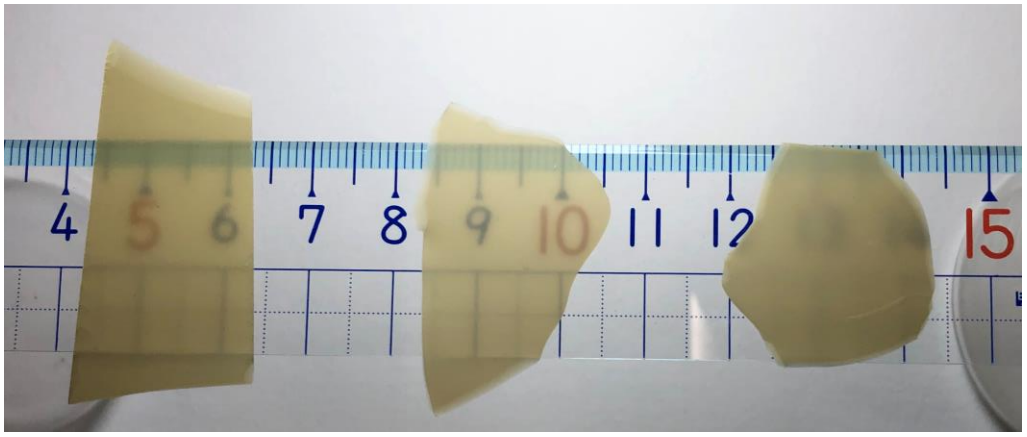

(d) 0.4PB; (e) 0.4PB-AA; (f) 0.4PB-AM

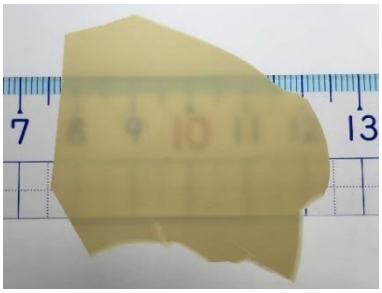

(g) 0.2PB

Fig. 3.12 Various drying PB

(a) 0.1PB

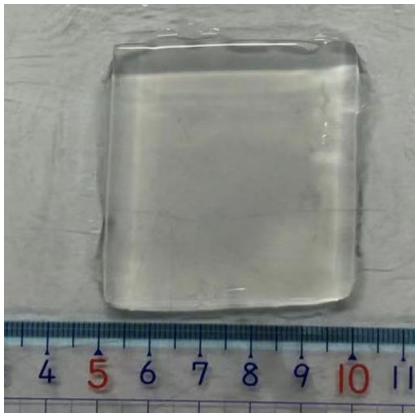

(b) 0.4PB

(c) 0.1PB-AA

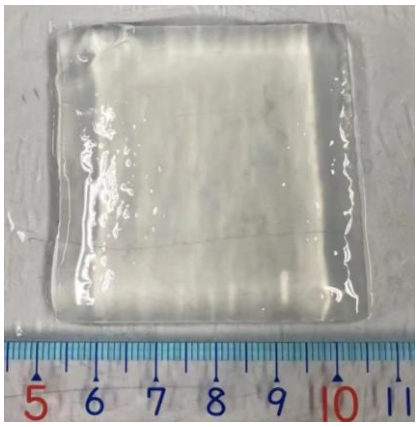

(d) 0.4PB-AA

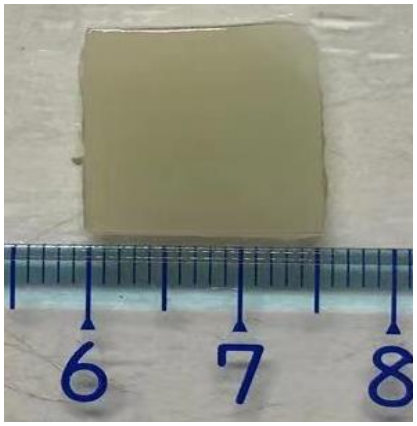

(e) 0.1PB-AM

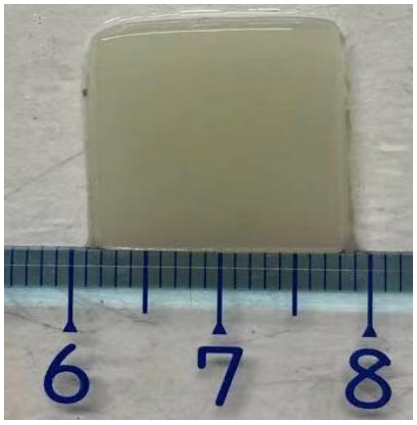

(f) 0.4PB-AM

Fig. 3.13 The imagines for after swelling of various PBs in DI-W.

(2) Results of UB and PBs

a) UB

Figs. 3.14 (a) and (b) present the SEM images with different size observed from UB. They were shown that the silicate layers of bentonite were interlaced with each other after swelling in deionized water.

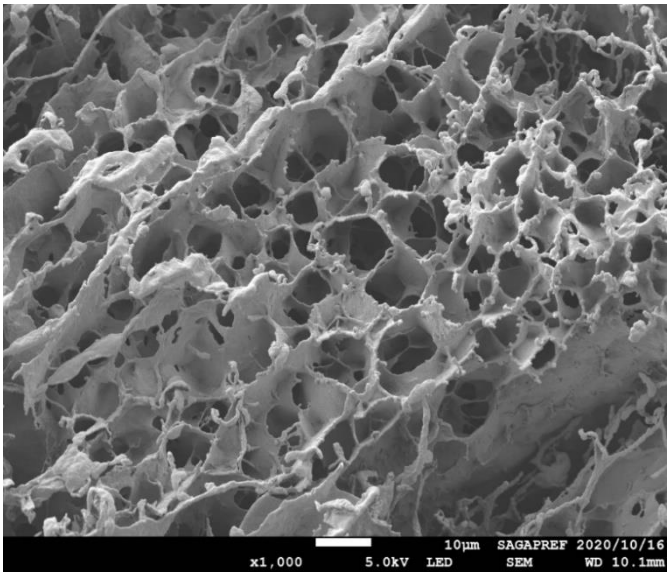

(a)

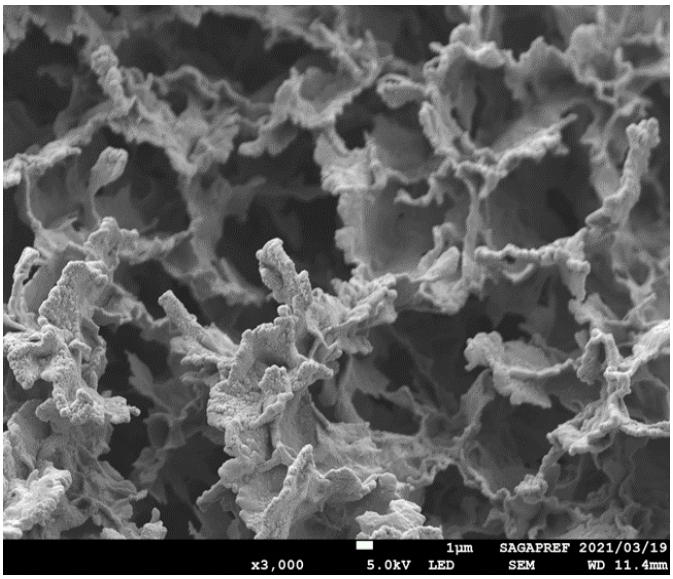

(b)

Fig. 3.14 SEM images of UB

b) 0.1PB and 0.1PB-AA

Fig. 3.15 shows that the sheet of dry 0.1 PB and 0.1PB-AA consists of two parts with different color. It is interpreted that the upper part is polymer and the lower part is bentonite.

Fig. 3.16 (a) and (b) show the SEM images of 0.1PB with upper part. It is clearly show that the amount of the polymer was interlaced with a little bentonite. Many polymer chains were observed in 0.1PB. Fig. 3.16 (c) and (d) show the SEM images of 0.1PB with lower part. A small number of polymer chains were observed between bentonite particles. Even these small amount polymer chains can improve swelling capacity of bentonite in cation solutions. The mechanism will describe in next section.

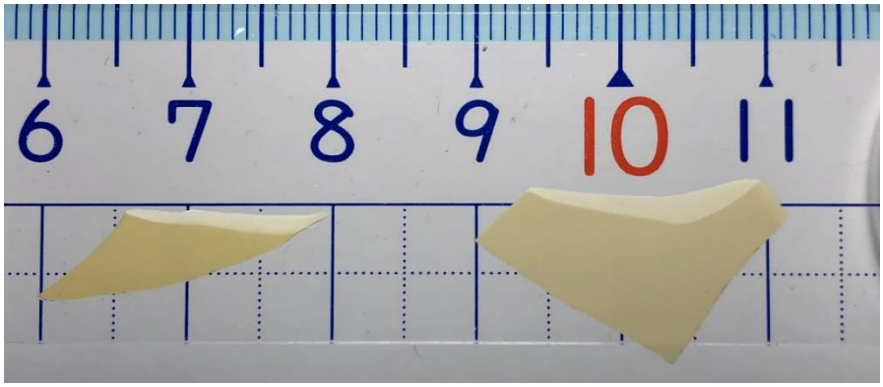

A sheet of 0.1PB-AA A sheet of 0.1PB

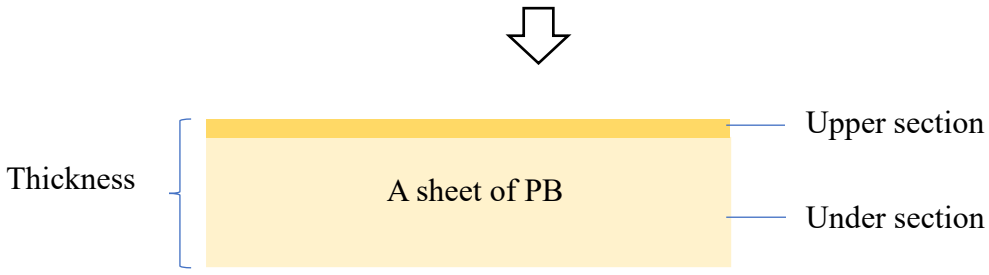

Fig. 3.15 Schematic diagram of a sheet of dry 0.1 PB and 0.1PB-AA

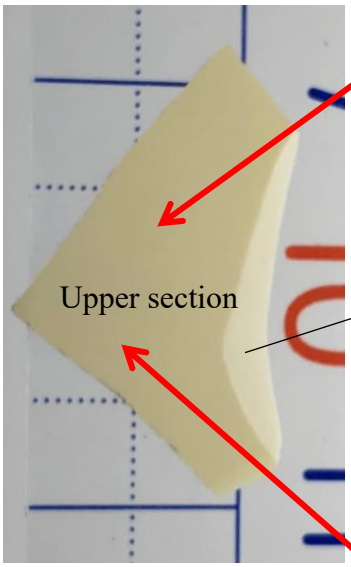
Upper section
Under section

0.1PB

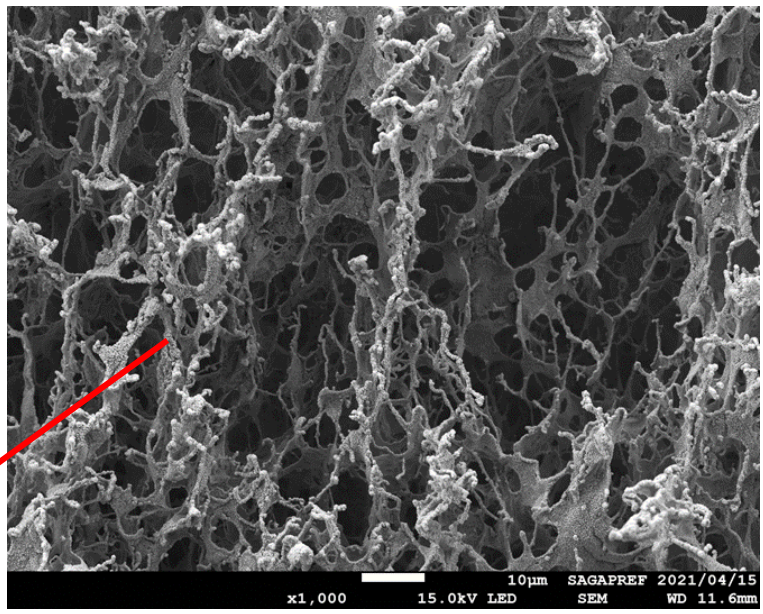
x1,000 15.0kV LED 10µm SAGAPREF 2021/04/15 SEM WD 11.6mm

(a)

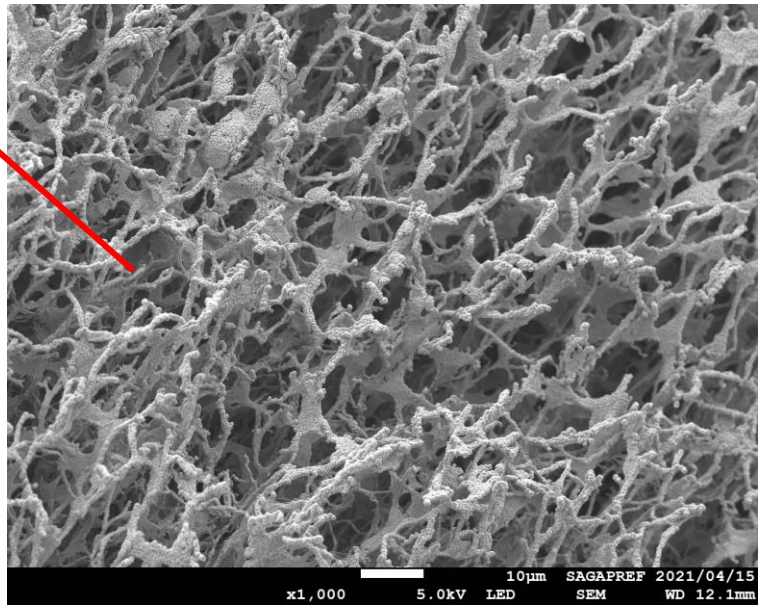
x1,000 5.0kV LED 10µm SAGAPREF 2021/04/15 SEM WD 12.1mm

(b)

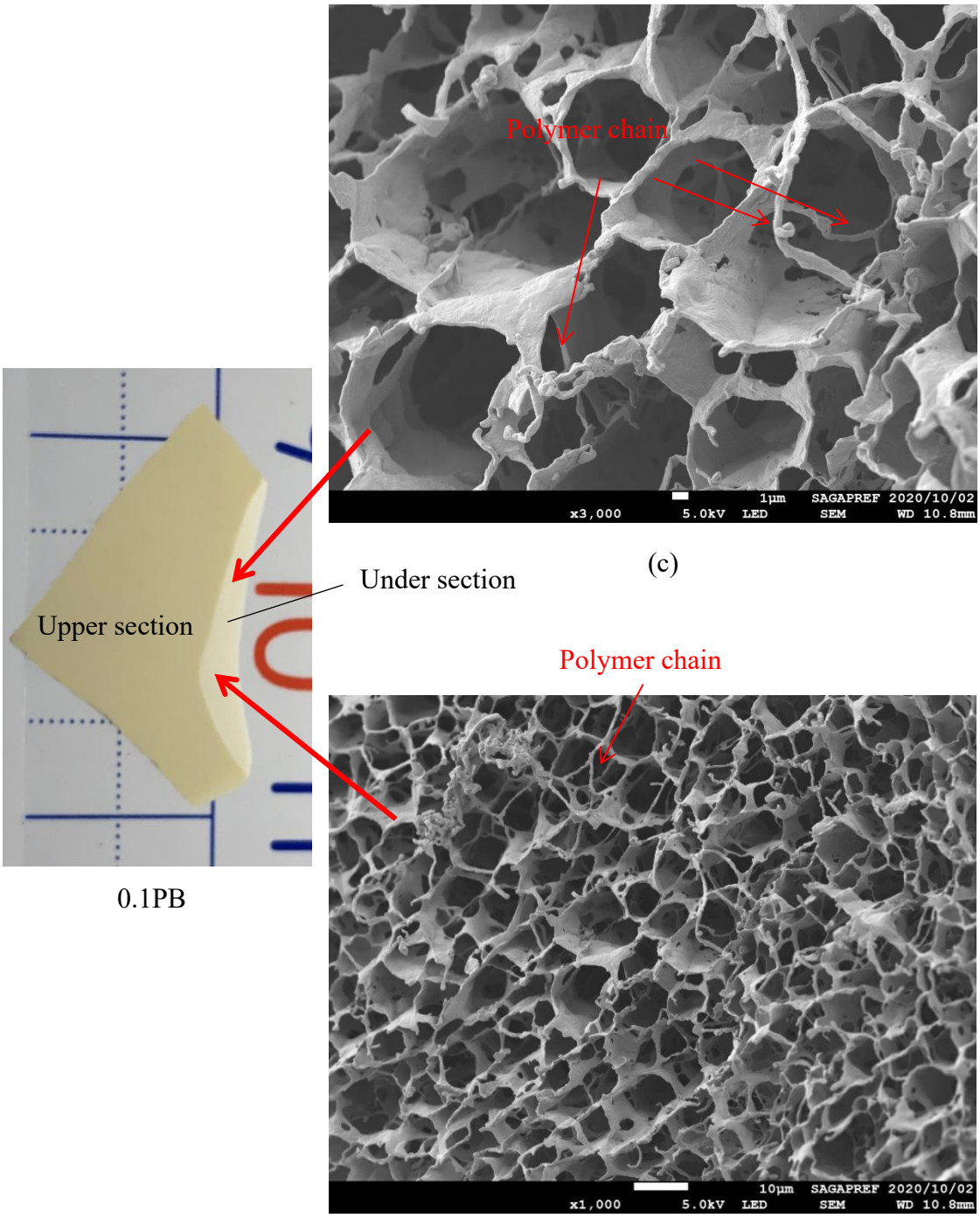

Fig. 3.16 SEM images of 0.1PB

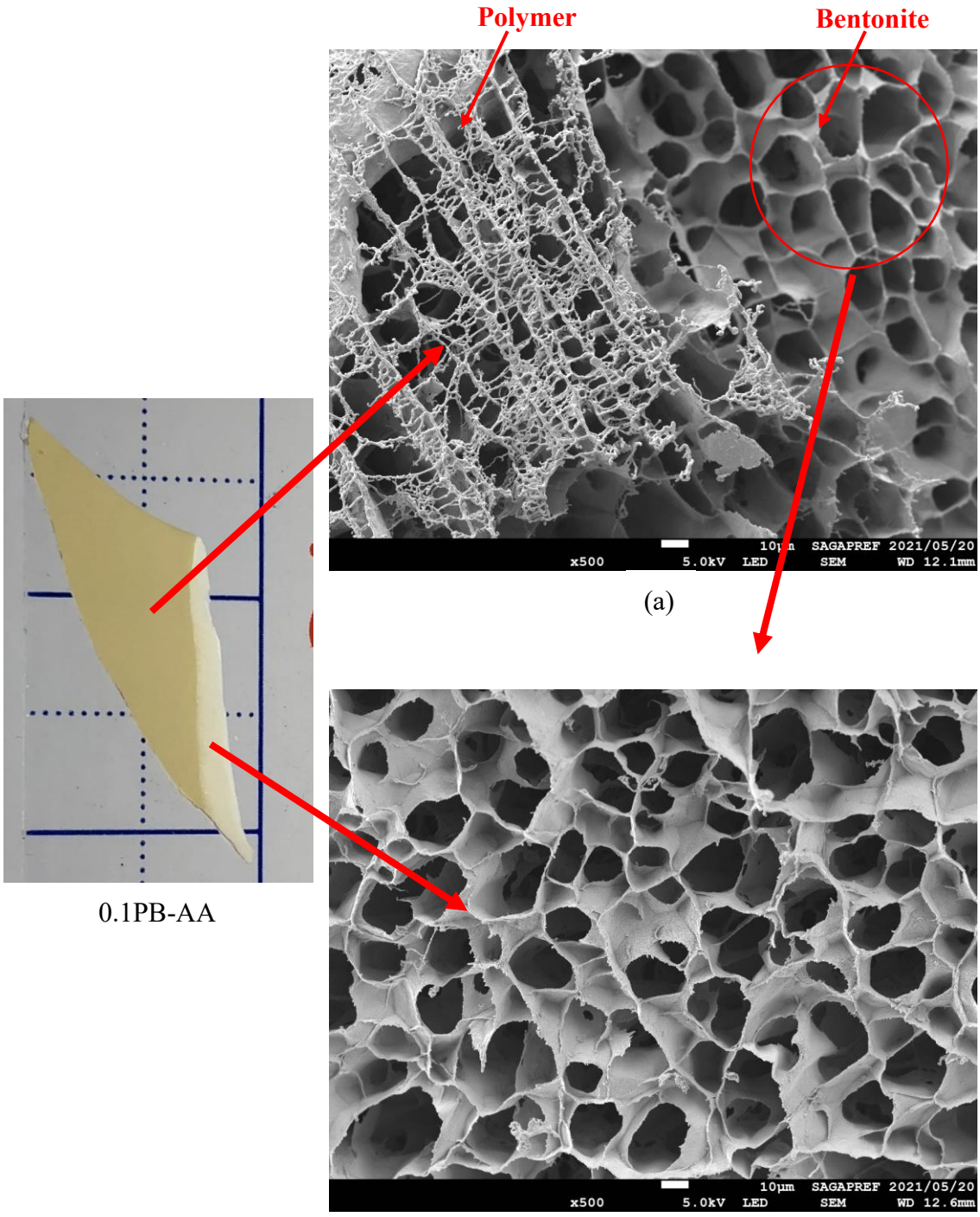

Fig. 3.17 SEM images of 0.1PB-AA

Fig. 3.17 (a) and (b) show the SEM images of 0.1PB-AA. It observed that the bentonite was covered by polymer net. Bentonite was clearly observed and they are regular cross-arrangement and contain amount of granular pore space. It is different with 0.1PB, the polymer chains were not found between bentonite particles like in 0.1PB.

c) 0.2PB

Fig 3.18 shows the SEM images of 0.2PB. It is clearly that high polymer content makes the bentonite like the reticular structure. The polymer and silicate of bentonite was connected uniformly. It is speculated that the silicate layers of bentonite were separated by intercalated polymer.

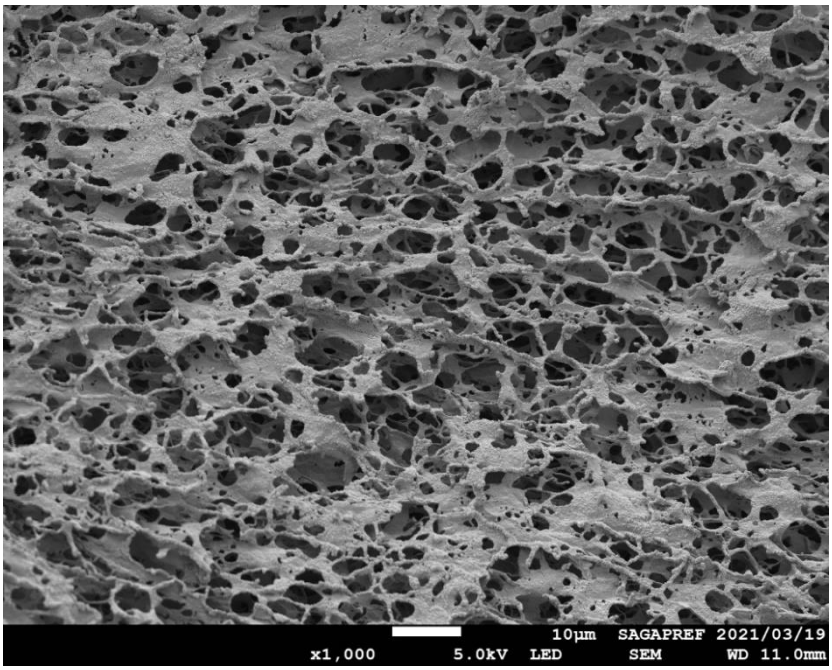

Fig. 3.18 SEM images of 0.2PB

d) 0.4 PB and 0.4PB-AA

Fig. 3.19 (a) and (b) show the SEM images of 0.4PB, and Fig. 3.20 (a) and (b) show the SEM images of 0.4PB-AA. we can find that both 0.4 PB and 0.4PB-AA, the large amount of polymers net was observed. Further, due to the existence of the amide groups ($-CONH_2$), the polymer networks of 0.4PB seems denser than that of 0.4PB-AA. which will be useful to keep the bentonite swelling in cation solutions.

e) 0.1PB-AM and 0.4PB-AM

Fig. 3.21 (a) and (b) show the SEM images of 0.1PB-AM and 0.4PB-AM. The linear polymer is not found in both 0.1PB-AM and 0.4PB-AM, it was observed that the polyacrylamide was around the bentonite particles.

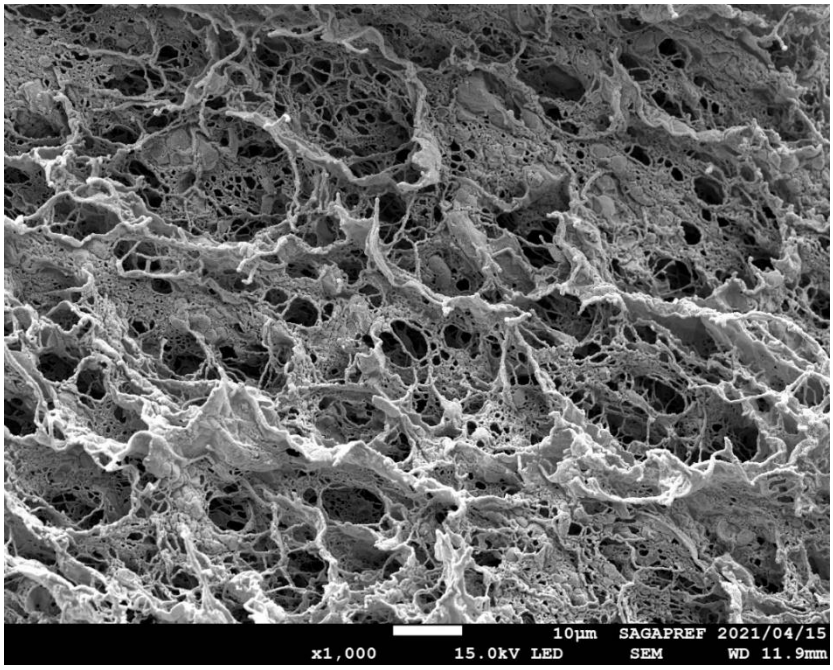

(a)

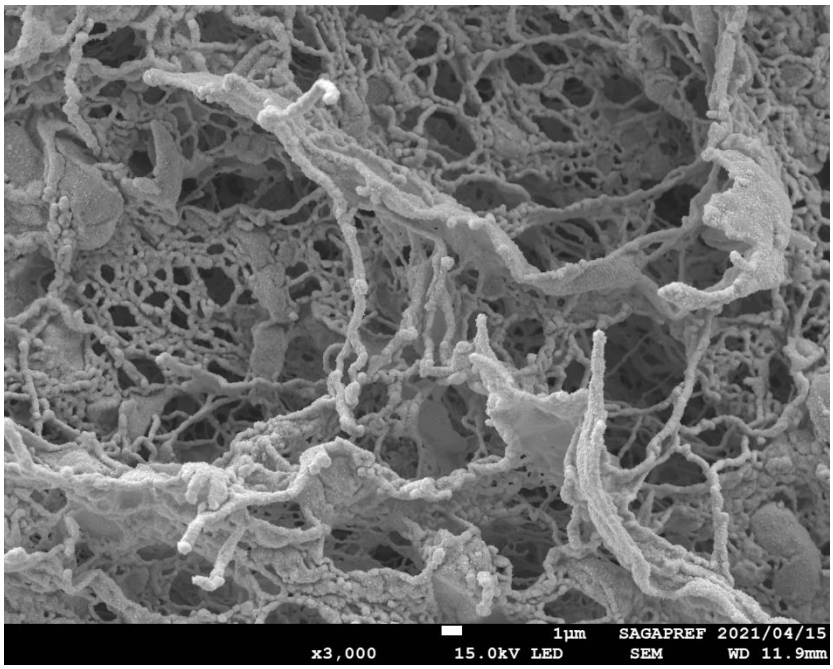

(b)

Fig. 3.19 Scanning Electron Microscopy (SEM) images of 0.4PB

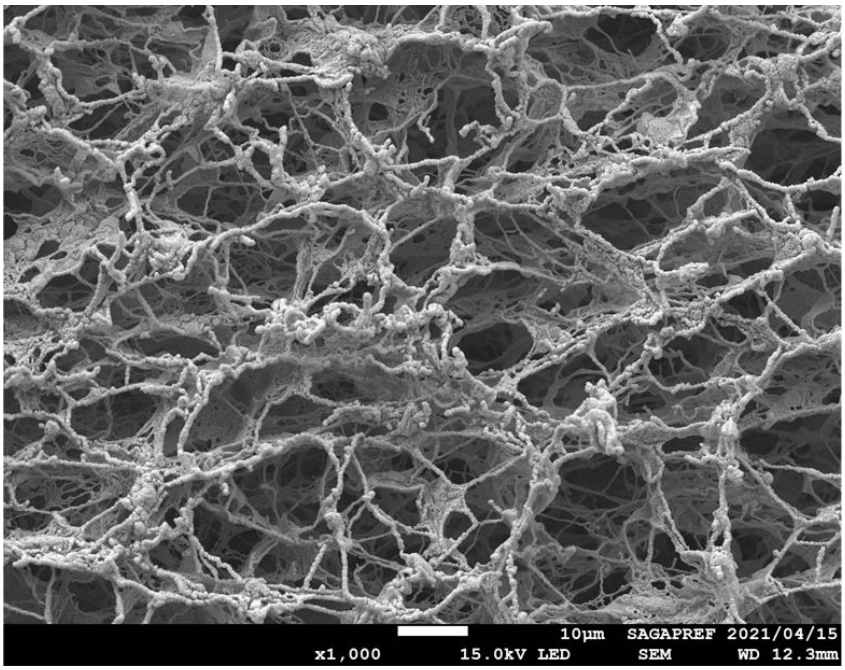

(a)

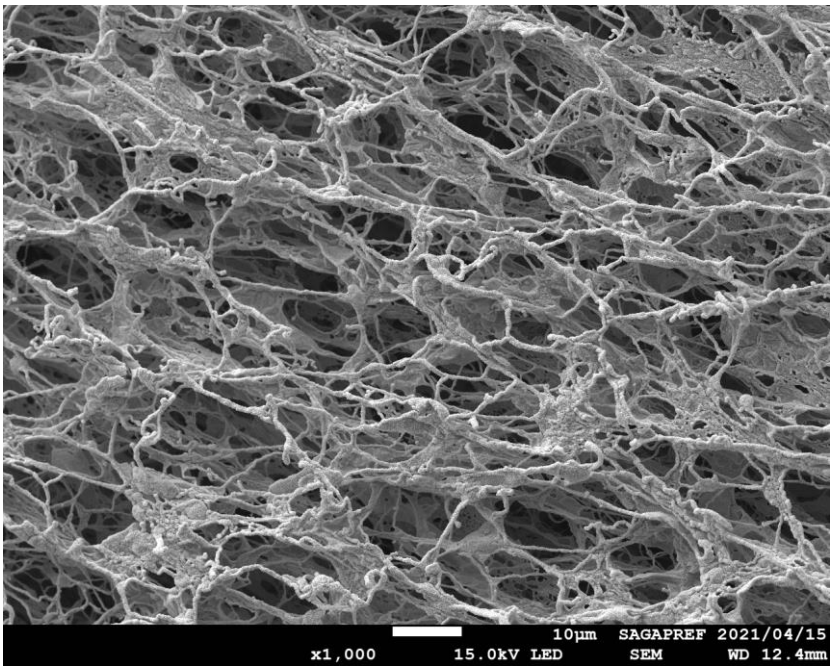

(b)

Fig. 3.20 Scanning Electron Microscopy (SEM) images of 0.4PB-AA

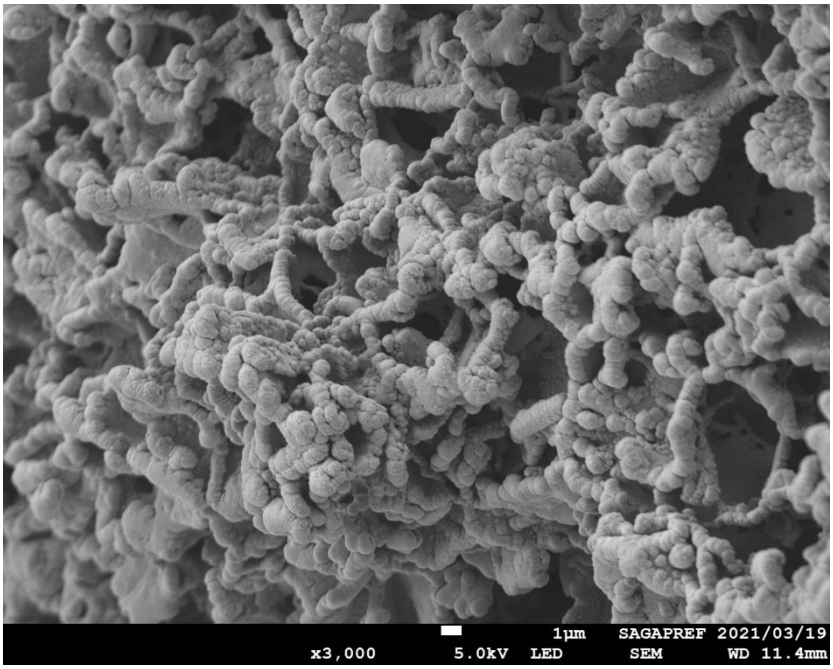

(a) 0.1PB-AM

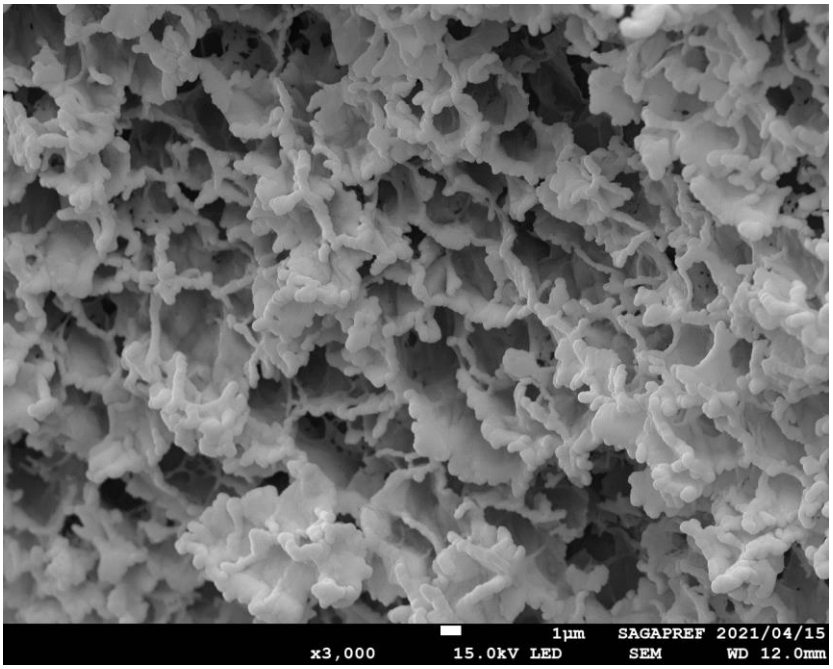

(b) 0.4PB-AM

Fig. 3.21 SEM images with (a) 0.1PB-AM; (b) 0.4PB-AM

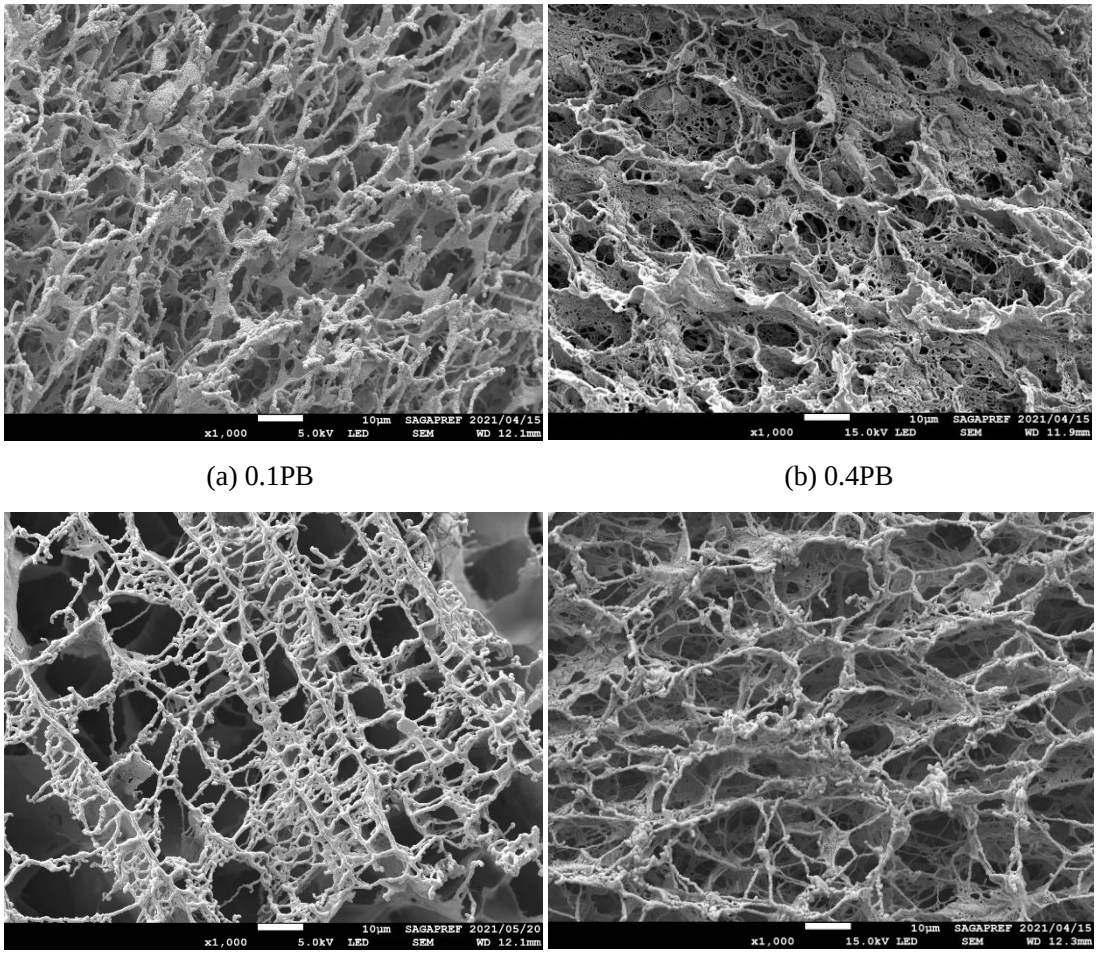

(a) 0.1PB (b) 0.4PB

(c) 0.1PB-AA (d) 0.4PB-AA

Fig. 3.22 Compared the SEM images PBs with different monomers and polymer content

The SEM images in Fig. 3.22 (a) and (b) were produced using PBs of two monomers acrylic acid and acrylamide, and Fig. 3.22 (c) and (d) were produced using PBs only using the acrylic acid. Under the polymer content 10%, it is observed that polymer and bentonite particle was combined uniformly when use two monomers (0.1PB), however, the 0.1PB-AA only using the acrylic acid shows the polymer covered the bentonite. Under the polymer content 40%, both 0.4PB and 0.4PB-AA show the large amount of polymer formed in the PBs. Due to the existence of the amide groups (-$CONH_2$), the polymer networks of 0.4PB seems denser than that of 0.4PB-AA.

3.5 Summary

New polymerized bentonites (PBs) were produced using natural sodium bentonite (UB) and two monomers, acrylic acid (M_1) and acrylamide (M_2) using a free radical polymerization method. The initiator (I) used was potassium persulfate. During the polymerization process, instead of using nitrogen gas, vacuum pressure was used to remove oxygen. It is aimed to simplify the procedure of polymerization. Base on the results of free swelling index (FSI) of produced PBs in 0.6 NaCl solution, the conditions identified/adopted for polymerization are: pH of 6, $I/(M_1 + M_2) = 0.5\%$, and $M_1/M_2 = 0.5$.

For the results of XRD, it is postulated that the structure of 0.1PB is the phase-separated type, and the product is a microcomposite. Others PBs (e.g., 0.2PB, 0.4PB, 0.1PB-AA, 0.4PB-AA, 0.1PB-AM and 0.4PB- AM), the d-spacing of the bentonite particles was increased, and it is postulated that the structure is intercalated and the product is a nanocomposite.

The SEM images of swelled PBs show large amount of polymer like net structures between bentonite particle of 0.1PB-AM and 0.4PB-AM. Higher polymer content, more polymer like networks in PBs. These polymers will have an important role to increase the resistance to aggressive cation solutions.

CHAPTER FOUR
EVALUATING THE PROPERTIES OF THE NOVEL PBs

4.1 Physical properties

(1) Items tested and test conditions

Physical properties of UB and PBs were examined through a series of Atterberg limits and specific gravity (G) test. Liquids tested were deionized water (DI-W), 0.6 M NaCl, 0.03 M $CaCl_2$ and 0.06 M $CaCl_2$ solutions. The liquid limit and plastic limit tests were performed following ASTM D4318 and the specimen gravity test followed ASTM D854.

(2) Test results

The values of specific gravity (G), liquids limits (w_l), and plastic limit (w_p) are listed in Table 4.1. Due to the existence of polymer strings in the PBs, which prevented the sample from breaking apart when the rounded rod reached 3 mm in diameter, the plastic limits of the PBs could not be determined by using the method of rolling the sample into rods as shown in Fig. 4.1. Bohnhoff and Shackelford (2013) reported the same phenomenon.

Fig. 4.1 The sample of 0.1PB in plastic limit test.

Table 4.1 Specific gravities, liquid limits and plastic limits of UB and PBs

liquids	**Materials**								
	UB			0.1PB			0.2PB		
	G (-)	w_l (%)	w_p (%)	G (-)	w_l (%)	w_p (%)	G (-)	w_l (%)	w_p (%)
DI-W	2.65	716	46	2.46	1005	-	2.41	2108	-
0.6 M NaCl		275	45		395	-		585	-
0.03 M $CaCl_2$		451	36		760			1207	
0.06 M $CaCl_2$		359	37		581	-		732	-

The values of w_l for PBs are much higher than that of UB, and the higher the polymer content is, the higher the w_l will be. The value of w_l of a soil is generally controlled by (1) water in the diffuse double layer (DDL) and (2) water in micropores of the soil (Sridharan and Prakash 1999). It is postulated that with the existence of polymers, more water can be held in micropores (Prongmanee et al. 2018; Tian et al. 2019), resulting in a higher w_l value. Since the polymer is lighter than the bentonite mineral, the G values of PBs were lower than that of UB. The G value of 0.2 PB was approximately 90% of that of the UB.

4.2 Swelling capacity

Swelling capacity of PBs and UB was evaluated by free swelling index (FSI) tests and swelling pressure tests using DI-W, 0.6 M NaCl and 0.03-0.06 M $CaCl_2$ solutions.

4.2.1 FSI values of PBs and UB

Fig. 4.2 shows the results of the FSI test with four different liquids. Generally, the PBs had higher FSI values than UB for all liquids tested except 0.1PB in 0.06 M $CaCl_2$, and the higher the polymer content, the higher the FSI. With DI-W, the FSI value of 0.1PB was more than 5 times that of UB and that of 0.2PB was more than 10 times higher. With 0.6 M NaCl solution, the FSI of 0.1PB was 29 mL/2g, and it was more than 40 mL/2g for 0.2PB. These results indicate that 0.1PB can potentially be used as a core

material of GCLs under seawater conditions (0.6 M NaCl). For 0.06 M $CaCl_2$ solution, the FSI of 0.1PB was almost the same as that of UB, and the FSI increased only for 0.2PB (nanocomposite). Prongmanee et al. (2018) reported some swelling and consolidation properties of polymerized bentonite (PB) when using acrylic acid as the monomer. For PB with a polymer to bentonite ratio of 0.1, the FSI value of PB reported by Prongmanee et al. (2018) was 35 mL/2g in DI-W and 21 mL/2g in 0.6 M NaCl solution. These values are lower than the values of 0.1PB from this study. Scalia et al. (2014) reported a bentonite-polymer composite (BPC) using a monomer to bentonite ratio greater than 0.1, and the FSI value in DI-W was also less than that of 0.1PB in this study.

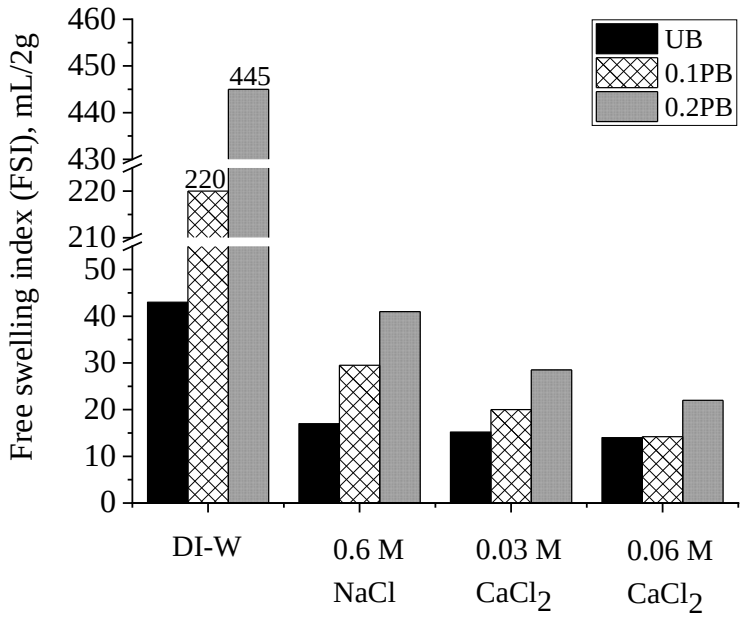

Fig. 4.2 FSI values of PBs and UB

4.2.2 Swelling pressure test

(1) Test method

1) Sample preparation. The specimen was formed by statically compressing 20 g of

air-dried powders of PBs or UB in a cylindrical rigid ring with a diameter of 60 mm and thickness of 60 mm. The compression machine used had a maximum compression capacity of 30 kN. The initial water content of UB and PBs was approximately 3%. The compression pressure adopted was 1.3-8.2 MPa; Before the swelling pressure test the thicknesses of the specimens were approximately 5.6 to 6.7 mm, and the initial dry density was 1.03 g/cm^3 - 1.26 g/cm^3.

2) Test set-up. The device for testing swelling pressure is shown in Fig. 4.3. After all flow pipes of the device were filled with water, saturated filter paper and porous stone were placed on the bottom pedestal. Then, the lower rigid ring with the specimen inside was carefully placed on saturated filter paper. After that, the lower rigid ring was fixed with the bolts. Next, saturated filter paper and a piston with a saturated porous stone were placed on the top of the specimen. The piston was fixed by tightening the fixing screws to prevent swelling of the specimen caused by sucking liquid from the saturated filter paper. After that, the load cell was connected to the piston.

3) Start of the test. The fixing screws of the piston were released, and the desired liquid was supplied to the bottom of the specimen under a 20 kPa pressure. The swelling pressure was recorded until it reached a steady value. The swelling pressure test was conducted under isochoric conditions (Schanz and Tripathy 2009), which is basically the same as ASTM D4546 (ASTM 2003) Method C. Note that the total height of the specimen and the load cell system were fixed, but during the test, the expansion of the specimen due to the compression of the load cell was allowed, and this was measured by a linear variable differential transducer (LVDT). With the measured vertical displacement of the specimen, the final dry density of the specimen was calculated.

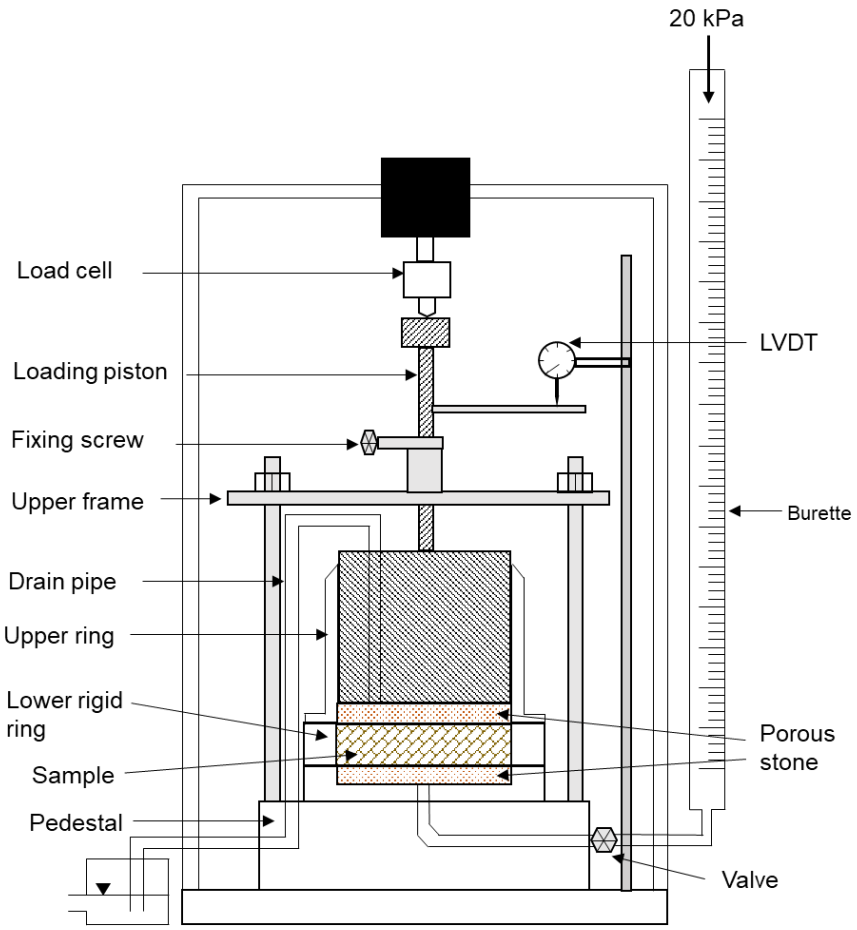

Fig. 4.3 Swelling pressure test apparatus

(2) Test results and discussion

For a given dry density (or void ratio) of bentonite (clay), generally, the higher the swelling pressure is, the lower the permeability will be (e.g., Prongmanee *et al*., 2018). Therefore, swelling pressure is an indirect indicator for evaluating the permeability of a GCL. Fig. 4.4 (a), (b) and (c) show the plots of swelling pressure versus time for the PBs and UB with DI-W and cation solutions with 0.6 M NaCl and 0.03 M $CaCl_2$, respectively. The swelling pressures of PBs reached steady values took a longer time than those of the UB, which is attributed to the fact that PBs have lower permeabilities, and this will be discussed in the section on consolidation test results. Because the higher swelling

pressure induced more compression of the load cell, the final dry densities of the PBs were less than that of the corresponding UB.

Fig. 4.5 shows the relationship of swelling pressure and final dry density in DI-W, 0.6 M NaCl and 0.03 M $CaCl_2$ solutions. They show that the swelling pressure increased with dry density of the specimens.

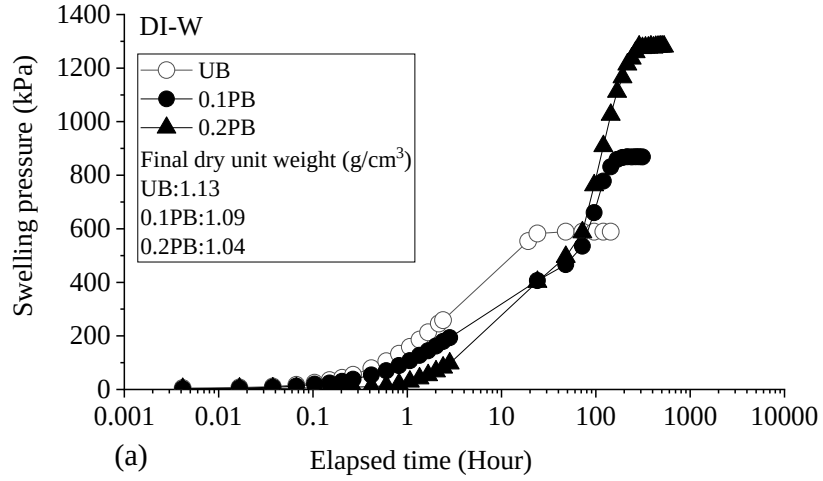

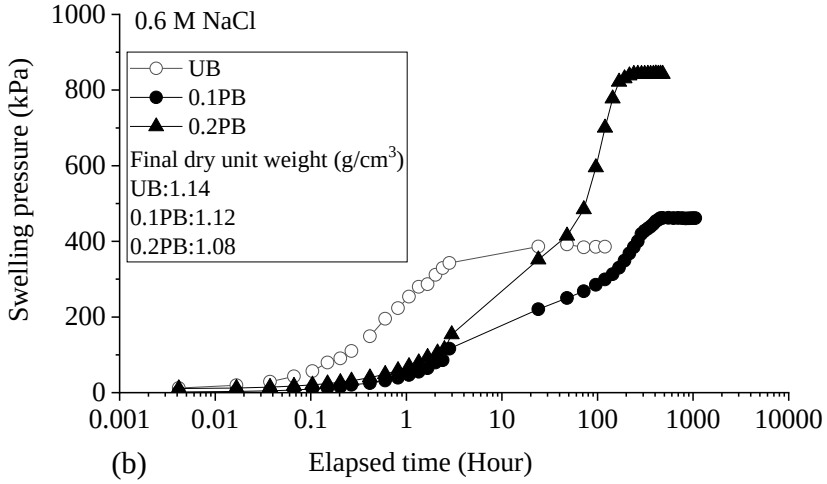

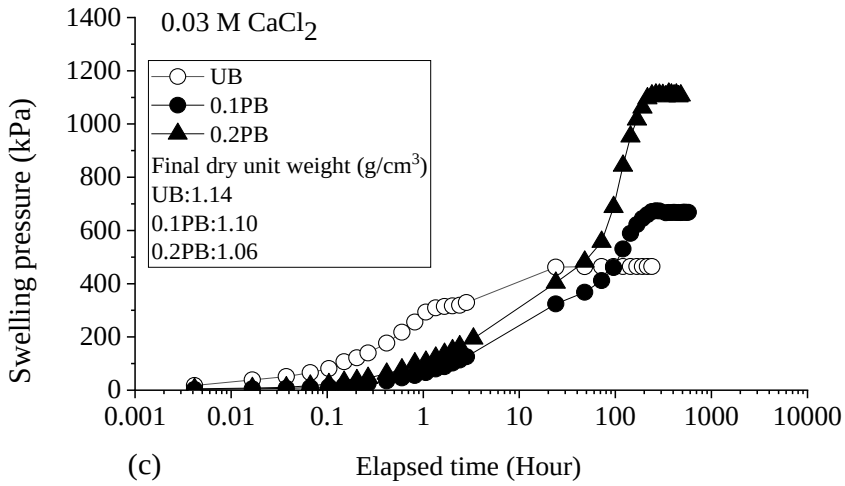

Fig. 4.4 Typical swelling pressure versus time curves (a) DI-W, (b) 0.6 M NaCl and (c) 0.03 M $CaCl_2$ solution

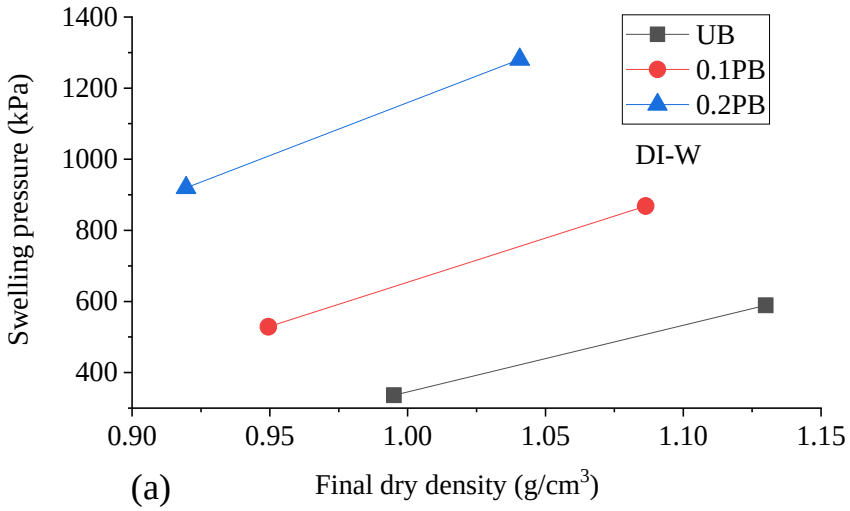

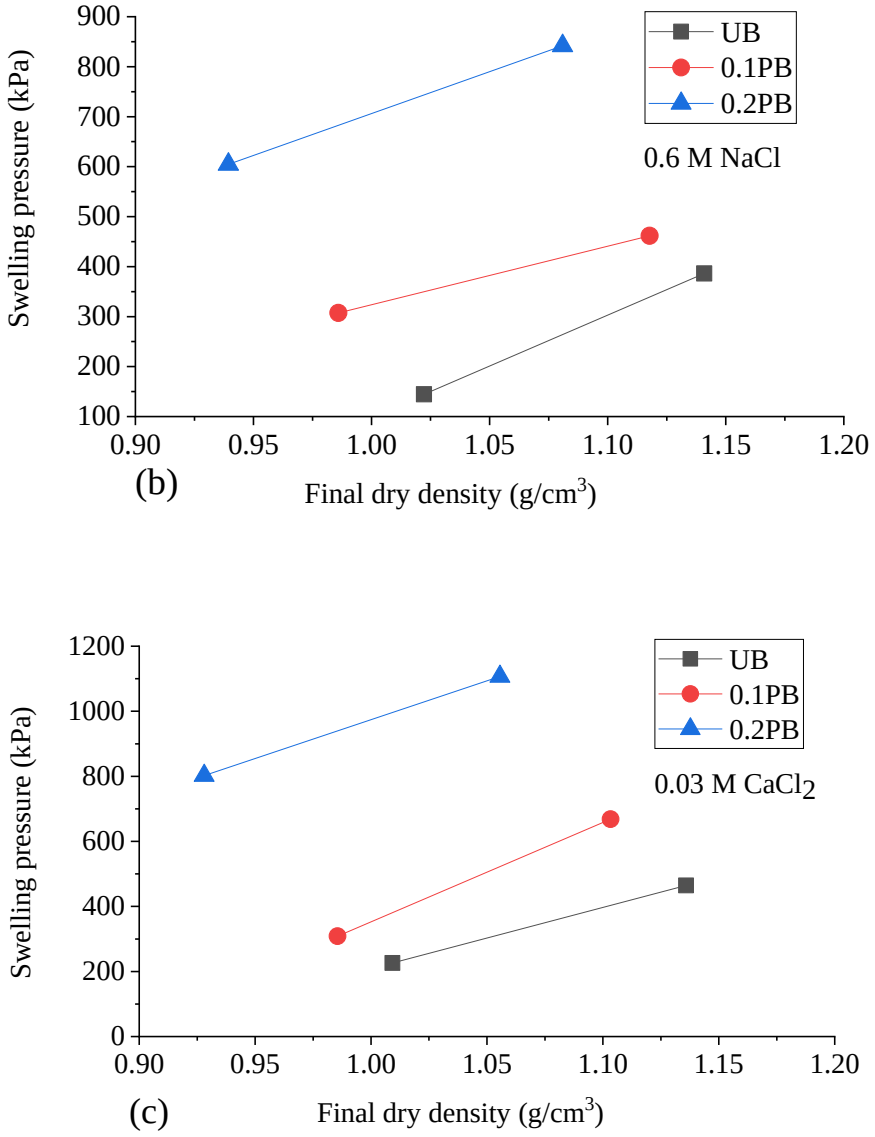

Fig. 4.5 Swelling pressure versus final dry density (a) DI-W, (b) 0.6 M NaCl and (c) 0.03 M $CaCl_2$ solution

Fig. 4.6 shows the relationship of swelling pressure and polymer content in DI-W, 0.6 M NaCl and 0.03 M $CaCl_2$ Solutions. This indicates that the swelling pressure of PBs increased as the polymer content increased under the same test conditions. 0.2PB had a higher swelling pressure than 0.1PB. It is deduced that the intercalated structure of 0.2PB (nanocomposite) absorbed more water molecules into the interlayer spaces of bentonite particles. In Fig. 4.6, swelling pressures with cation solutions exhibit the same

tendency as DI-W; in particular, the swelling pressure of 0.2PB almost doubled the value of 0.1PB.

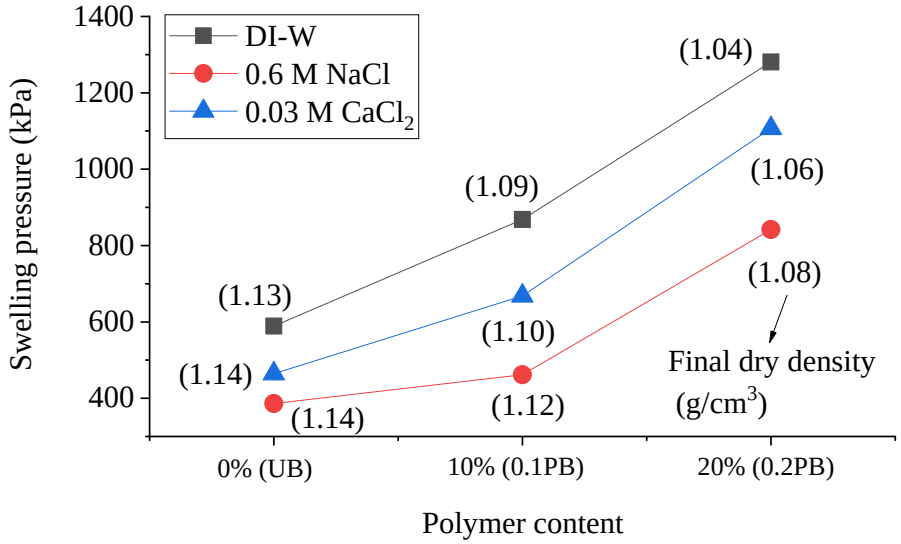

Fig. 4.6 Relationship of swelling pressure and polymer content in DI-W, 0.6 M NaCl solution and 0.03 M $CaCl_2$ solution

4.3 Swelling mechanism of PB

Polymers produced using both acrylic acid and acrylamide as monomers have two hydrophilic groups, -$CONH_2$ and –COONa (Fig. 4.7 (a)) (Liu and Rempel 1997), which are dipoles (Deng et al. 2006). The formed polymer is anionic type. For a PB, polymer can wrap around bentonite particles. As illustrated in Fig. 4.7 (b), the bonds between the polymer and bentonite particles involve (1) ion-dipole interactions between exchangeable cations and the carbonyl oxygens (C=O) of amide groups -$CONH_2$, and (2) H-bonding between the amide groups and water molecules in the hydration shells of exchangeable cations (Deng et al. 2006). Both groups, -$CONH_2$ and -COONa, have the ability to connect with exchangeable cations directly or indirectly by physical interaction (Deng et al. 2006), which can reduce the amount of cations entering the diffuse double layers of bentonite particles. As a result, PB exhibits higher swelling in solutions of

cations.

Other mechanisms explaining the higher swelling capacity of the anionic acrylamide polymer are hydration, ionization and osmosis (Kim et al. 2010; Liu and Rempel 1997), and these are discussed below.

1) Hydration. Before absorbing water, anionic polyacrylamide chains are contracted and intertwined with each other to form a net structure. Anionic polyacrylamide has hydrophilic groups comprising sodium carboxylate (-COONa) and amide (-$CONH_2$). When water molecules diffuse into the net structure, hydrophilic groups -COONa and -$CONH_2$ are hydrated. In anionic polyacrylamide, nonionic hydrophilic groups -$CONH_2$ and ionic hydrophilic groups –COONa are interlaced with each other on the polymer chain. Both -$CONH_2$ and -COONa will be hydrated in an aqueous solution, and the total hydration potential will be higher than that of the ionic hydrophilic groups, -COONa, alone.

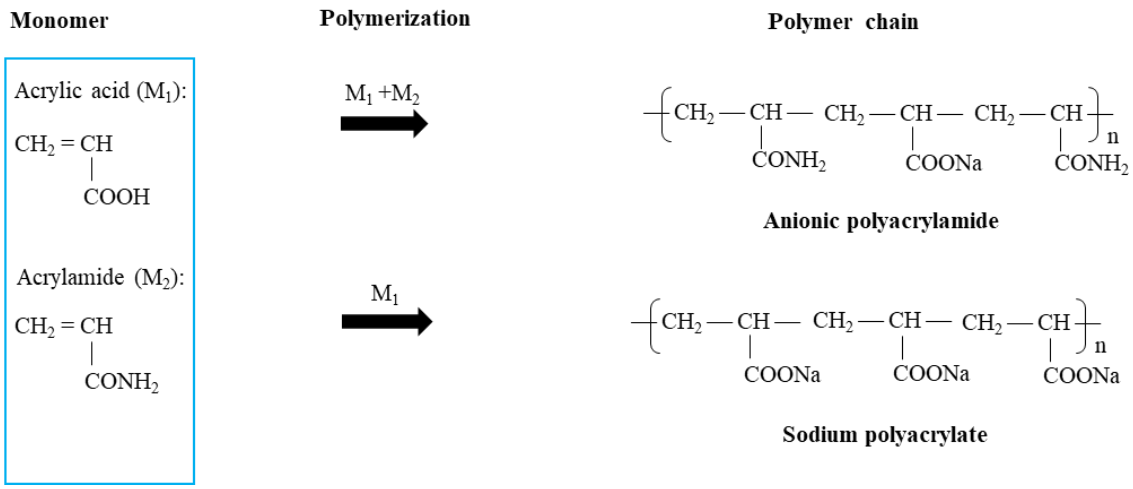

(a) The molecular structure formula of monomers and polymer

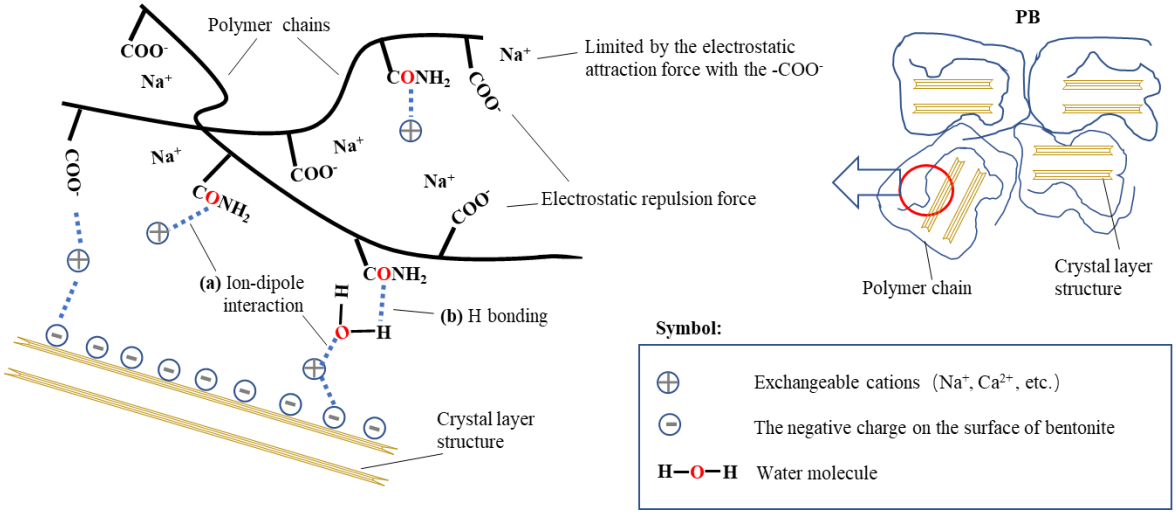

(b) Swelling mechanism of PBs in cation solutions

Fig. 4.7 Mechanism of anionic polyacrylamide protecting higher cation replacement into the interlayer of bentonite particles; (a) the molecular structure formula of monomers and polymer; (b) swelling mechanism of PBs in cation solutions

2) Ionization. The ionic functional group -COONa will be ionized to $-COO^-$ and Na^+. The functional group $-COO^-$ is attached to the polyacrylamide chains. Free Na^+ ion can move away from the polyacrylamide chains to a limited distance (limited by the electrostatic attraction force of $-COO^-$). Due to the electrostatic repulsion force operating between the functional groups $-COO^-$, the chains of anionic polyacrylamide expand to increase the inside space of the net structure.

3) Osmosis. Free Na^+ exists in the network of the polyacrylamide chains, resulting in different concentrations of Na^+ inside and outside the net structure, which generates osmotic pressure and prompts water molecules to infiltrate into the net structure of the anionic polyacrylamide.

4.4 Consolidation tests

4.4.1 Test condition

(1) Sample preparation

Three types of liquids were tested, i.e., DI-W, 0.6 M NaCl, 0.06 M $CaCl_2$ and 0.03 M $CaCl_2$ solutions. Dry 0.1PB, or 0.2PB or UB powder was thoroughly mixed with desired liquid with a liquid content of two times the corresponding liquid limit of the sample. Then of the suspension was vacuumed two hours at 0.1 MPa, and cured for at least 24 hours after that. Next, the slurry was preconsolidated under a vertical effective stress of 40 kPa in an odometer ring 60 mm in diameter and 60 mm in height until the rate of vertical deformation was less than 0.003 mm/h. The specimens for consolidation tests were cut from the preconsolidated samples. It was found that if the preconsolidation pressure was less than 40 kPa, the preconsolidated sample was too soft and difficult to handle. Therefore, a preconsolidation pressure of 40 kPa was adopted in this study.

Then, consolidation test specimens of 60 mm in diameter and 10 mm in height were trimmed from the preconsolidated samples. Due to the very low permeability of UB and PBs (under two-way drainage conditions), one loading step with a 20 mm thick specimen would take more than one week. To shorten the test duration, we used specimens 10 mm thick with which each loading step took approximately 3 days.

(2) Test method

The multiple stage loading (MSL) consolidation test was conducted following ASTM D2435 (ASTM 2018) with vertical consolidation pressures ranging from 40 kPa to 1280 kPa. The values of permeability (k) of the specimen were calculated from the test results using Taylor's (1948) method.

4.4.2 Test results

The consolidation test results of three specimens (e.g., UB, 0.1PB and 0.2PB) are presented for three liquids, DI-W, 0.6 M NaCl, 0.03 M $CaCl_2$ and 0.06 M $CaCl_2$ solutions respectively. The initial water contents (w_i), void ratios (e_i) and compression indexes (C_c) of UB, 0.1PB, and 0.2PB with various solutions are summarized in Table 4.2. Since the curves of e – log(σ_v') are almost linear for effective vertical stresses up to 314 kPa, the values of C_c were calculated using the effective vertical stresses ranging from 40 kPa to 314 kPa.

Table 4.2 Initial water content (w_i), initial void ratio (e_i), and compression index (C_c) of UB and PBs

Liquid	**UB**			**0.1PB**			**0.2PB**		
	w_i	e_i	C_c	w_i	e_i	C_c	w_i	e_i	C_c
DI-W	438	11.48	9.03	559	13.76	9.85	865	20.85	14.49
0.6 M NaCl	184	4.78	2.88	237	5.22	3.14	292	7.05	5.45
0.03 M $CaCl_2$	175	4.64	3.002	181	4.45	3.58	203	4.89	3.85
0.06 M $CaCl_2$	161	4.27	2.48	169	4.28	2.67	187	4.51	3.11

(1) In DI-W

Fig. 4.8 shows e – log(σ_v') relationships for UB and 0.1PB and 0.2PB with DI-W. Under a given pressure, the void ratios e of PBs are larger than that of UB. The compression indexes (C_c) of PBs are higher than that of UB, as listed in Table 4.2.

As mentioned before, PBs have higher liquid limits (Table 4.1) and larger FSIs (Fig. 4.2). Therefore, they contain more macropores under lower consolidation pressure. However, when the consolidation pressure was increased, these macropores were crushed /compressed, and this resulted in a larger value of C_c. The relationships of permeability and void ratio of UB and PBs are plotted in Fig. 4.9. For a given void ratio,

the order of the calculated hydraulic conductivities was $k_{UB} > k_{0.1PB} > k_{0.2PB}$ (subscripts indicate the corresponding materials).

(2) In 0.6 M NaCl

The $e - \log(\sigma_v')$ relationships of UB and 0.1PB and 0.2PB with 0.6 M NaCl solution are depicted in Fig 4.10. The C_c values of PB was higher than that of UB, and the higher the polymer content, the higher the C_c value. When $\sigma_v' < 200$ kPa, under a given pressure, the void ratios of PBs were higher than that of UB, and when $\sigma_v' > 200$ kPa, the void ratio of 0.2PB was less than that of UB. The relationships of permeability versus void ratio with 0.6 M NaCl solution is depicted in Fig 4.11. With the conditions tested, for a given void ratio, the order of hydraulic conductivities was $k_{UB} > k_{0.1PB} > k_{0.2PB}$. The difference was reduced with decreasing void ratio. For void ratios up to 5 for 0.1PB and 7 for 0.2PB, the calculated values of k for PBs are still smaller than 10^{-11} m/s for both the 0.6 M NaCl and 0.03-0.06 M $CaCl_2$ solutions.

(3) In 0.03 M $CaCl_2$ - 0.06 M $CaCl_2$

The $e - \log(p')$ relationships of UB and 0.1PB and 0.2PB with 0.03 M $CaCl_2$ and 0.06 M $CaCl_2$ solutions are depicted in Figs 4.12 (a) and (b), respectively. In both solutions, the C_c values of PBs were higher than that of UB, and the higher the polymer content, the higher the C_c value as shown in Table 4.2.

The relationships of permeability versus void ratio with 0.03 M $CaCl_2$ and 0.06 M $CaCl_2$ solutions are depicted in Figs 4.13 (a) and (b) respectively. With the conditions tested, in both solutions, for a given void ratio, the order of hydraulic conductivities was $k_{UB} > k_{0.1PB} > k_{0.2PB}$.

According to the above the discussions, in DI-W and cation solutions, the permeability k of 0.1PB and 0.2PB calculated from consolidation test were all lower than that of UB. The higher polymer content, the lower permeability. For clayey soils, the value of permeability from the flow test and the value interpreted from consolidation

test were comparable (e.g., Bohnhoff and Shackelford 2014, Quang and Chai 2015). Therefore, the values of permeability from consolidation test results represented the permeability of UB and PBs with different pore water chemistry. While there is a limitation that chemical equilibrium in the pore water was not checked, and the value of permeability cannot be treated as the final value for the corresponding liquid used (Scalia et al. 2018).

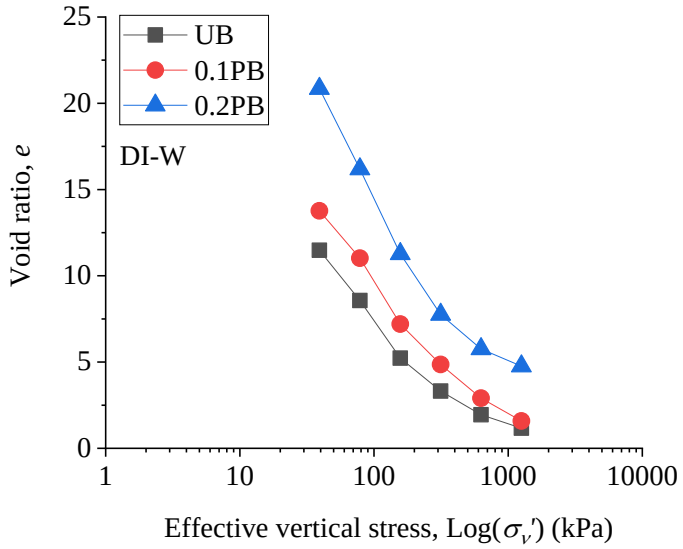

Fig. 4.8 e – log(σ_v') relationships (DI-W)

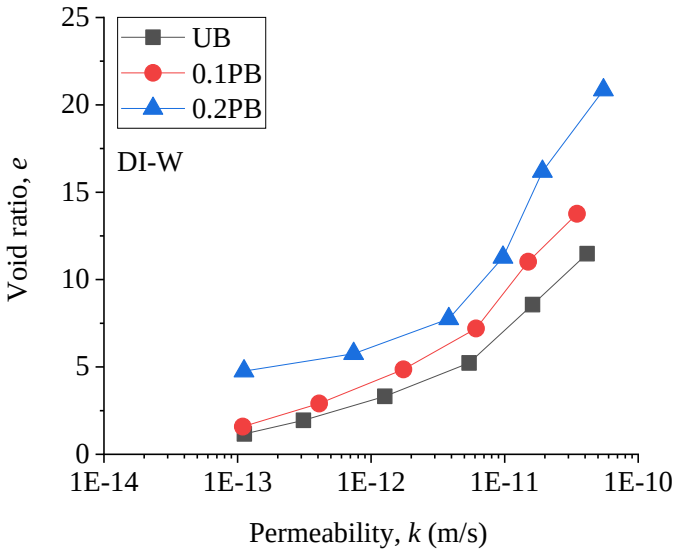

Fig. 4.9 Relationship of *k* and *e* (DI-W)

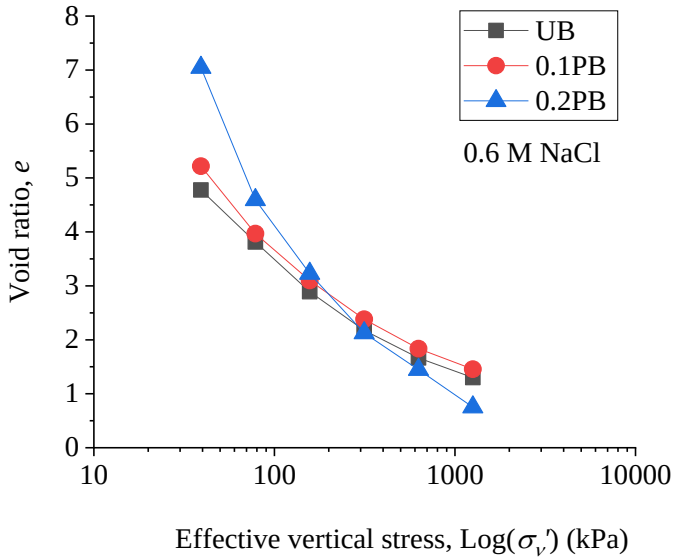

Fig. 4.10 e – log(σ_v') relationships (0.6 M NaCl solution)

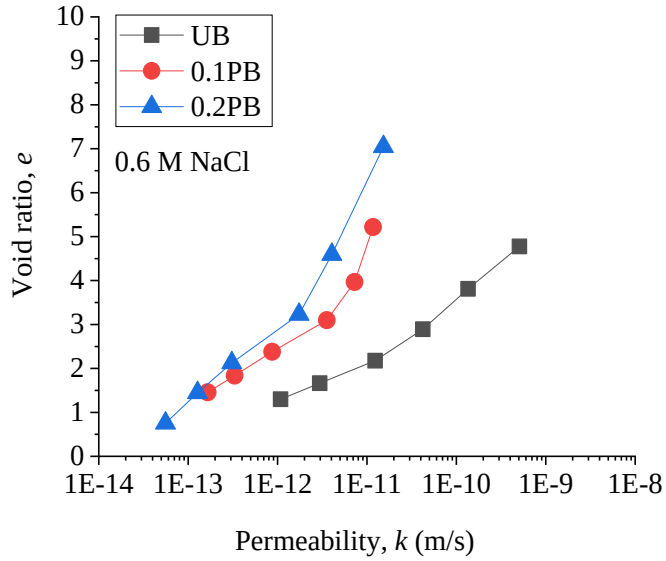

Fig. 4.11 Relationship of *k* and *e* (0.6 M NaCl solution)

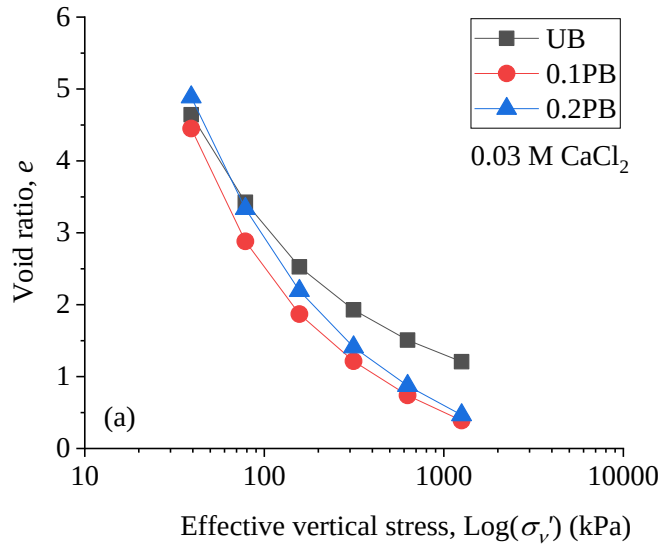

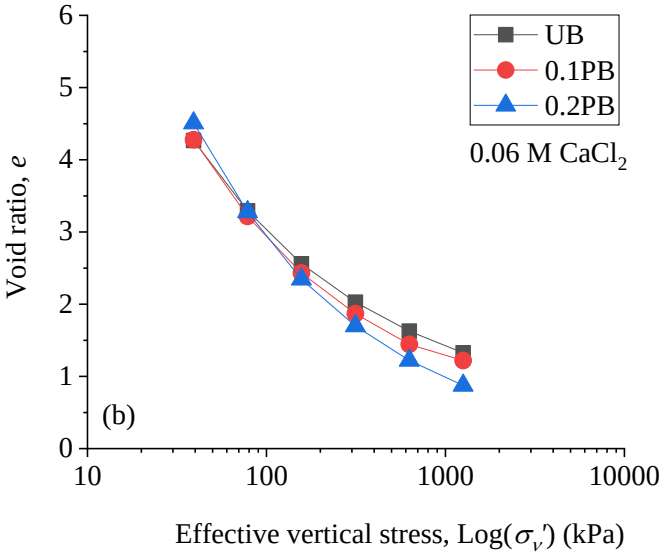

Fig. 4.12 e – log(σ_v') relationships (DI-W)

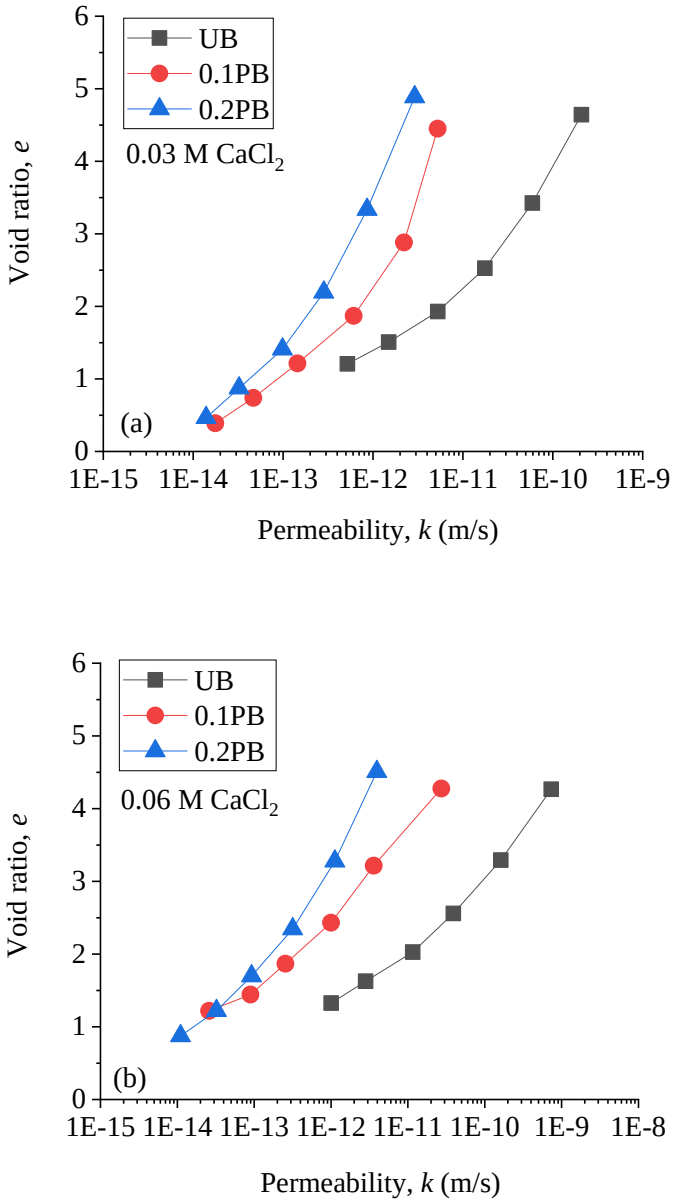

Fig. 4.13 Relationship of *k* and *e* (DI-W)

The consolidation test results from Prongmanee et al. (2018) for a PB with a polymer to bentonite ratio of 0.1, using DI-W and 0.6 M NaCl solution, are compared in Fig.4.14 with the results for 0.1PB from this study. It is evident that for a given void ratio, the permeability of 0.1PB from this study was lower than that reported by Prongmanee et al.'s (2018). It is implied that with the same polymer content (10%), the 0.1PB has better barrier properties than those of Prongmanee et al.'s (2018).

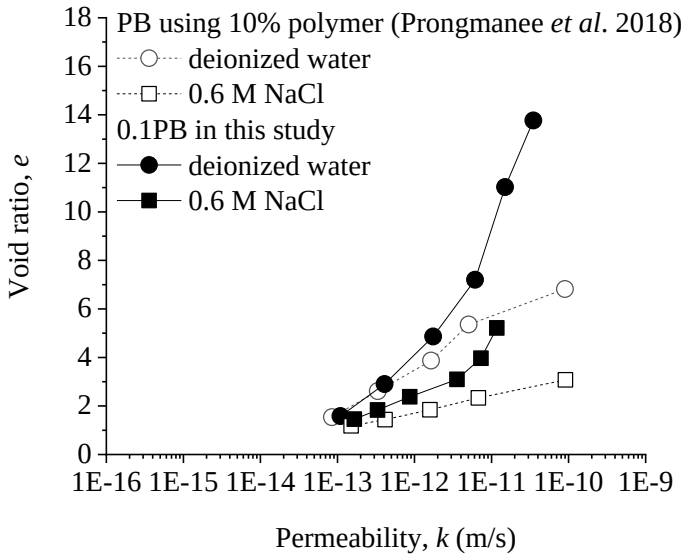

Fig. 4.14 Comparison of the relationships of *k* and *e*

4.5 Permeability test

4.5.1 Test method and conditions

0.1PB and UB were used for permeability test with DI-W and, 0.6 M NaCl and 0.03 M $CaCl_2$ solutions. Tests were carried out in a rigid wall permeameters (De Camillis et al. 2016).

(1) Sample preparation

Dry 0.1PB or UB powder was thoroughly mixed with the desired liquid with a liquid content of two times the liquid limits of the samples, and the suspension was vacuumed two hours at 0.1 MPa, and then cured for at least 24 hours. After that, the slurry was preconsolidated under a vertical effective stress of 20 kPa in an odometer ring 60 mm in diameter and 60 mm in height for 6 days. The specimens of 10 mm were cut from the preconsolidated samples. During the flow rate test, hydraulic gradient used was 345-245.

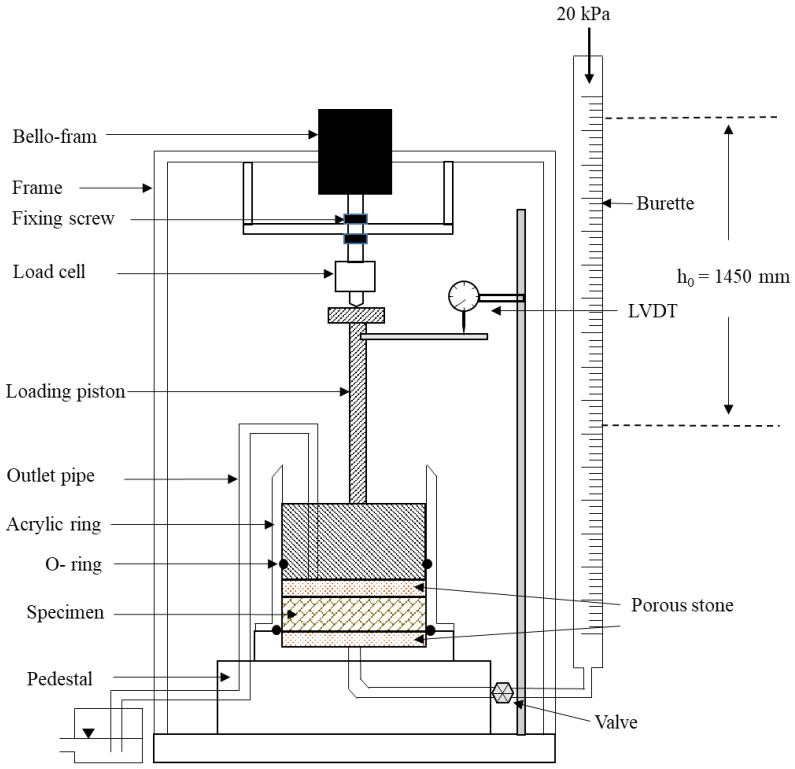

(a) Sketch

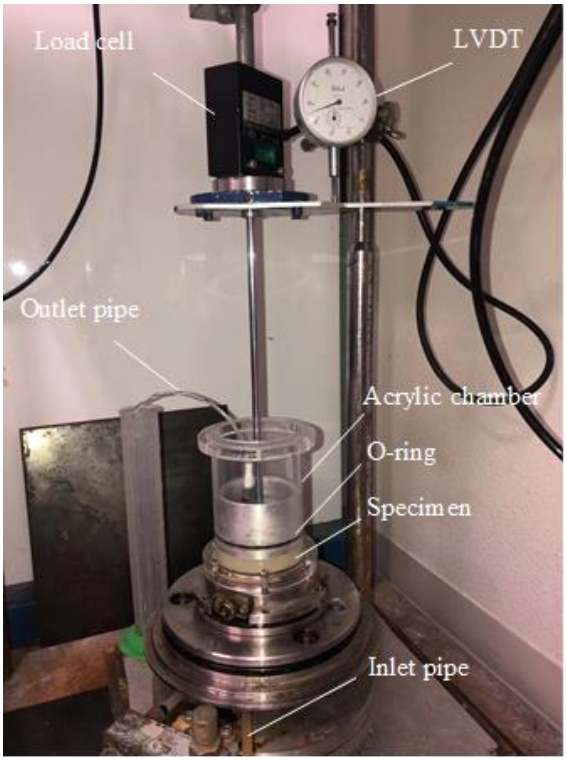

(b) Photo

Fig. 4.15 The apparatus of rigid wall permeability test (a) sketch; (b) photo.

(2) Test equipment and method

1) The device for testing permeability is shown in Fig. 4.15. After all flow pipes of the device were filled with the corresponding liquid, saturated filter paper and porous stone were placed on the bottom pedestal. Then, the acrylic rigid ring with the specimen inside was carefully placed on saturated filter paper. After that, the acrylic rigid ring was fixed with the bolts. Then, saturated filter paper and a piston with a saturated porous stone inserted into it were placed on the top of the specimen.

2) Start of the test. The vertical pressure of 20 kPa was supplied. Then, the fixing screws of the load cell was fixed, and the desired liquid was supplied to the bottom of the specimen under a 30 kPa pressure. The water level change in the burette was recorded periodically. The collection of effluent samples for periodical electrical conductivity (EC) and pH measurements. Termination criteria for the permeability tests were defined according to ASTM D6766, which was the ratio of outflow to inflow to be within in 1.0 ± 0.25, and chemical termination criteria require that the ratio of effluent to influent EC and pH to fall within 1.0 ± 0.1. The initial void ratios of 0.1PB were higher than those of UB in various solutions tested as listed in Table 4.3.

Table 4.3 Initial void ratio e_0

	UB	**0.1PB**
DI-W	13.51	15.02
0.6 M NaCl	5.78	7.46
0.03 M $CaCl_2$	6.98	7.33

4.5.2 Results of permeability test

(1) In DI-W

Fig. 4.16 shows the permeability of UB and 0.1PB versus elapsed time approximately 60 days in DI-W. The permeability k of 0.1PB was 4.1 $\times 10^{-11}$ m/s, which was lower than that of UB with 1.6 $\times$ 10^{-10} m/s.

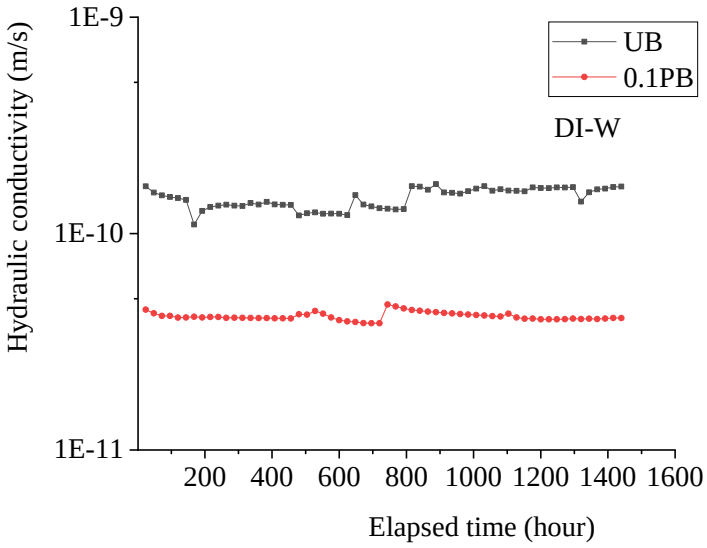

Fig. 4.16 Permeability versus elapsed time in DI-W

(2) In 0.6 M NaCl solution

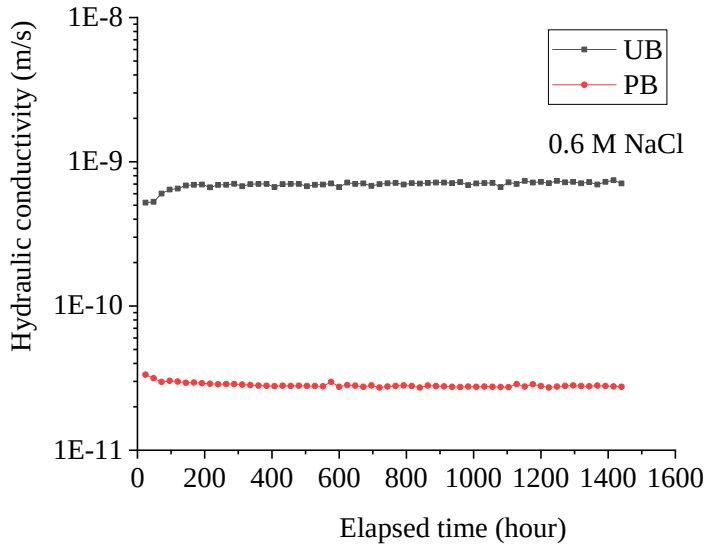

Fig. 4.17 Permeability versus elapsed time in 0.6 M NaCl solution

Fig. 4.17 shows the permeability of UB and 0.1PB versus elapsed time approximately 60 days in 0.6 M NaCl. The permeability k of 0.1PB was 2.8 $\times 10^{-11}$ m/s, which was lower than that of UB with 7.1 $\times$ 10^{-10} m/s.

(3) In 0.03 M $CaCl_2$ solution

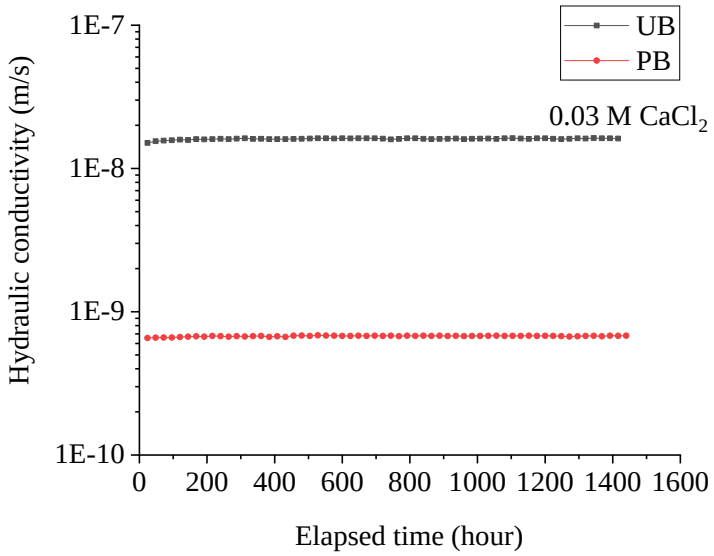

Fig. 4.18 Permeability versus elapsed time in 0.03 M $CaCl_2$ solution

Fig. 4.18 shows the permeability of UB and 0.1PB versus elapsed time approximately 60 days in 0.03 M $CaCl_2$ solution. The permeability k of 0.1PB was 6.8 $\times 10^{-10}$ m/s, which was 1-2 order magnitude lower than that of UB with 1.6×10^{-8} m/s.

4.5.3 Compared the results of consolidation test and permeability test

Fig. 4.19 show the results of comparing the k from consolidation test and permeability test with (a) DI-W, (b) 0.6 M NaCl solution and (c) 0.03 M $CaCl_2$ solution. Based on these figures, the following observations can be made: (1) the value k from the consolidation test and permeability test are scattered in three solutions. (2) Although both test data was scatter, the directly measured k values is approach the extend tendence line of k calculated from the consolidation test. This show that both k values were comparable.

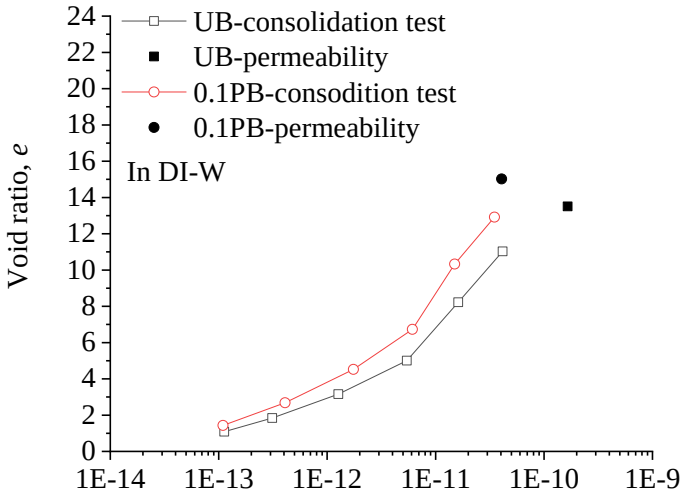
UB-consolidation test
UB-permeability
0.1PB-consodition test
0.1PB-permeability
In DI-W
Void ratio, e
Permeability, k (m/s)
1E-14
1E-13
1E-12
1E-11
1E-10
1E-9

(a)

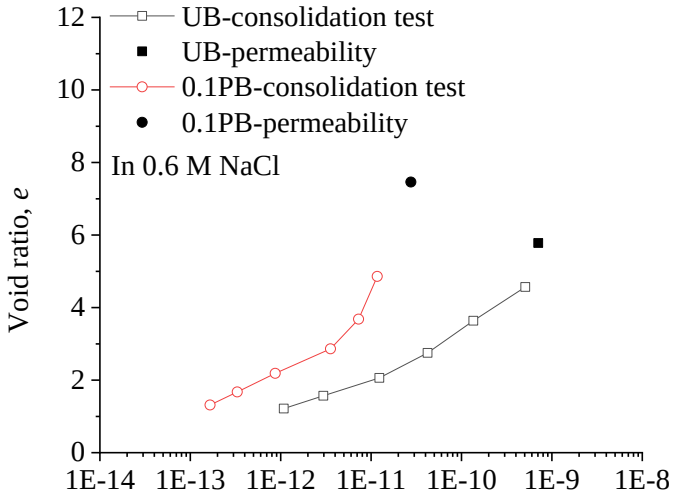
UB-consolidation test
UB-permeability
0.1PB-consolidation test
0.1PB-permeability
In 0.6 M NaCl
Void ratio, e
Permeability, k (m/s)
1E-14
1E-13
1E-12
1E-11
1E-10
1E-9
1E-8

(b)

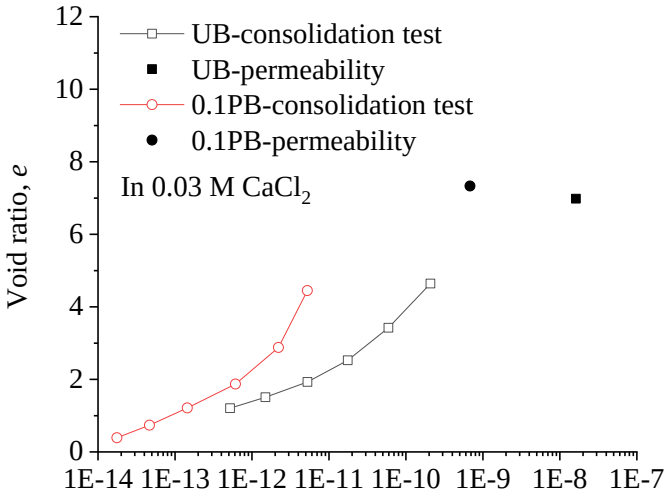
UB-consolidation test
UB-permeability
0.1PB-consolidation test
0.1PB-permeability
In 0.03 M CaCl2
Void ratio, e
Permeability, k (m/s)
1E-14
1E-13
1E-12
1E-11
1E-10
1E-9
1E-8
1E-7

(c)

Fig. 4.19 Compared the *k* from consolidation test and permeability test

4.6 Summary

The values of liquid limit (w_l) for PBs (0.1PB and 0.2PB) are much higher than that of UB, and the higher the polymer content is, the higher the w_l will be. Since the polymer is lighter than the bentonite mineral, the *G* values of PBs were lower than that of UB.

The 0.1PB, 0.2PB and UB were evaluated by a series of experiment test, e.g., FSI test, swelling pressure test, consolidation test and permeability test. For FSI test, the PBs have higher FSI values than those of the UB. With 0.6 M NaCl solution, the FSI of 0.1PB is approximately 30 mL/2g and that of 0.2PB is more than 40 mL/2g, both of which exceed the requirements for GCLs (24 mL/2g). The results of the swelling pressure tests indicate that the PBs have higher swelling capacities than those of UB in DI-W and cation solutions (e.g., 0.6 M NaCl and 0.03-0.06 M $CaCl_2$).

The novel PBs (0.1PB, 0.2PB and 0.4PB) have two hydrophilic groups, -$CONH_2$ and -COONa. Due to both groups can be connected with exchangeable cations directly or indirectly by physical interaction, the amount of cations were reduced entering the diffuse double layers of bentonite particles. This will improve the swelling capacity of the novel PBs in the aggressive cation solutions (0.6 M NaCl solution).

The results of the consolidation tests show that for all liquids tested, the compression indexes (C_c) of PBs are higher than that of UB. For a given void ratio, the order of the permeability is $k_{UB} > k_{0.1PB} > k_{0.2PB}$ (subscripts indicate the corresponding materials). For void ratios up to 5 for 0.1PB and 7 for 0.2PB, the calculated values of *k* for PBs are still smaller than 10^{-10} m/s for both the 0.6 M NaCl and 0.03-0.06 M $CaCl_2$ solutions. The results from the direct permeability test were show that the 0.1PB have lower permeability than that of the UB in DI-W, 0.6 M NaCl and 0.03 M $CaCl_2$ solutions.

Although k values from consolidation test and permeability test were scatter, the directly measured *k* values is approach the extend trendline of *k* calculated from the consolidation test, hence, both *k* values were comparable. Therefore, it is suggested that the novel PBs have potential for use as core materials for GCLs designed for use in a high Na^+ concentration environment (e.g., sea water).

CHAPTER FIVE
BEHAVIOR OF GCLS USING POLYMERIZED BENTONITE

5.1 Introduction

Due to their low permeability and the ease of field installation, geosynthetic clay liners (GCLs), are widely used as an essential component in linear system of municipal solid-waste landfills (Bouazza 2002; Rowe et al. 2019; Scalia et al. 2018). A geotextile encased GCL consists of two layers of geotextiles and a sandwiched thin layer (4-5 mm) of bentonite, which controls the permeability of the GCL. Since the bentonite layer is thin, and during its installation, holes and/or spots without bentonite may be formed on the GCLs due to existence of sharp subjects in subgrade or ballast cover layers (FOX et al. 1998; Mazzieri and Pasqualini 1997; Rowe and Li 2020). Further, after GCLs installed in the field and covered with a layer of geomembrane, before placing the waste materials over it, the defects (spots without bentonite) can be formed due to so called down-slope moisture migration resulting from daily thermal cycles (Brachman et al. 2015; Rowe et al. 2016b, 2019; Take et al. 2015). Fortunately, expansion of hydrated bentonite can enter the defect spots and block the liquid flow through them. This is called self-healing of GCLs (Babu et al. 2001; Chai et al. 2016; Chai and Prongmanee 2020; Mazzieri and Pasqualini 2000; Prongmanee et al. 2018; Sari and Chai 2013; Shackelford et al. 2000).

Self-healing capacity of a GCL depends on the swelling capacity of the bentonite in it (Chai and Prongmanee 2020). For natural sodium bentonite, when it meets cation solution, its swelling capacity will decrease significantly (Katsumi et al. 2008; Prongmanee et al. 2018; Rowe 2020). To increase the swelling capacity of bentonite used in GCLs, several researches were conducted on using polymerized bentonite (De Camillis et al. 2017; Chai and Prongmanee 2020; Di Emidio et al. 2015; Ozhan 2018;

Prongmanee and Chai 2019). In this study, a novel polymerized bentonite (PB) using two monomers was developed, which has a higher swelling capacity, for example, its free swelling index (FSI) in 0.6 M NaCl solution was about 29 mL/2g. In engineering practice, it is desirable to predict self-healing capacity of a GCL to be used in a particular site under a particular environment, i.e., possible leakages to permeate into it. Chai et al. (2016) proposed a semi-empirical method for predicting self-healing capacity of GCLs with circular damage-holes. Further the method by Chai et al. (2016) is for GCLs with natural bentonites. In this chapter, Chai et al.'s method has been modified to be applicable for using PB as a core material.

In this section, the hydraulic properties of geotextile encased GCL using the novel PB as core was investigated by permeability test, and self-healing capacity test using deionized water (DI-W) and 0.6 M NaCl solution. Further, the predicted and measured self-healing ratios (healed area divided by the total damage area) were compared with the measured data.

5.2 Leakage rate and self-healing test

5.2.1 GCL specimen

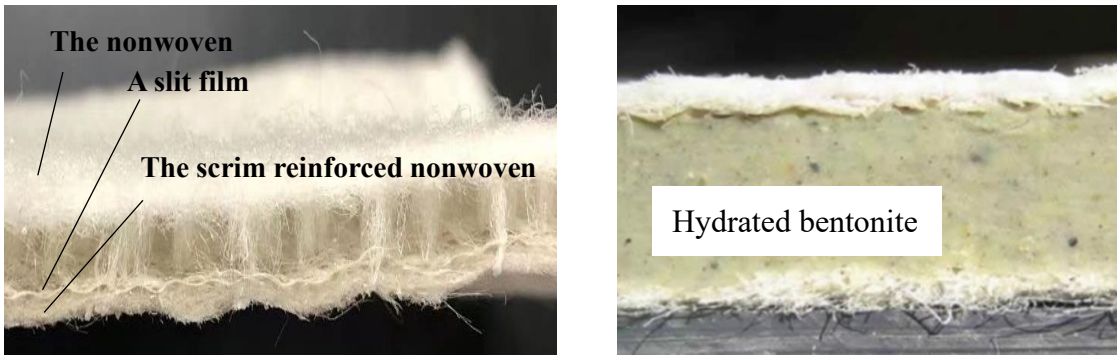

Fig. 5.1 (a) The GCL without original granular bentonite and (b) hydrated GCL sample

The geotextiles were obtained from a commercial GCL by removing the original bentonite. The cover geotextile is a nonwoven one, and the carrier geotextile has a slit film woven layer with scrim reinforced nonwoven as in Fig. 5.1 (a) and hydrated GCL sample in Fig. 5.1 (b). In addition, for easy to embed the UB (UB-GCL) or the PB (PB-GCL) uniformly between the two geotextiles, the cover and the carrier geotextiles were separated by cutting the bundle fibers. Therefore, the handmade GCLs were different from the commercial GCLs with the needle-punched bundle fibers. The detailed procedures will be described in the test method section.

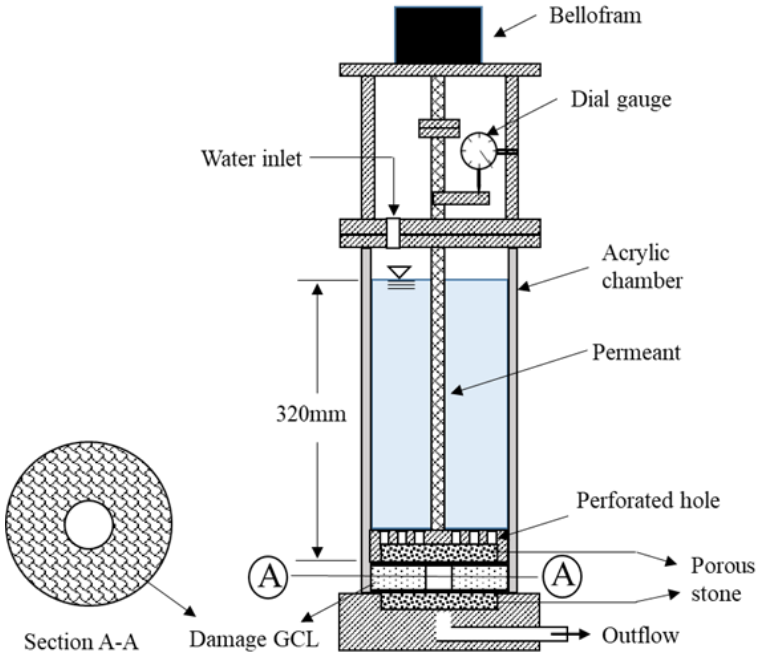

Fig. 5.2 Leakage rate test apparatus

5.2.2 Test method of leakage rate test

A rigid-wall constant head permeability cell was used to measure the leakage rate of the GCLs with and without a damage hole. The equipment was mainly composed of a piston loading system and an acrylic cell with an inner diameter of 150 mm. An overburden pressure of 20 kPa was applied using compressed air through a Bellofram cylinder system.

A porous stone was inserted into the perforated piston. The vertical displacement was measured with a dial gauge. A schematic view of the equipment is shown in Fig. 5.2. A constant water head of 320 mm was used in this study.

The detailed procedures are as follows:

(1) Calibration of the device

For GCL specimen with a damage hole, the flow rate will be basically controlled by the hydraulic resistance of the device itself (porous stones). A flow test without a GCL specimen was conducted. From the test result, the permeability of the porous stone used in the device of approximately 10^{-5} m/s was obtained (Prongmanee 2018).

(2) Test method

A rigid-wall constant head permeability cell was used to measure the leakage rate of the GCLs with a circular damage-hole. The liquids used were deionized-water (DI-W) and 0.6 M NaCl solution (simulating sea water). A constant water head of 320 mm was used in this study. The test procedures are as follows:

(a) A 150 mm diameter disk of the GCL specimen was cut from a sheet of a commercial GCL. Then, the original bentonite was removed out and replaced with the dry 0.1PB (0.1PB-GCL) and UB (UB-GCL). The dry mass per unit area of dry PB and UB used was 4 kg/m^2. To control the uniformity of handmade 0.1PB-GCL, for one 0.1PB-GCL sample, the amount of the PB was divided into four equal parts and carefully spread them on each quarter part of the carrier geotextile. Then added the cover geotextile and sealed the periphery of the sample by a tape and shook the specimen to make it as uniform and possible. Finally, the thickness of the specimen was measured at least at four different points and make sure that the difference was within 0.1 mm.

(b) A damage-hole was marked at the center of the specimen and trimmed using a sharp cuter, such as, the case of GCL's hole with diameter of 100 mm and 20mm were shown in Fig. 5.3.

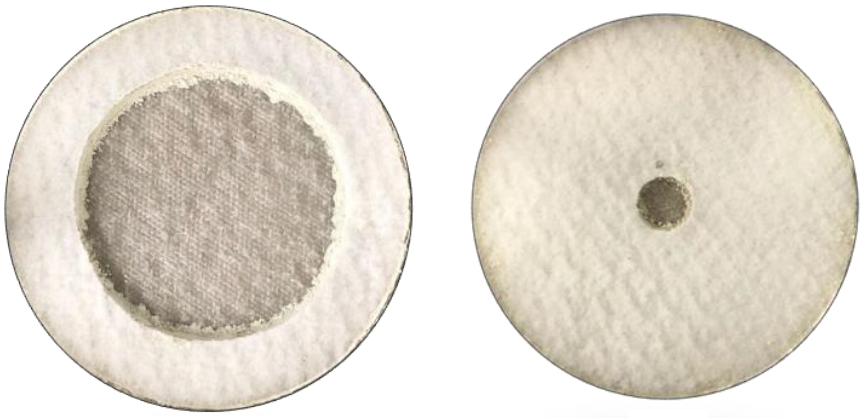

(a) (b)

Fig. 5.3 The GCL's hole with (a) diameter of 100 mm and (b) diameter of 20 mm

(c) The specimen was placed carefully into the apparatus. The piston was installed. A pressure of 20 kPa was applied. The liquid was poured into the chamber of the device.

(d) The drainage valve was opened, and leakage rate test was started. The liquid was added periodically to maintain the constant head of 320 mm. The flow rate as well as the vertical movement of the specimen were recorded periodically (Chai and Prongmanee 2020). After steady state flow was reached, the leakage rate test was stopped, and the mass and water content of the hydrated bentonite entered the damage hole were measured.

The tests were terminated after the flow rate stabilized or no measurable flow rate. The duration for each test was varied between 15 days to 30 days. After the test, the specimens were photographed both under natural light ("normal photo") and placed it on a transparent light box ("light box photo") in which a 40w fluorescent light bulb was placed as shown in Fig.5.4. Further, the indentation of the damage-hole was measured using a laser distance measuring device in case the holes were not fully filled by the UB or 0.1PB entered them. The properties of UB-GCL and 0.1PB-GCL with DI-W and 0.6 M NaCl solution are shown in Table 5.1 and Table 5.2, respectively. After self-healing

test, the final water content of the self-healed zone was higher than that of around zone. It is postulated that in the damage hole, UB or 0.1PB had more space to swell.

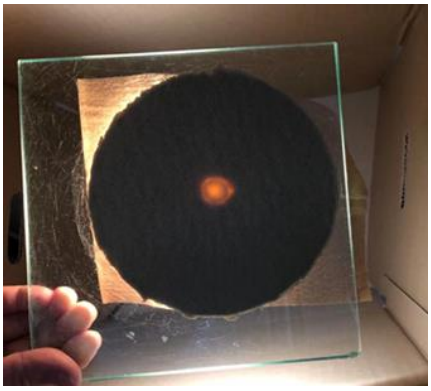

Fig. 5.4 A transparent light box

5.3 Results and discussions

5.3.1 Permeability *k* of intact GCL

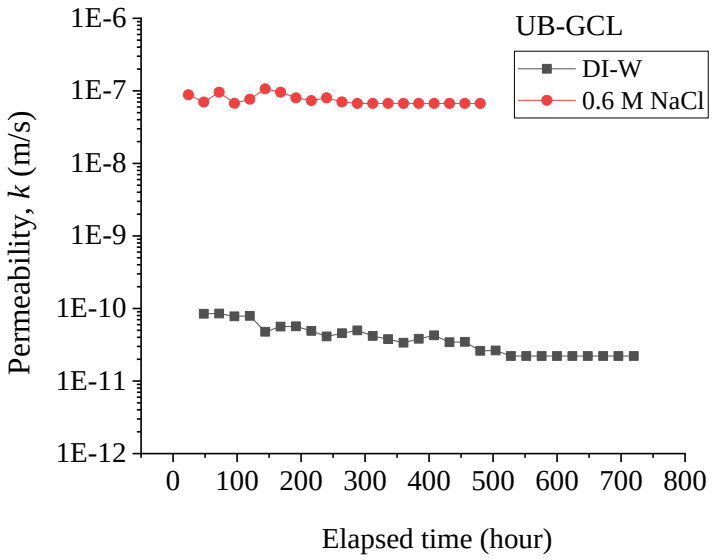

Fig. 5.5 Permeability of intact GCL in DI-W and 0.6 M NaCl solution

Fig. 5.5 show the results of permeability test of intact GCL in DI-W and 0.6 M NaCl solution. At the constant head of 320 mm, the value *k* of UB in DI-W is 2.21×10^{-11} m/s and in 0.6 M NaCl solution is 6.71×10^{-8} m/s. However, for 0.1PB, there were no liquid flow out from the leakage rate test, hence, the results of 0.1PB were not demonstrated.

Table 5.1 Properties of UB-GCL and 0.1PB-GCL with DI-W

Test-DI-W	Test duration (days)	Dry mass (g/m^2)	Initial water content w_i (%)	Final w_f (%)			Self-healed mass (g)	Initial hole diameter (mm)	Initial thickness (mm)	Final thickness (mm)
				Damage zone	Near damage zone	Edge of specimen zone				
0.1PB-80 mm	10	4000	0	876.2	521.7	247.3	3.13	80	7.5	11.6
0.1PB-90 mm	10	4000	0	890.1	561.9	301.8	3.62	90	7.5	11.8
0.1PB-100 mm	30	4000	0	831.8	682.6	585.1	6.16	100	7.5	15.4
UB-60 mm	25	4000	0	701.1	392.3	281.8	2.24	60	7.5	11.4
UB-80 mm	15	4000	0	754.9	278.5	276.5	1.99	80	7.5	9.6

Table 5.2 Properties of UB-GCL and 0.1PB-GCL with 0.6 M NaCl solution

Test-0.6 M NaCl	Test duration (days)	Dry mass (g/m^2)	Initial water content w_i (%)	Final w_f (%)			Self-healed mass (g)	Initial hole diameter (mm)	Initial thickness (mm)	Final thickness (mm)
				Damage zone	Near damage zone	Edge of specimen zone				
0.1PB-30 mm	20	4000	0	446.2	151.2	122.9	0.65	30	7.5	8.5
0.1PB-20 mm	20	4000	0	516.6	209.8	131.4	0.30	20	7.5	8.6
0.1PB-15 mm	20	4000	0	503.8	168.2	148.2	0.26	15	7.5	8.6
0.1PB-10 mm	20	4000	0	555.6	202.8	186.8	0.09	10	7.5	8.7
UB-10 mm	20	4000	0	500.1	133.6	115.3	0.01	10	7.5	7.8
UB-5 mm	20	4000	0	222.2	144.4	108.1	0.09	5	7.5	7.9

5.3.2 Self-healing capacity

(1) 0.1PB-GCL and UB-GCL in DI-W

(a) Photos of the specimens

The photos of the 0.1PB-GCL and UB-GCL specimens after the leakage rate tests are shown in Figs. 5.6 and 5.7 for using DI-W respectively. For the 0.1PB-GCL, the "normal photos" show that the damaged-holes of 80 mm, 90 mm and 100 mm in diameters were fully self-healed, and for UB-GCL, the damaged-hole up to 60 mm was self-healed. For GCLs with natural bentonite, Sari and Chai (2013) reported using tap water, a hole up to 30 mm in diamter can be self-healed; and Li and Rowe (2020) reported using DI-water, a hole up to about 40 mm can be self-healed. Therefore, the results in Fig. 5.6 demonstrate the high self-healing capacity of the PB-GCL. While the "light box photos" show that the light partialy penetrated the healed damage-holes. The closer to the center, the stronger the light. This indicates that the PB entered the damage-holes had higher water content and lower dry density.

(b) Indentations of the damage-holes for using DI-W

As shown in Fig. 5.6, for the three cases using DI-W, the holes were fully filled by hydrated PB. Fig. 5.9 shows the thickness variaitions of UB-GCL and 0.1PB-GCL specimens after the leakage rate tests using DI-W, which were measured by a laser distance measuring device as shown in Fig. 5.8. For the case 0.1PB-GCL with an initial damage-hole of 100 mm in diameter, and UB-GCL with an initail damage-hole of 60 mm, there were no indentation remained at the damage-hole location, but for the case UB-GCL of 80 mm damage-hole, there was a hole of about 20 mm in diameter remained. The self-healing ratio (healed damage area divided by the total damage area) was calculated using soft of Auto CAD measured areas. The UB-GCL of 80 mm damage-

hole is about 70.5%.

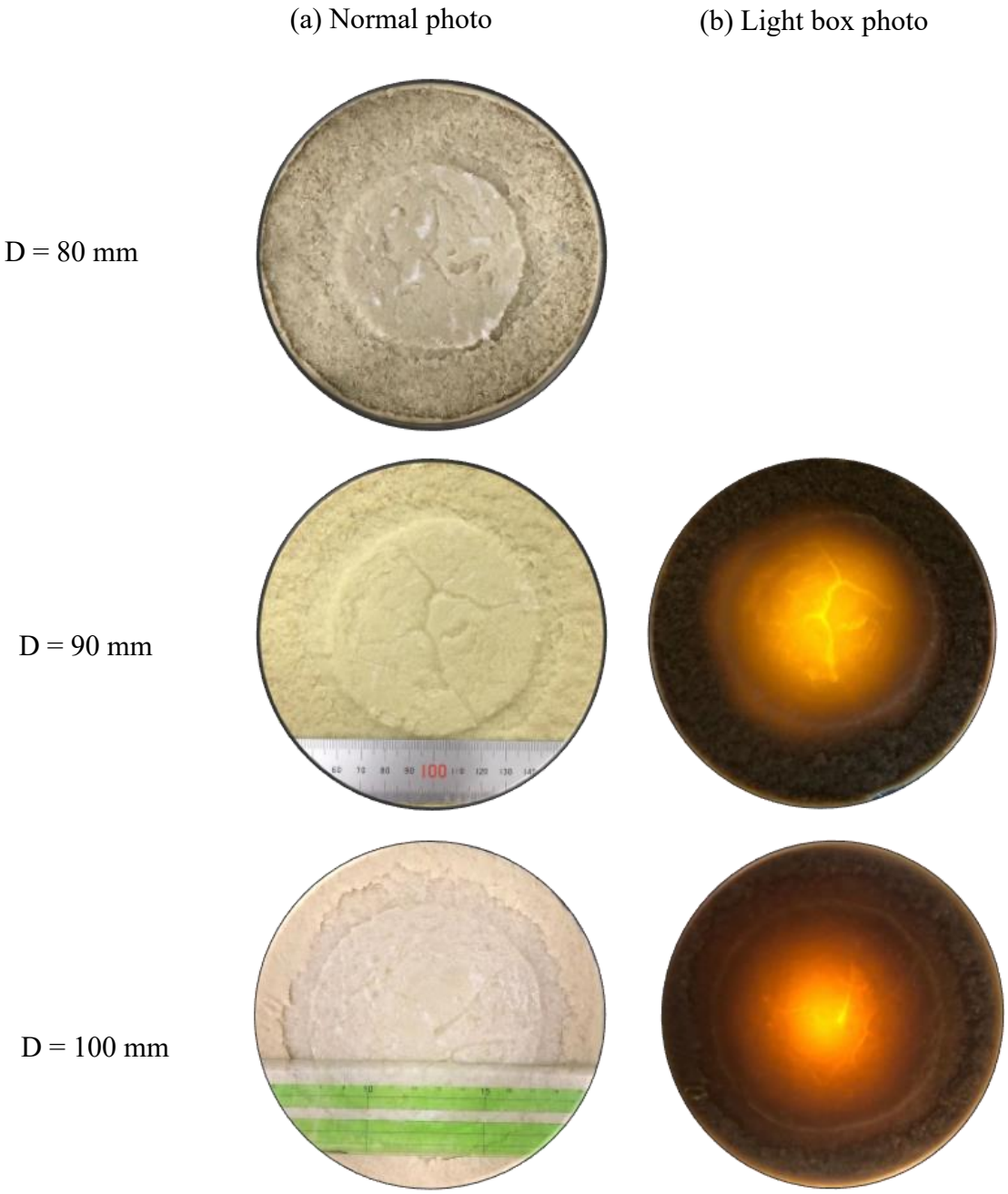

0.1PB-GCL in DI-W; specimen diameter: 150 mm

Fig. 5.6 Photos of damaged 0.1PB-GCL specimens after leakage rate test using DI-W

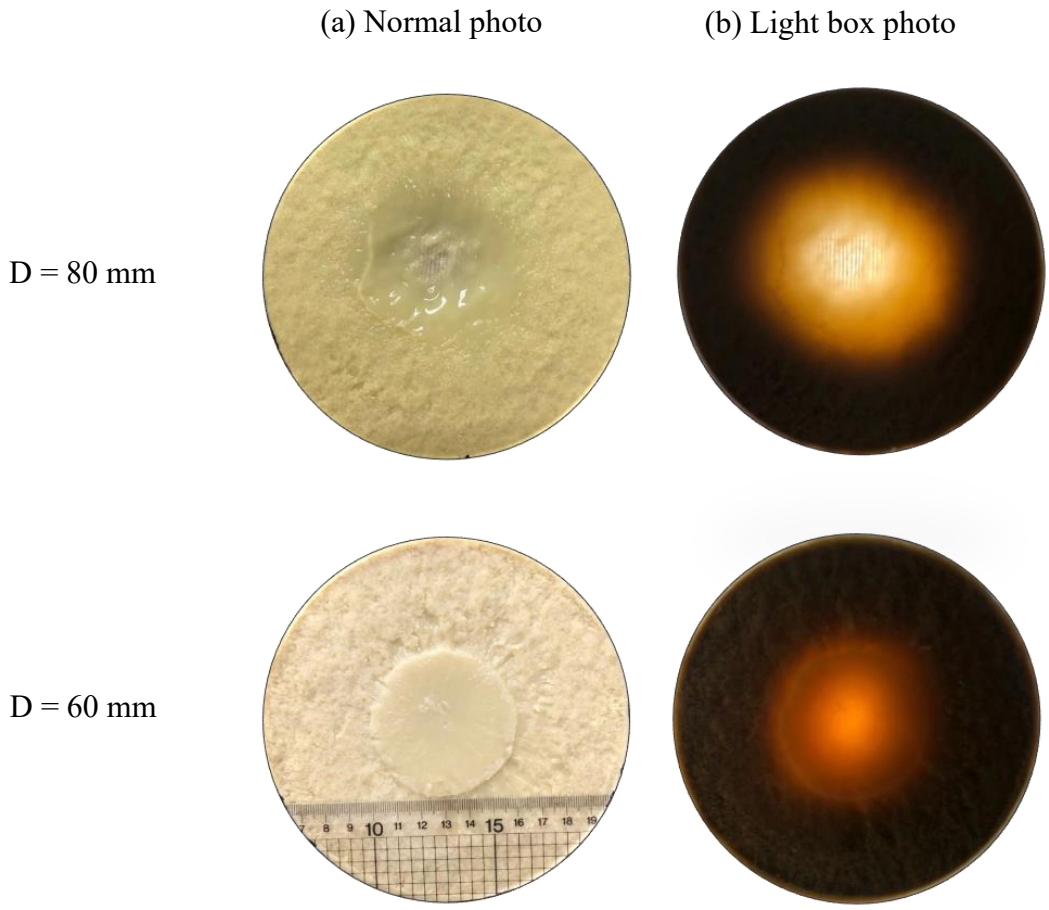

UB-GCL in DI-W; specimen diameter: 150 mm

Fig. 5.7 Photos of damaged 0.1PB-GCL specimens after leakage rate test using DI-W

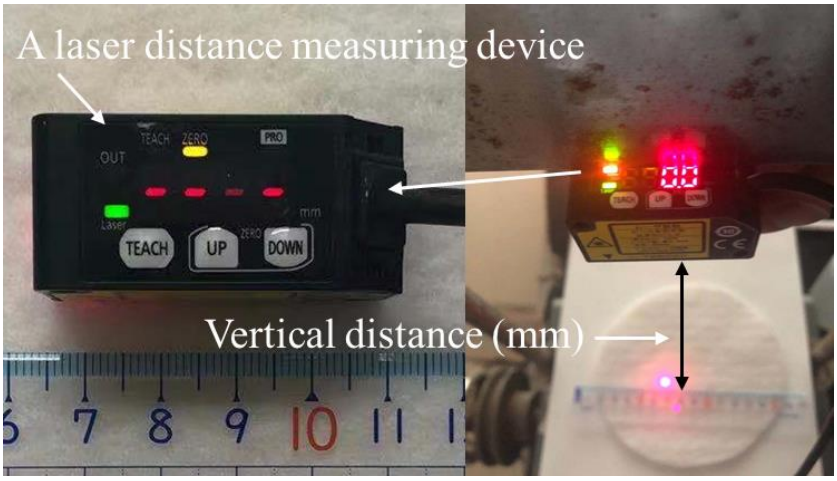

Fig. 5.8 A laser distance measuring device

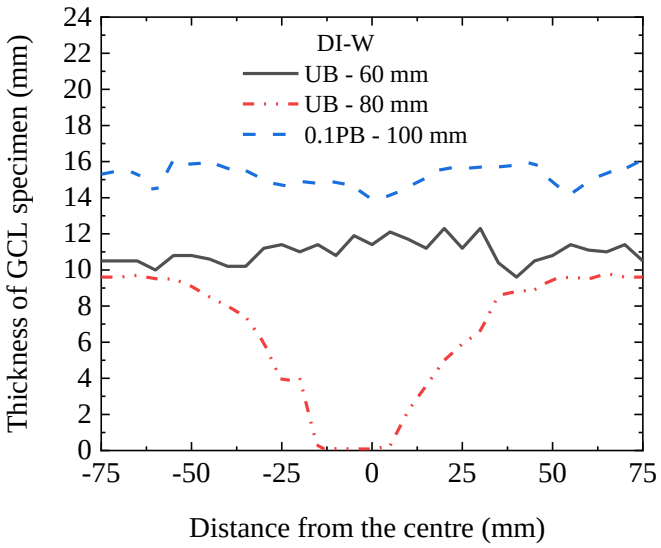

Fig. 5.9 Thickness variations of GCL specimens

(c) Permittivity of the damage holes

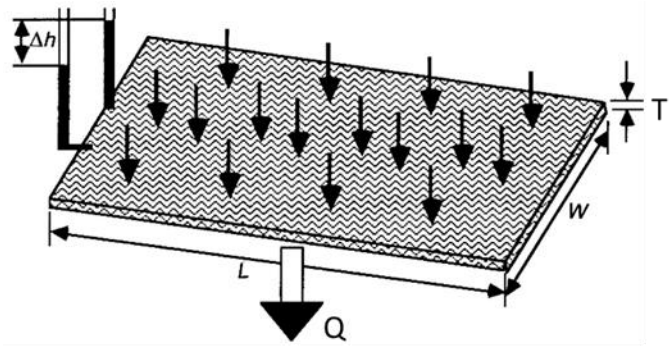

Fig. 5.10 The schematic diagram of the flow in the clay

Due to the thickness of the damage hole in GCL is not uniform and can not measure clear, the permittivity (ψ) of the damage hole was adopted. In Fig. 5.10 shows the schematic diagram of the flow in the clay, according to the Darcy law, the permeability (k) was calculated as follow Eq. (5.0):

$$k = (T \bullet Q)/(\Delta h \bullet A) \tag{5.0}$$

The permittivity (ψ) can be defined as follow Eq. (5.0a):

$$\psi = k/T = Q/(\Delta h \bullet A) \tag{5.0a}$$

Where k is the permeability, T is the thickness of specimen, Q is the steady of flow rate, Δh is head difference, A is the flow area.

The permittivity of the damage-hole (ψ_{hole}) was calculated as follows Eq. (5.0b):

$$\psi_{hole} = \frac{Q_{damage} - Q_{intact}(1 - A_{damage} / A_{total})}{A_{damage} \cdot \Delta h} \tag{5.0b}$$

where Q_{intact} is the steady flow rate of the intact sample, Q_{damage} is the steady flow rate of the damaged sample, A_{damage} is the damage area, A_{total} is the total cross-sectional area of the specimen, and Δh is the water head difference. For the conditions adopted, there were no flow measured for intact specimens of PB-GCL with DI-W for a duration of more than four weeks (Q_{intact} = 0). Therefore, the measured flow rates of PB-GCL was all from the damage-holes. The values of PB-GCL permittivity of 80 mm, 90 mm and 100 mm damage-holes with DI-W are shown in Fig. 5.10. The initial values of 10^{-2} -10^{-3} s^{-1} can be considered as the values of the porous stone used. After about 13 hours elapsed time, there was no measurable flow rate under a total head of 320 mm. Assuming the thickness of the PB entered the holes as T, the corresponding permeability of the healed damage hole will be, $k = T \cdot \psi_{hole}$. With the final value of ψ_{hole} in Fig. 5.11 and T = 15 mm (measured value), the permeability of the healed damage-holes can be evaluated as in 10^{-9} m/s order. For the UB-GCL permittivity of 60 mm and 80 mm damage-hole with DI-W are shown in Fig. 5.12. After steady state flow was reached, measured both T of 60 mm and 80 mm damage-hole is 11.4 mm and 9.6 mm, respectively in table 5.1. The permeability of 60 mm and 80 mm the healed damage-holes can be evaluated as in 10^{-10} m/s and 10^{-5} m/s order respectively.

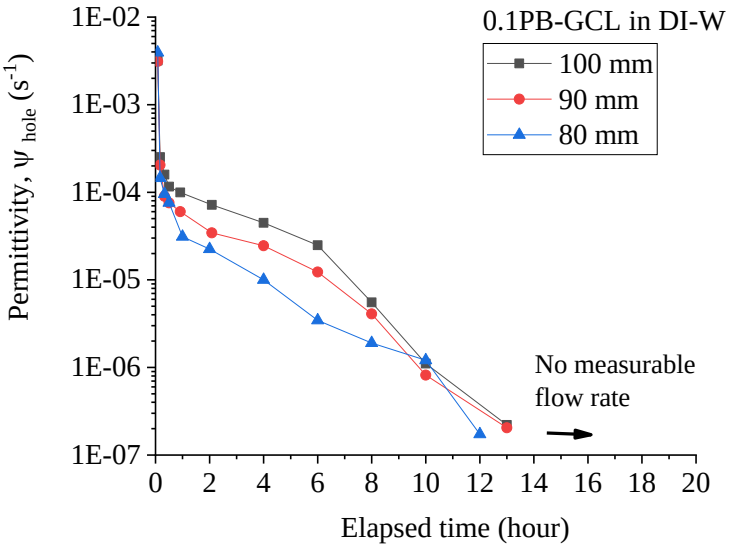

Fig. 5.11 Permittivity (ψ_{hole}) versus elapsed time of the 0.1PB-GCL in DI-W

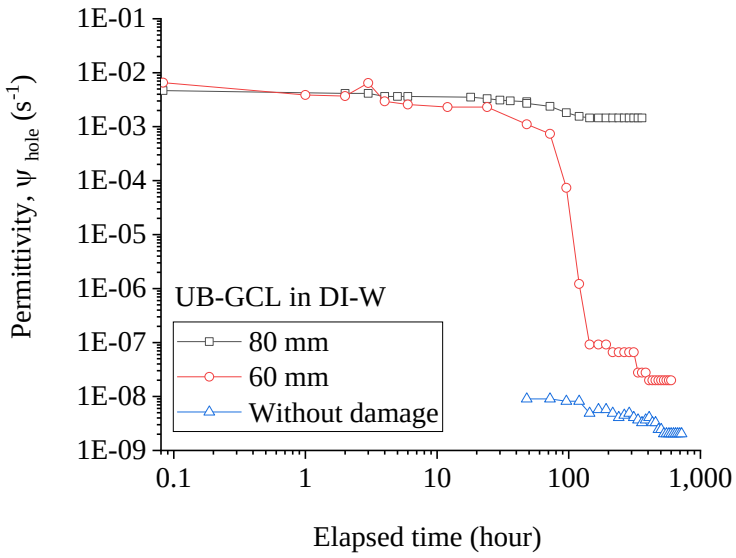

Fig. 5.12 Permittivity (ψ_{hole}) versus elapsed time of the UB-GCL in DI-W

(2) PB-GCL and UB-GCL in 0.6 M NaCl solution

(a) Photos of the specimens

The photos of the 0.1PB-GCL and UB-GCL specimens after the leakage rate tests are shown in Figs. 5.13 and 5.14 for using 0.6 M NaCl solution respectively. It is observed that the "normal photos" show that for 0.1PB-GCL damage-holes up to 15 mm

in diameters were self-healed (Fig. 5.13), for UB-GCL damage-holes up to 5 mm in diameters were self-healed (Fig. 5.14). The same as for using DI-water, even for the self-healed cases, light partially penetrated the healed areas in the “light box photos”.

(b) Indentations of the damage-holes for using 0.6 M NaCl solution

As shown in Fig. 5.15 (a), for UB-GCL, the case with an initial damage-hole of 5 mm in diameter was fully filled by hydrated UB and the hole with 10 mm, there is a 5.5 mm depth and 4 mm in diameter hole remained. In Fig. 5.15 (b), for the case of 0.1PB-GCL with an initial damage-hole of 15 mm in diameter, there was no indentation remained at the damage-hole location, but for the case of 20 mm damage-hole, there was a hole of about 5 mm in diameter remained. The self-healing ratio of 0.1PB-GCL with 20 mm and 30 mm damage-hole is about 90.0% and 65.0% respectively. Self-healing ratio of UB-GCL with 10 mm damage-hole is about 9.6%.

(c) Permittivity of the damage holes using 0.6 M NaCl

The variations of permittivity for 0.1PB-GCL damage-holes of 10 to 30 mm in diameters with 0.6 M NaCl solution are shown in Fig. 5.16. It can be seen that after about 15 days elapsed time, the measured flow rates were becoming steady. For these cases, the measured thickness of the GCL specimens was about 9 mm (Table 5.2), and the permeability of the healed damage-holes of 10 mm and 15 mm in diameters was in the order of 10^{-8} m/s.

Fig. 5.17 shows the variations of permittivity for UB-GCL damage-holes of 5 and 10 mm in diameters. The measured thickness of the GCL specimens was about 8 mm (Table 5.2), and the permeability of the healed damage-holes of 5 mm and 10 mm in diameters was in the order of 10^{-7} and 10^{-5} m/s respectively.

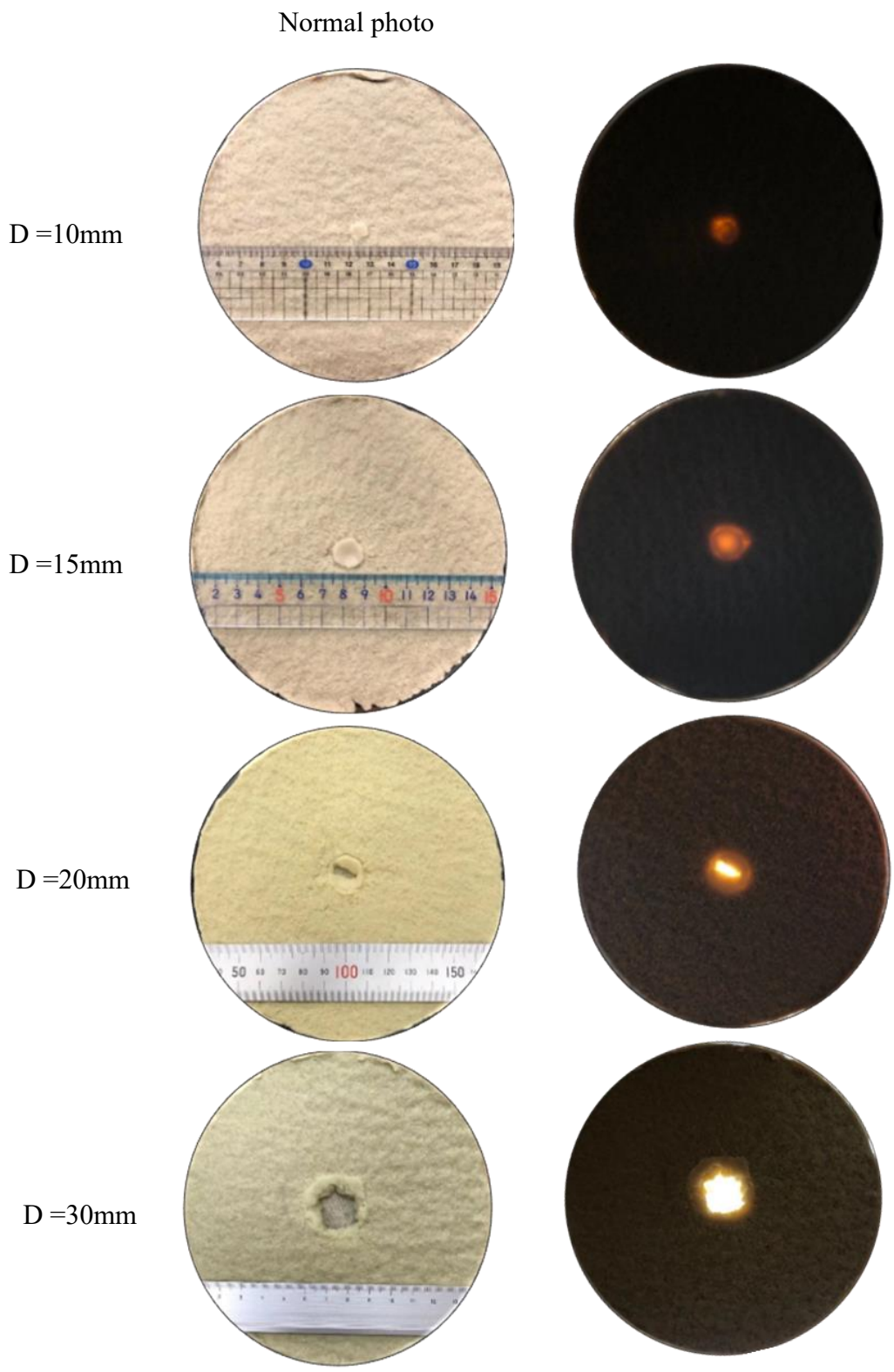

Fig. 5.13 Photos of damaged 0.1PB-GCL specimens after leakage rate test using 0.6 M NaCl solution

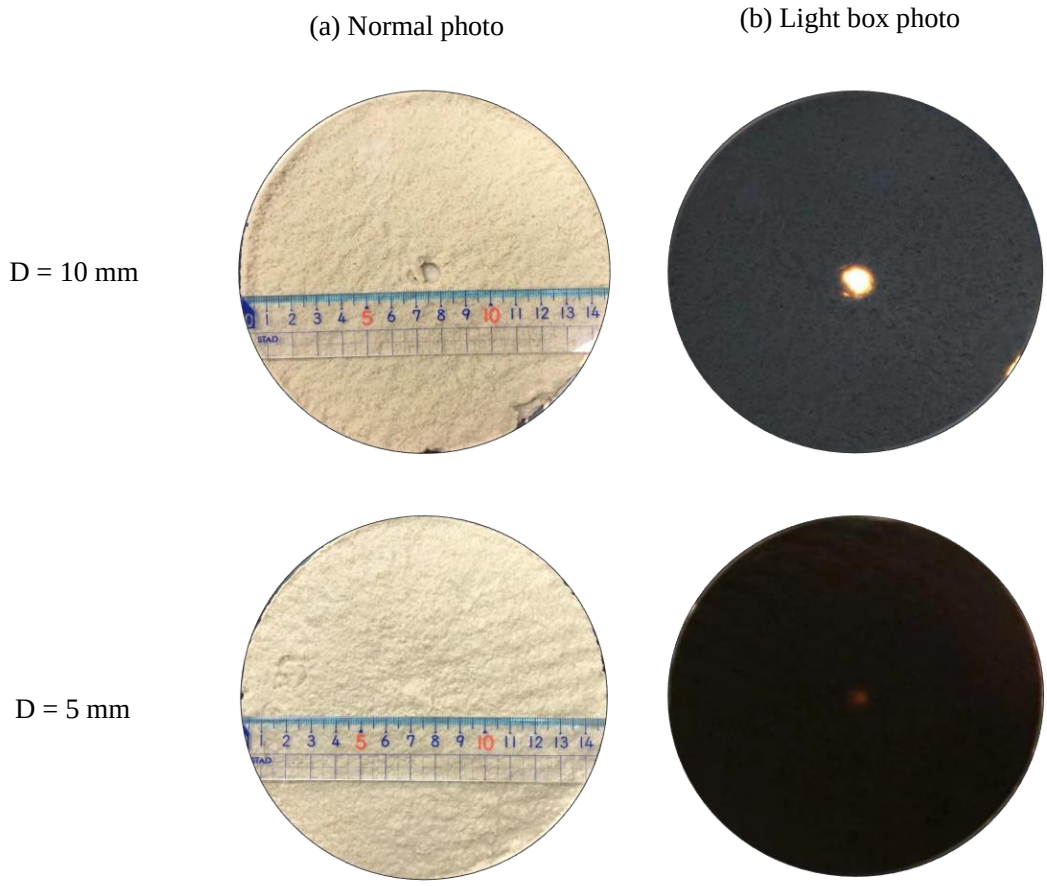

Fig. 5.14 Photos of damaged UB-GCL specimens after leakage rate test using 0.6 M NaCl solution

For a different PB, Chai and Prongmanee (2020) reported that, under the same void ratio condition, the permeability of the PB with 0.6 M NaCl solution was much higher than that with DI-W.

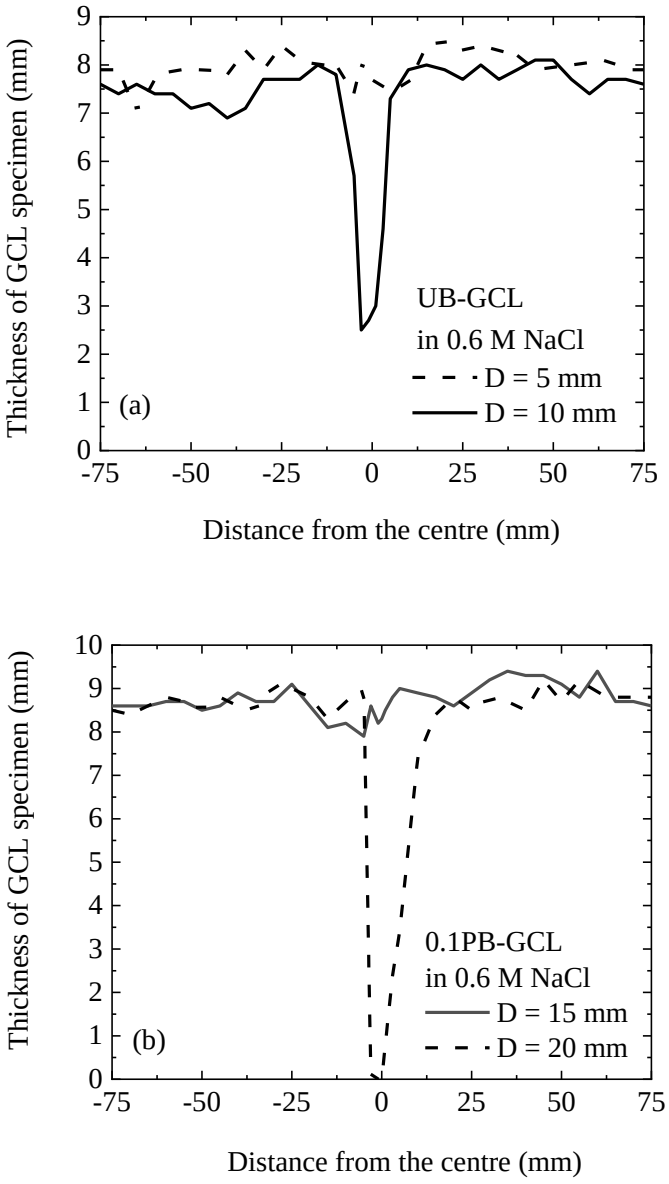

Fig. 5.15 Thickness variations of GCL specimens (a) UB-GCL and (b) 0.1PB-GCL

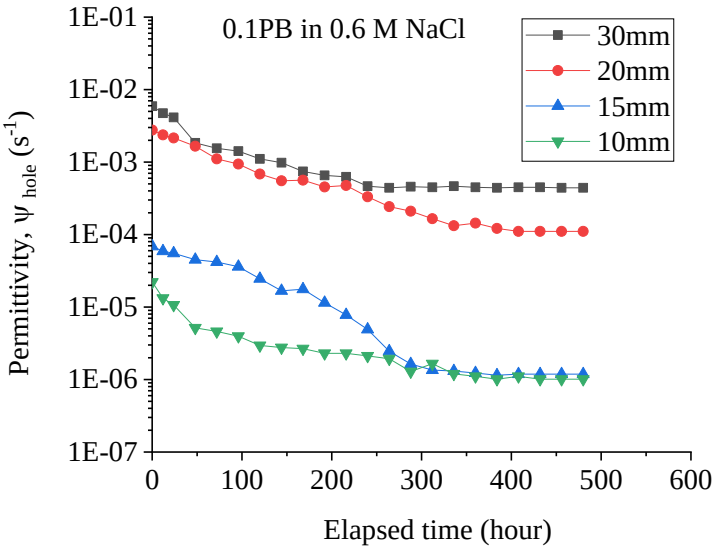

Fig. 5.16 Permittivity (ψ_{hole}) versus elapsed time of the 0.1PB-GCL in 0.6 M NaCl solution

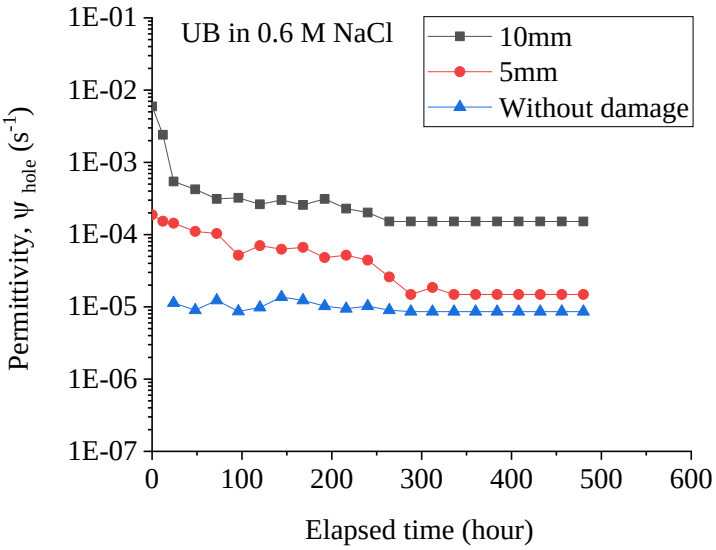

Fig. 5.17 Permittivity (ψ_{hole}) versus elapsed time of the UB-GCL in 0.6 M NaCl solution

5.4 Predicting self-healing capacity of GCLs with circular damages

5.4.1 Modified prediction method

The self-healing ratio (α) is defined as the ratio of healed damage area (A_1) and total damage area (A): $\alpha = A_1/A$. A_1 is a function of the amount (mass) of bentonite (m_b) entered a damage-hole; water content (w) of the bentonite in the damage-hole; and (c) the thickness (t) of the hydrated GCL. For circular damage-hole, Chai et al. (2016) proposed the following equations for predicting the value of m_b, w and t.

$$m_b = m_0 \frac{D}{D_0} \frac{t_b}{t_{b0}} \left(\frac{w_l}{w_{l0}} \right)^{0.55} \left(1 - 0.2 \left(\frac{p'}{2 \cdot p_a} \right)^{0.1} \right) \qquad (p' \le 200 \text{ kPa}) \qquad (5.1)$$

where D is the diameter of a damage-hole, D_0 is a constant (= 50 mm), m_0 is a constant (= 3 g for natural bentonite), w_l is the liquid limit of bentonite with the liquid tested, w_{l0} is the liquid limit of bentonite using DI-W, p_a is atmospheric pressure, p' is the overburden pressure on the GCL, t_b is the initial thickness of bentonite layer in the GCL, and t_{b0} = 4 mm (a reference thickness).

$$w = w_l \left(\frac{D}{D_0} \right)^{0.35} \left(1 - 0.25 \left(\frac{p'}{2 \cdot p_a} \right)^{0.05} \right) \qquad (p' \le 200 \text{ kPa}) \qquad (5.2)$$

$$t = t_g + (1 + e_0) \frac{M_s}{G \rho_w} \left[1 - \frac{\gamma \cdot C_s}{1 + e_0} \log \left(\frac{p'}{p'_0} \right) \right] \qquad (5.3)$$

where t_g is the thickness of geomembrane in case of geomembrane supported GCL (GM-GCL), and the thickness of geotextiles in case of geotextile encased GCL (GT-GCL), e_0 is the initial void ratio of the bentonite, G is specific gravity of the bentonite particles, ρ_w is density of water, p'_0 is a reference pressure, and γ is a reduction factor. For GT-GCL, considering the hydrated bentonite can enter the pores of the geotextiles, an effective thickness t_g = 0.5 mm was suggested. The original equation for calculating the thickness, t, did not contain the parameter γ, and Eq. (5.3) is a modified one. The

original equation considers the effect of swelling on the thickness of a GCL, but ignored the effect of the bentonite entering the damage-hole. The latter is a function of size of the damage-hole to the size of the sample tested, and amount of bentonite entered the hole. To avoid too complicity, a reduction factor, γ is adopted to approximately consider this effect. The value of γ has been back-estimated as 0.9. Further, the initial thickness of bentonite layer t_b in the original equation has been replaced by $(1+e_0)M_s/G\rho_w$ (M_s is the dry bentonite mass per unit area in a GCL).

In Eq. (5.1), t_b and t_{b0} are parameters representing amount of bentonite in a GCL. Therefore, it has been modified to use dry bentonite mass per unit area (M_s) instead. The modified Eq. (5.1) becomes:

$$m_b = m_0 \frac{D}{D_0}\frac{M_s}{M_{s0}}\left(\frac{w_l}{w_{l0}}\right)^{0.55}\left(1-0.2\left(\frac{p'}{2\cdot p_a}\right)^{0.1}\right) \qquad (p' \le 200 \text{ kPa}) \quad (5.1a)$$

M_{s0} is a reference dry bentonite mass per unit area, and the value is related to the value of m_0. The geotextile encased GCL tested by Chai et al. (2016) had a dry bentonite mass per unit area of approximately 4,100 g/m^2, and therefore, M_{s0} = 4,100 g/m^2.

Then α can be calculated as (Chai et al. 2016):

$$\alpha = min\left(1, \beta\frac{v_1}{v_0}\right) \quad (5.4)$$

$$v_1 = (1+wG)\frac{m_b}{G\rho_w} \quad (5.5)$$

$$v_0 = \frac{\pi D^2}{4}t \qquad \text{(Circular damage)} \quad (5.6)$$

where v_1 is the volume of the hydrated bentonite entered the damage-hole, v_0 is the volume of the damage-hole, and β is a factor linking ratio of volume (v_1/v_0) to ratio of area (α is defined as the ratio of area), and β = 1.1 was proposed (Chai et al. 2016).

5.4.2 Comparing predicted and measured self-healing ratios

The modified prediction method was applied to the 0.1PB-GCL. The swelling index (Cs) of 0.1PB is 4.18 using DI-W and 0.67 using 0.6 M NaCl solution. It was found that the prediction under estimated the self-healing ratio significantly. One of the key parameters affect the predicted self-healing ratio is the predicted amount of bentonite entered a damage-hole (Eqs (5.1a). In Eqs (5.1a), the constant m_0 = 3 g was calibrated from GCLs using natural bentonite. The PB has higher swelling capacity, and there would be more PB entering a damage-hole. Using the test results in this study, it has been back evaluated that using m_0 = 5.5 g in Eqs (5.1a), reasonable predictions can be resulted. Therefore, the predicted results presented below using m_0 = 5.5 g in Eqs (5.1a). In prediction calculation, the referring pressure p'_0 in Eq (5.3) of 300 kPa was assumed. The PB-GCL used powder PB (passing 75 μm sieve), under an overburden pressure of 20 kPa, the measured void ratio was 2.5.

Table 5.3 Sizes of damages as well as self-healing ratios for the test data from this study

No	**Dry mass per unit area (kg/m^2)**	**Liquid**	***D*** **(mm)**	**Measured** α_m	**Predicted** α_p	**Remark**
C1	4.0	DI-water	90	1.00	1.00	Polymerized bentonite (0.1PB)
C2	4.0		100	1.00	0.98	
C3	4.0	0.6 M NaCl	10	1.00	1.00	
C4	4.0		15	1.00	1.00	
C5	4.0		20	0.90	0.89	
C6	4.0		30	0.65	0.67	

The measured and predicted self-healing ratios are listed in Table 5.3 and compared

in Fig. 5.18, and agreement between them is good.

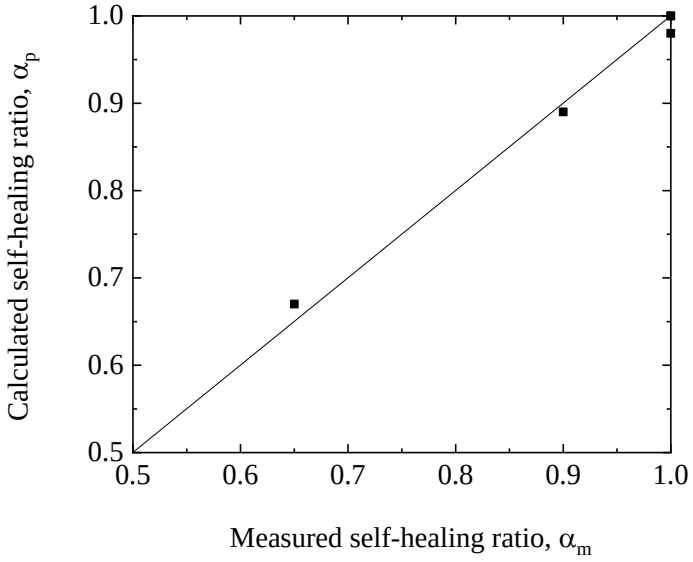

Fig. 5.18 Comparison of measured and predicted self-healing ratio for the test data from this study

5.5 Summary

In this chapter, the permeability and self-healing capacity of GCLs using the novel polymerized bentonite (PB) or UB as a core material were evaluated through laboratory leakage rate tests. The liquids used were deionized-water (DI-W) and 0.6 M NaCl. Further, the method for predicting self-healing capacity of a GCL with a damage hole was investigated by comparing the predictions with the measured data. Based on the experimental results and analysis, following conclusions can be drawn.

(1) For PB-GCL, the test results show that with DI-W, a circular damage-hole up to 100 mm in diameter, and with 0.6 M NaCl solution (simulating sea water), a damage-hole up to 15 mm in diameter were self-healed. While in the case of the PB-GCL specimen with 20 mm and 30 mm damage-hole, the self-healing ratios were about 90% and 65%, respectively. For UB-GCL in DI-W, a damage hole up to 60 mm in diameter

was self-healed and in 0.6 M NaCl solution up to 5 mm was self-healed.

(2) The method for predicting self-healing capacity of GCL with a circular damage-hole proposed by Chai et al. in 2016 has been modified to be applicable for PB-GCL. The analysis results indicate that a key model parameter, a reference mass of bentonite entered a damage-hole has to be modified from 3 g (for UB) to 5.5 g (for PB). With this modification, good agreement between the measured and predicted self-healing ratios (healed area divided by the total damage area) of PB-GCL was obtained.

CHAPTER SIX
CONCLUSIONS AND RECOMMENDATIONS

6.1 Conclusions

Polymerized bentonites (PBs) as new barrier material used in GCL system because they can keep lower permeability and high swelling pressure when in contact with aggressive chemical environments. However, PB (10% polymer content) still cannot meet the requirement (free swelling index (FSI) > 24 mL/2g) to be used as the core of geosynthetics clay liner (GCL) under aggressive environment, such as 0.6 M NaCl solution (simulated sea water condition).

In this study, a novel PB was developed to meet the FSI value more than 24 mL/2g in 0.6 M NaCl. A simple polymerization procedure as well as suitable conditions for polymerization were established. The properties tested were morphologies determined by X-ray diffraction (XRD), physical properties (w_l, w_p, and G), swelling properties (FSI and swelling pressure), consolidation properties (compression indexes (C_c) and the calculated and directly measured permeability value (k)). Finally, the self-healing capacity of the novel GCL with PB as core material (PB-GCL) was evaluated by leakage rate test and the new method of predicting self-healing capacity was proposed. Based on the test results, the following conclusions can be drawn.

6.1.1 Polymerized bentonite

(1) developing a novel PB

New polymerized bentonites (PBs) were produced using natural sodium bentonite (UB) and two monomers, acrylic acid (M_1) and acrylamide (M_2), using the free radical polymerization method. The initiator (I) used was potassium persulfate. For simplifying the procedure of polymerization process, instead of using nitrogen gas, vacuum pressure

was used to remove oxygen from the mixture of the bentonite and the monomers. The conditions established for polymerization were: pH of 6, $I/(M_1 + M_2) = 0.5\%$, and $M_1/M_2 = 0.5$, which were evaluated using FSI of produced PBs with 0.6 M NaCl solution.

From the results of XRD, it is postulated that the structure of 0.1PB is the phase-separated type, and the product is a microcomposite. Others PBs, e.g., 0.2PB and 0.4PB mean polymer/bentonite ratio of 0.2, 0.4 and using two monomers; 0.1PB-AA and 0.4PB-AA mean polymer/bentonite ratio of 0.1, 0.4 and using acrylic acid as monomer; and 0.1PB-AM and 0.4PB-AM mean polymer/bentonite ratio of 0.1, 0.4 and using acrylamide as monomer, the d-spacing of the bentonite particles was increased, and it is postulated that the structure is intercalated and the products are nanocomposite. The SEM images of swelled PBs show there were large amount of polymer like net structures between bentonite particles. Higher polymer content, more polymer like networks in PBs. These polymers networks will have an important role in increasing the resistance to aggressive cation solutions.

(2) Properties of the PB

The 0.1PB, 0.2PB and UB were evaluated by a series of experiment test, e.g., FSI test, swelling pressure test, consolidation test and permeability test. The results from FSI test show that the PBs had higher FSI values than those of UB. With 0.6 M NaCl solution, the FSI of 0.1PB was approximately 30 ml/2g which exceed the requirements to be used in GCLs (24 mL/2g). The results of the swelling pressure tests indicate that the PBs had higher swelling capacities than those of UB in DI-W and cation solutions (e.g., 0.6 M NaCl and 0.03-0.06 M $CaCl_2$). The novel PBs (0.1PB, 0.2PB and 0.4PB) have two hydrophilic groups, $-CONH_2$ and -COONa. Due to both groups can be connected with exchangeable cations directly or indirectly by physical interaction, the amount of cations entering the diffuse double layers of bentonite particles were reduced. This increased the

resistance of PBs to the cation solutions with high concentration (0.6 M NaCl solution) and kept high swelling capacity.

The results of the consolidation tests show that for all liquids tested, the compression indexes (C_c) of PBs were higher than that of UB. The higher the polymer content, the higher the C_c value. For a given void ratio, the order of permeability is $k_{UB} > k_{0.1PB} > k_{0.2PB}$ (subscripts indicate the corresponding materials). For void ratios up to 5 for 0.1PB and 7 for 0.2PB, the calculated values of k from the consolidation test results for PBs are still smaller than 10^{-10} m/s for both the 0.6 M NaCl and 0.03-0.06 M $CaCl_2$ solutions. The result from the direct permeability test, for void ratio at 7.46, the k of 0.1PB is approximately 2.8×10^{-11} m/s in 0.6 M NaCl solution. Although k values from consolidation test and permeability test were scatter, the directly measured k values is approach the extend trendline of k calculated from the consolidation test, hence, both k values were comparable.

Therefore, it is suggested that the novel PBs have a potential for use as core materials for GCLs to be used in a high Na^+ concentration environment (e.g., sea water).

6.1.2 Self-healing capacity of GCL with polymerized bentonite

(1) For PB-GCL, the test results show that with DI-W, a circular damage-hole up to 100 mm in diameter, and with 0.6 M NaCl solution, a damage-hole up to 15 mm in diameter were self-healed. While in the case of the PB-GCL specimen with 20 mm and 30 mm damage-hole, the self-healing ratios were about 90% and 65%, respectively. For UB-GCL in DI-W, a damage hole up to 60 mm in diameter was self-healed and in 0.6 M NaCl solution up to 5 mm was self-healed.

(2) The method for predicting self-healing capacity of GCL with a circular damage-hole proposed by Chai et al. in 2016 has been modified to be applicable for PB-GCL. The analysis results indicate that a key model parameter, a reference mass of bentonite

entered a damage-hole has to be modified from 3 g (for UB) to 5.5 g (for PB). With this modification, good agreement between the measured and predicted self-healing ratios (healed area divided by the total damage area) of PB-GCL was obtained.

6.2 Recommendations for future work

The present study uses two monomers for producing the novel polymerized bentonite (PB). The novel PB has been proved that it has higher swelling capacity and lower permeability in aggressive solution (sea water). However, durability and effect of possible drying and wetting cycle on the properties of the novel PB are still not clear. These issues should be investigated in the future.

REFERENCES

ASTM D5890. Standard test method for swell index of clay mineral component geosynthetic clay liners ASTM International, West Conshohocken, PA, USA.

ASTM D4546. Standard test methods for one-dimensional swell or settlement potential of cohesive soils ASTM International, West Conshohocken, PA, USA.

ASTM D2435. Standard test methods for one dimensional consolidation properties of soils using incremental loading ASTM International, West Conshohocken, PA, USA.

ASTM D4972. Standard test methods for pH of soils ASTM International, West Conshohocken, PA, USA.

ASTM D4318. Standard test methods for liquid limit, plastic limit, and plasticity index of soils. American Society for Testing and Materials, West Conshohocken, PA, USA.

ASTM D854. Standard test methods for specific gravity of soil solids by water pycnometer method, American Society for Testing and Materials, West Conshohocken, Pennsylvania, USA.

ASTM D5887. Standard Test Method for Measurement of Index Flux Through Saturated Geosynthetic Clay Liner Specimens Using a Flexible Wall Permeameter. American Society for Testing and Materials, West Conshohocken, Pennsylvania, USA.

Abhilash, V., Rajender, N., and Suresh, K. (2016). X-ray diffraction spectroscopy of polymer nanocomposites. Spectroscopy of Polymer Nanocomposites, Elsevier Inc.

Ahmed, E. M. (2015). Hydrogel: Preparation, characterization, and applications: A review. Journal of Advanced Research, Cairo University, 6(2), 105–121.

Alexandre, M., and Dubois, P. (2000). Polymer-layered silicate nanocomposites:

Preparation, properties and uses of a new class of materials. Materials Science and Engineering R: Reports, 28(1), 1–63.

Ashmawy, A. K., El-Hajji, D., Sotelo, N., and Muhammad, N. (2002). Hydraulic performance of untreated and polymer-treated bentonite in inorganic landfill leachates. Clays and Clay Minerals, 50(5), 546–552.

Babu, G. L. S., Sporer, H., Zanzinger, H., and Gartung, E. (2001). Self-healing properties of geosynthetic clay liners. Geosynthetics International, 8(5), 461–470.

Barvenik, F. W. (1994). Polyacrylamide characteristics related to soil applications. Soil Science, 158(4), 235–243.

Behera, S., and Mahanwar, P. A. (2020). Superabsorbent polymers in agriculture and other applications: a review. Polymer-Plastics Technology and Materials, 59(4), 341–356.

Benson, C. H., and Meer, S. R. (2009). Relative abundance of monovalent and divalent cations and the impact of desiccation on geosynthetic clay liners. Journal of Geotechnical and Geoenvironmental Engineering, 135(3), 349–358.

Billmeyer, F. W. (1984).Textbook of polymer science, third ed. Wiley, New York, USA.

Bohnhoff, G. L., and Shackelford, C. D. (2013). Improving membrane performance via bentonite polymer nanocomposite. Applied Clay Science, Elsevier B.V., 86, 83–98.

Bohnhoff, G. L., and Shackelford, C. D. (2014). Consolidation Behavior of Polymerized Bentonite-Amended Backfills. Journal of Geotechnical and Geoenvironmental Engineering, 140(5), 04013055.

Bouazza, A. (2002). Geosynthetic clay liners. Geotextiles and Geomembranes, 20(1), 3–17.

Brachman, R. W. I., Rentz, A., Rowe, R. K., and Take, W. A. (2015). Classification and

quantification of downslope erosion from a geosynthetic clay liner (GCL) when covered only by a black geomembrane. Canadian Geotechnical Journal, 52(4), 395–412.

De Camillis, M., Di Emidio, G., Bezuijen, A., and Verástegui-Flores, R. D. (2016). Hydraulic conductivity and swelling ability of a polymer modified bentonite subjected to wet–dry cycles in seawater. Geotextiles and Geomembranes, 44(5), 739–747.

De Camillis, M., Di Emidio, G., Bezuijen, A., Verastegui Flores, D., Van Stappen, J., and Cnudde, V. (2017). Effect of wet-dry cycles on polymer treated bentonite in seawater: swelling ability, hydraulic conductivity and crack analysis. Applied Clay Science, 142, 52–59.

Chai, J. C., Sari, K., Shen, S. L., and Cai, Y. (2016). Predicting self-healing ratio of GCL with a damage hole. Geotextiles and Geomembranes, 44(5), 761–769.

Chai, J. C., and Shen, S.L. (2018). Predicting Swelling Behavior of a Na^{+}-Bentonite Used in GCLs. International Journal of Geosynthetics and Ground Engineering, 4(1).

Chai, J. C., and Prongmanee, N. (2020). Barrier properties of a geosynthetic clay liner using polymerized sodium bentonite. Geotextiles and Geomembranes, Elsevier, 48(3), 392–399.

Chen, J. N., Benson, C. H., and Edil, T. B. (2018). Hydraulic conductivity of geosynthetic clay liners with sodium bentonite to coal combustion product leachates. Journal of Geotechnical and Geoenvironmental Engineering, 144(3).

Chen, J., Salihoglu, H., Benson, C. H., Likos, W. J., and Edil, T. B. (2019). Hydraulic Conductivity of Bentonite-Polymer Composite Geosynthetic Clay Liners Permeated with Coal Combustion Product Leachates. Journal of Geotechnical and Geoenvironmental Engineering, 145(9).

Christian, W., Zainab, B., Tian, K., and Abichou, T. (2020). Effect of specimen preparation on the swell index of bentonite-polymer GCLs. Geotextiles and Geomembranes, 48, 875-885.

Deng, Y., Dixon, J. B., White, G. N., Loeppert, R. H., and Juo, A. S. R. (2006). Bonding between polyacrylamide and smectite. Colloids and Surfaces A: Physicochemical and Engineering Aspects, 281(1–3), 82–91.

Di Emidio, G., Van Impe, W. F., and Flores, R. D. V. (2011). Advances in geosynthetic clay liners: Polymer enhanced clays. Geotechnical Special Publication, 1931–1940.

Di Emidio, G., Mazzieri, F., Verastegui-Flores, R.-D., Van Impe, W., and Bezuijen, A. (2015). Polymer-treated bentonite clay for chemical-resistant geosynthetic clay liners. Geosynthetics International, 22(1), 125–137.

EPA. (2017). Geosynthetic clay liners used in municipal solid waste landfills.

FOX, P. J., Triplett, E. J., Kim, R. H., and Olsta, J. T. (1998). Filed study of installation damage for geosynthetic clay liners. Geosynthetics International, 5(5), 491–520.

Gao, D., Heimann, R. B. (1993). Structure and Mechanical Properties of Superabsorbent Poly(acrylamide)-Montmorilionite Composite Hydrogels. Polymer Gels and Networks, 1(4), 225–246.

GI (Geosynthetic Institute). (2016). GRI test method GCL3:Test methods, required properties, and testing frequencies of geosynthetic clay liners (GCLs). Geosynthetic Institute, Folsom, USA.

Guyonnet, D., Gaucher, E., Gaboriau, H., Pons, C.-H., Clinard, C., Norotte, V., and Didier, G. (2005). Geosynthetic clay liner interaction with leachate: Correlation between permeability, microstructure, and surface chemistry. Journal of Geotechnical and Geoenvironmental Engineering, 131(6), 740–749.

Guyonnet, D., Touze-Foltz, N., Norotte, V., Pothier, C., Didier, G., Gailhanou, H., Blanc, P., and Warmont, F. (2009). Performance-based indicators for controlling

geosynthetic clay liners in landfill applications. Geotextiles and Geomembranes, 27(5), 321–331.

Katsumi, T., Ishimori, H., Onikata, M., and Fukagawa, R. (2008). Long-term barrier performance of modified bentonite materials against sodium and calcium permeant solutions. Geotextiles and Geomembranes, 26(1), 14–30.

Kim, S., Iyer, G., Nadarajah, A., Frantz, J. M., and Spongberg, A. L. (2010). Polyacrylamide hydrogel properties for horticultural applications. International Journal of Polymer Analysis and Characterization, 15(5), 307–318.

Kim, S., and Palomino, A. M. (2011). Factors influencing the synthesis of tunable clay-polymer nanocomposites using bentonite and polyacrylamide. Applied Clay Science, Elsevier B.V., 51(4), 491–498.

Koerner, R. M. (1990). Design with Geosynthetics, 2nd ed. Prentice Hall: Englewood Cliffs, NJ, USA.

Kolstad, D. C., Benson, C. H., and Edil, T. B. (2004). Hydraulic conductivity and swell of nonprehydrated geosynthetic clay liners permeated with multispecies inorganic solutions. Journal of Geotechnical and Geoenvironmental Engineering, 130(12), 1236–1249.

Kong, D. J., Wu, H. N., Chai, J. C., and Arulrajah, A. (2017). State-of-the-art review of geosynthetic clay liners. Sustainability (Switzerland), 9(11), 1–18.

Lee, J.-M., and Shackelford, C. D. (2005). Impact of Bentonite Quality on Hydraulic Conductivity of Geosynthetic Clay Liners. Journal of Geotechnical and Geoenvironmental Engineering, 131(1), 64–77.

Li, T.-K., and Rowe, R. K. (2020). GCL self-healing: Fully penetrating hole/slit hydrated with RO water and 10 mM Ca solution. Geosynthetics International, 27(1), 34–47.

Liu, Z. S., and Rempel, G. L. (1997). Preparation of Superabsorbent Polymers by

CrosslinkingAcrylic Acid and Acrylamide Copolymers. Applied polymer, 64(7), 1345–1353.

Matyjaszewski, K., and Davis, T. P. (2002). Handbook of Radical Polymerization. WILEY-INTERSCIENCE.

Mazzieri, F., and Pasqualini, E. (1997). Field performance of GCLs: a case study. In: Proceedings of the First ANZ Conference on Environmental Geotechnics, Melbourne, 289–294.

Mazzieri, F., and Pasqualini, E. (2000). Permeability of damaged geosynthetic clay liners. Geosynthetics International, 7(2), 101–118.

McBride, M. B. (1994). Environmental chemistry of soils. Environmental chemistry of soils.

Mishra, M. K., and Yagci, Y. (2016). Handbook of Vinyl Polymers: Radical Polymerization, Process, and Technology: Second Edition. Handbook of Vinyl Polymers: Radical Polymerization, Process, and Technology: Second Edition.

Mitchell, J. K., and Soga, K. (2005). Fundamentals of soil behavior. ew York: John Wiley & Sons.

Nie, J. X., and Chai, J.C. (2021). Swelling Behavior and Permeability of Polymerized Bentonite with Due Monomers. Springer Singapore.

Nie, J. X., Tanaka, R., and Chai, J.C. (2020). Effect of polymerization on the swelling properties of a sodium bentonite and its mechanism. Materials Science Forum.

Norrish, K., and Quirk, J. P. (1954). Crystalline swelling of montmorillonite: Use of electrolytes to control swelling. Nature, 173(4397), 255–256.

Ozhan, H. O. (2018). Hydraulic capability of polymer-treated GCLs in saline solutions at elevated temperatures. Applied Clay Science, 161, 364–373.

Painter, P. C., and Coleman, M. M. (1998). Fundamentals of polymer science: An introductory text.

Petrov, R. J., and Rowe, R. K. (1997). Geosynthetic clay liner (GCL) - Chemical compatibility by hydraulic conductivity testing and factors impacting its performance. Canadian Geotechnical Journal, 34(6), 863–885.

Prongmanee, N. (2018). Polymerized bentonites and their applications in geosynthetic clay liner (Doctoral dissertation, Saga University).

Prongmanee, N., and Chai, J.-C. (2019). Performance of Geosynthetic Clay Liner with Polymerized Bentonite in Highly Acidic or Alkaline Solutions. International Journal of Geosynthetics and Ground Engineering, 5(3).

Prongmanee, N., Chai, J. C., and Shen, S. (2018). Hydraulic properties of polymerized bentonites. Journal of Materials in Civil Engineering, 30(10), 1–10.

Quang, N. D., and Chai, J. C. (2015). Permeability of lime- and cement-treated clayey soils. Canadian Geotechnical Journal, 52(9), 1221–1227.

Rowe, R. K. (2020). Geosynthetic clay liners: Perceptions and misconceptions. Geotextiles and Geomembranes, 48(2), 137–156.

Rowe, R. K., Brachman, R. W. I., Hosney, M. S., Take, W. A., and Arnepalli, D. N. (2017). Insight into hydraulic conductivity testing of geosynthetic clay liners (GCLs) exhumed after 5 and 7 years in a cover. Canadian Geotechnical Journal, 54(8), 1118–1138.

Rowe, R. K., Brachman, R. W. I., Take, W. A., Rentz, A., and Ashe, L. E. (2016a). Field and laboratory observations of down-slope bentonite migration in exposed composite liners. Geotextiles and Geomembranes, 44(5), 686–706.

Rowe, R. K., Garcia, J. D. D., Brachman, R. W. I., and Hosney, M. S. (2019). Chemical interaction and hydraulic performance of geosynthetic clay liners isothermally hydrated from silty sand subgrade. Geotextiles and Geomembranes, 47(6), 740–754.

Rowe, R. K., and Li, T.-K. (2020). Self-healing of circular and slit defects in GCLs upon hydration from silty sand under applied stress. Geotextiles and Geomembranes, 48(5), 667–683.

Rowe, R. K., Rentz, A. K., Brachman, R. W. I., and Take, W. A. (2016b). Effect of GCL type on downslope erosion in an exposed composite liner. Journal of Geotechnical and Geoenvironmental Engineering, 142(12).

Sari, K., and Chai, J. (2013). Self healing capacity of geosynthetic clay liners and influencing factors. Geotextiles and Geomembranes, 41, 64–71.

Sawada, Y., Nakazawa, H., Take, W. A., and Kawabata, T. (2019). Full scale investigation of GCL damage mechanisms in small earth dam retrofit applications under earthquake loading. Geotextiles and Geomembranes, 47(4), 502–513.

Scalia IV, J., Benson, C. H., Bohnhoff, G. L., Edil, T. B., and Shackelford, C. D. (2014). Long-term hydraulic conductivity of a bentonite-polymer composite permeated with aggressive inorganic solutions. Journal of Geotechnical and Geoenvironmental Engineering, 140(3), 1–13.

Scalia, J., Benson, C. H., Edil, T. B., Bohnhoff, G. L., and Shackelford, C. D. (2011). Geosynthetic clay liners containing bentonite polymer nanocomposite. Geotechnical Special Publication, 2001–2009.

Scalia, J., Bohnhoff, G. L., Shackelford, C. D., Benson, C. H., Sample-Lord, K. M., Malusis, M. A., and Likos, W. J. (2018). Enhanced bentonites for containment of inorganic waste leachates by GCLs. Geosynthetics International, 25(4), 392–411.

Schanz, T., and Tripathy, S. (2009). Swelling pressure of a divalent-rich bentonite: Diffuse double-layer theory revisited. Water Resources Research, 45(2).

Shackelford, C. D., Benson, C. H., Katsumi, T., Edil, T. B., and Lin, L. (2000). Evaluating the hydraulic conductivity of GCLs permeated with non-standard liquids. Geotextiles and Geomembranes, 18(2–4), 133–161.

Shear, I. (2001). Geosynthetic Clay Liners Solid Waste Landfills. General.

Sposito, G. (2008). The Chemistry of Soils. Oxford University Press; New York.

Sridharan, A., and Prakash, K. (1999). Influence of clay mineralogy and pore-medium chemistry on clay sediment formation. 36(5), 961–966.

Stutzmann, T., and Siffert, B. (1977). Contribution to the adsorption mechanism. 25, 392–406.

Swann, J. M. G., Bras, W., Topham, P. D., Howse, J. R., and Ryan, A. J. (2010). Effect of the Hofmeister anions upon the swelling of a self-assembled pH-responsive hydrogel. Langmuir, 26(12), 10191–10197.

Take, W. A., Brachman, R. W. I., and Rowe, R. K. (2015). Observations of bentonite erosion from solar-driven moisture migration in GCLs covered only by a black geomembrane. Geosynthetics International, 22(1), 78–92.

Taylor. (1948). Fundamentals of soil mechanics. New York: Chapman and Hall.

Theng. (1982). Clay-polymer interactions: summary and perspectives. Clay and Clay Minerals, 30(1), 1–10.

Theng, B. K. G. (1979). Formation and prospecties of clay- polymer complexes.

Tian, K., Benson, C. H., and Likos, W. J. (2016a). Hydraulic conductivity of geosynthetic clay liners to low-level radioactive waste leachate. Journal of Geotechnical and Geoenvironmental Engineering, 142(8), 04016037.

Tian, K., Likos, W. J., and Benson, C. H. (2016b). Pore-Scale Imaging of Polymer-Modified Bentonite in Saline Solutions. Geotechnical Special Publication, 468–477.

Tian, K., Likos, W. J., and Benson, C. H. (2019). Polymer Elution and Hydraulic Conductivity of Bentonite-Polymer Composite Geosynthetic Clay Liners. Journal of Geotechnical and Geoenvironmental Engineering, 145(10), 1–12.

Williams, P. A. (2007). Handbook of Industrial Water Soluble Polymers. Handbook of Industrial Water Soluble Polymers.